Investigations of interaction between gold and palladium in alcohol oxidation reactions

XIAOYANG HUANG

2020

PROF. G. J. HUTCHINGS

ABSTRACT

Synergistic interactions between Au and Pd in supported heterogeneous catalysts have long been attributed to the performance enhancements exhibited by AuPd bimetallic catalysts in the liquid phase oxidation of alcohols. However, conclusive experimental evidence for this synergy is somewhat limited and remains a subject of debate, which indirectly inhibits catalyst design. In this PhD thesis, a new explanation is provided for synergistic interactions between Au and Pd in supported AuPd bimetallic catalysts. The aqueous phase aerobic oxidation of 5-Hydroxymethylfurfural (HMF) was selected as a probe reaction for these studies, given the platform chemicals current significance within this field of research and the abundance of work documented on this reaction.

It is proposed that the performance of either Au or Pd in AuPd bimetallic catalysts can be enhanced by facilitating the movement of electrons from one metallic component to the other, indicating that synergy is attributable to a redox co-operation between the two metals. This synergy is markedly enhanced when the two metals are not alloyed, which is demonstrated with spatially separated Au and Pd nanoparticles, noted as (Au + Pd)/C, and physical mixtures of the monometallic counterparts. This theory is evidenced through careful experimental design, utilizing both chemical and electrochemical measurements, *e.g.*, cyclic voltammetry (CV), Short Circuit Current (SCC). Furthermore, it is also demonstrated that this phenomenon is independent of the reaction substrate; similar trends in catalytic performance were also observed for the aqueous phase aerobic oxidation of glycerol and ethanol. The catalysts used in this work were characterized by a number of different techniques, including: Scanning Transmission Electron Microscopy (STEM), Temperature Programmed Reduction (TPR), ultraviolet–visible spectroscopy (UV-vis), X-ray photoelectron spectroscopy (XPS), to further validate the proposed theory.

It is considered that this discovery will provide a new approach to the design and synthesis of highly efficient bimetallic heterogeneous catalysts and contains potential applications in fuel cell research.

ACKNOWLEDGEMENT

To complete this PhD thesis, it is not a simple work by myself alone, behind which a lot of people have made and are continuously making their great contributions to my work. For every progress we achieve, it involves the wisdom from everyone working as a team. Herein I would like to give my special thanks to those people who provided me advice on my research and gave me encouragement during my PhD studies.

First of all, I would like to express my biggest thanks to my supervisor: Prof. Graham Hutchings, who gives me the chance to perform my PhD work at Cardiff Catalysis Institute (CCI) and the financial support for my living in Cardiff. With his patient and considerable supervision, it motivates me to become one of the most excellent scientists in the future. At the same time, I would also acknowledge sincerely to Dr. Ouardia Akdim, Dr. Peter. Miediazk, Dr. Mark Douthwaite, Dr. Richard Lewis, Dr. Samuel Pattisson and Liang Zhao, for all the good suggestions and proposals that they provide during every group meeting that we have. Especially thanks to Kai Wang for running experiments on error bars for this work and Dr. David Morgan for running and analyzing XPS. Furthermore, I would like to warmly acknowledge the input from Prof. Christopher Kiely, Dr. Sultan M. Althahban and Dr. Qian He for the work of microscopy in Lehigh University and National University of Singapore; Prof. Donald Bethell and Prof. Steven Mclntosh for their crucial discussions on electrochemistry.

Secondly and importantly, I would like to give my special thanks to my parent: Jianbiao Huang (黄建标) and Yuemin Yang (羊月敏), who have always stayed behind me and given me countless number of confidence and cheers, sharing all the happiness or unhappiness that I had experienced. Without them, I would not have completed my PhD studies that easy.

A Final acknowledgement must be given to my colleagues Fei Wang and Helena Royle who had done good jobs on their master thesis with me. I can't adequately express my gratitude to Prof. Lei Liu, Prof. Yilai Jiao, Dr. Jile Fu, Prof. Xiaoliang Li and Dr. Rena Oh, during their academic visit to CCI, spending numerous time with me and making my life happy!

LIST OF ABBREVIATIONS

cm	Centimetre
cm^{-1}	Reciprocal centimetre
cm^2	Square Centimeter
mm	millimetre
nm	nanometre
g	Gram
mg	Milligram
wt. %	Weight percent
L	Litre
mL	Millilitre
µL	Microlitre
M	Molarity
mM	Millimolar
mmol	Millimole
h	Hour
min	Minute
min^{-1}	Reciprocal minute
s	Second
s^{-1}	Reciprocal second
kV	Kilovolt
V	Volt
eV	Electronvolt
mA	Milliamps
°C	Degree Celsius
K	Kelvin
rpm	Revolutions per minute

TABLE OF CONTENTS

CHAPTER 1: Introduction

CHAPTER 2: Experimental

CHAPTER 3: Preliminary research on physical mixture of Au/C + Pd/C

CHAPTER 4: Derivation of the reaction mechanism over the Au/C + Pd/C physical mixture

CHAPTER 5: Catalysis promotion and its application

CHAPTER 6: Conclusions and future plans

Appendix

Includes:

1 Introduction

Chapter 1 gives a brief introduction to the concept of catalysis, with focus on the discovery and development of Au catalysis and its enhanced activity when combined with a second metal, especially Pd, a phenomenon known as enhancement effect. This rate enhancement is observed in alcohol oxidation from biomass derived molecules such as benzyl alcohol and glycerol. Corresponding reviews on Au and Pd catalysts as physical mixtures and alloys are covered. Furthermore, a specific review of 5-hydroxymethylfurfural (HMF) oxidation, including the reaction pathway and mechanism over Au based catalysts, is given. This review covers both thermal and electrocatalytic oxidation with focus on the observed rate enhancement over catalytic performance of Au and Pd on various supports and at different molar ratios of metals. Finally, the structure and main purpose of this PhD thesis is introduced, which, in short, is to provide an explanation for the nature of this synergistic effect between Au and Pd, with HMF being used as a probe molecule for study.

1.1 Catalysis and Au catalysis

Catalysis is generally a process by which a catalyst is used for making a reaction occur with a lower activation energy and at a higher reaction rate[1], Scheme 1.1. Reaction with a catalyst shows changed kinetics due to catalysis, but the equilibrium of the reaction remains unchanged, therefore the thermodynamics are also the same comparing to the reaction without a catalyst. A key principle of catalysis is that the catalyst remains the same before and after reaction. Different kinds of catalysis include heterogeneous, homogeneous and bio-catalysis[1]. Catalysis is intimately associated with the chemical industry, for the large production of thousands of chemical products, *e.g.*, methanol formation from syngas[2]; production of ethanol through direct hydration of ethylene[3]; polyvinyl chloride (PVC) produced from polymerization of monomer of vinyl chloride, which is a product through the hydrochlorination of ethyne[4]. Taking vinyl chloride monomer as an example from an environmentally friendly aspect, the highly used mercuric chloride catalyst can trigger serious pollution to natural life and human society due to its high toxicity. However the industrialization of VCM production is crucial as VCM has many applications in daily life[5]. Herein, scientists look for a more stable and environmentally friendly catalyst for this process.

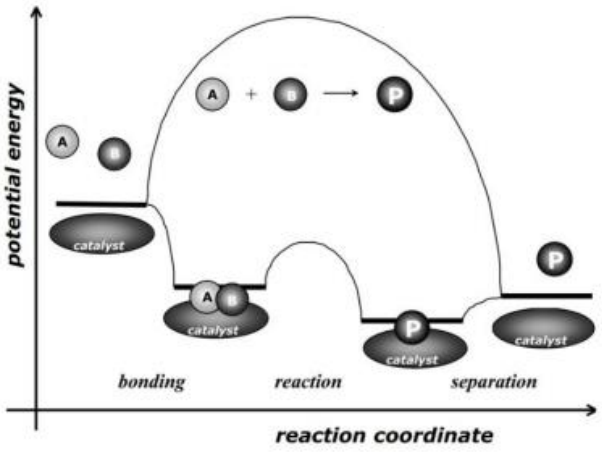

Scheme 1.1. Energy level diagram comparing a catalytic reaction to a reaction without catalyst[6].

Au catalysis is one of the most popular topics in the field of both heterogeneous and homogeneous catalysis. In the 1980s, Haruta and Hutchings independently and simultaneously found the excellent catalytic activity of Au for carbon monoxide oxidation at low temperature (Fig. 1.1) and hydrochlorination of ethyne to vinyl chloride. The latter was marked as a major breakthrough due to the potential replacement of the mercuric chloride catalyst, widely used for the production of VCM (Scheme 1.2)[4]. Au appeared more environmentally friendly than mercury. Since then, Au nanoparticles have found applications in a wide range of reactions such as the oxidation of organic molecules (*e.g.*, propene to propene oxide; propene epoxidation) for the synthesis of commercial products including adhesives, paints, and cosmetics[7]. Au has become increasingly popular over recent decades and is now studied by many different research groups worldwide[8–14].

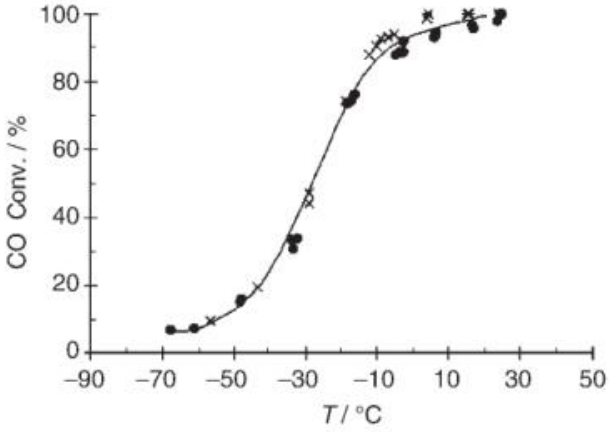

Figure 1.1. CO conversion as a function of temperature for uncalcined catalysts[15]; standard test conditions: (×) 0.47 % Au/TiO_2 and (●) 0.55 % Au/TiO_2.

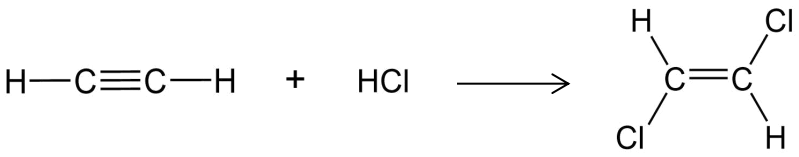

Scheme 1.2. Hydrochlorination of ethyne to vinyl chloride.

In 2002, Hutchings and his co-workers discovered another promising application of Au catalysis in research and industry; the direct synthesis of hydrogen peroxide (Scheme 1.3), a crucial but challenging reaction. Hydrogen peroxide is synthesized industrially without direct contact of hydrogen and oxygen in order to achieve high concentrations[16]. Supported Au catalysts were found to be considerably selective in the direct synthesis of hydrogen peroxide at a low temperature of 2 °C, and the reaction rate could be enhanced by addition of Pd, attributed to the formation of an Au-Pd alloy[17]. Later in 2009, an acid pretreated carbon supported Au-Pd alloy catalyst was found to successfully switch off the subsequent decomposition of H_2O_2, resulting in a high hydrogen selectivity greater than 95 %[8]. In 2016, another article demonstrated that the Pd-Sn alloy supported on commercial SiO_2 and TiO_2 supports can achieve the same activity as the Au-Pd alloy in the direct H_2O_2 synthesis from hydrogen and oxygen. The successful replacement of Au by Sn makes the reaction more economical[9].

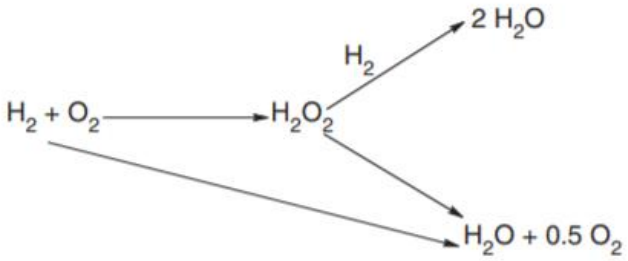

Scheme 1.3. Reaction scheme for the synthesis of hydrogen peroxide[18].

During the same period, several other groups were investigating the water gas shift (WGS) reaction (Scheme 1.4) using Au catalysts too. For example, Venugopal *et al.* found Au/Fe_2O_3 and $Au\text{-}Ru/Fe_2O_3$ showed good activity for this reaction at 120 °C, and the addition of Ru into Au in the formation of an alloy had promoted catalytic performance[11]. Thompsett *et al.* found a highly active $Au/CeZrO_4$ catalyst for clean hydrogen production from WGS at low temperatures. Data is presented in Fig. 1.2,

however the commercialization process is hindered by the deactivation of the catalyst possibly due to the feed composition[19].

$$CO + H_2O \rightarrow CO_2 + H_2$$

Scheme 1.4. Reaction diagram of water gas shift.

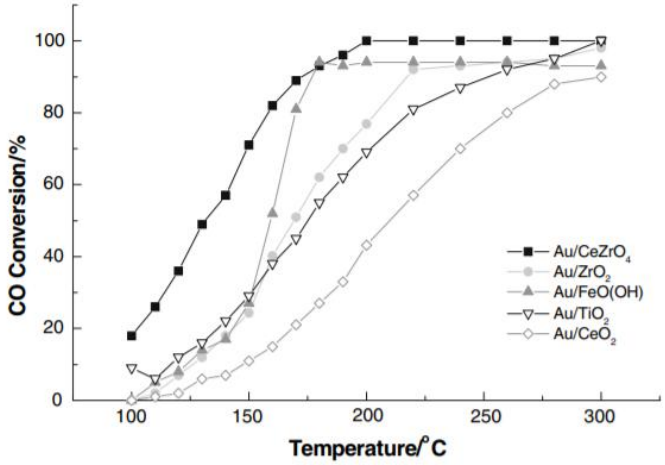

Figure 1.2. WGS activity as a function of temperature for a series of 2 wt.% Au catalysts on a range of supports (5 % CO, 30 % H_2O, 65 % N_2, 40,000 $cm^2\,g^{-1}\,h^{-1}$)[20].

Based on the description above, it appears that in both hydrogen peroxide synthesis and water gas shift reaction, by alloying a second metal to Au could greatly improve the catalysis with evidence of an observed higher reaction rate/conversion. To gain provide a more comprehensive understanding of the bimetallic system, the next section will review more studies which focus on the promotion effect observed by addition of a second metal to Au.

1.2 Activity enhancement in Au catalysis by adding a second metal

As above, bimetallic catalysts are generally known in many cases to exhibit an enhanced activity compared to the monometallic counterparts due to the combination

of physical and chemical properties from each of the substituents[21–24]. This phenomenon of enhancement effect has also been widely reported in a variety of chemical reactions[12–14,19,25–29], such as glycerol, cyclohexane, D-sorbitol and methanol oxidation. The nature of this synergistic effect, and the relation between activity and catalyst structure, is of high importance for the future catalyst design.[23] Therefore, several publications are reviewed here to elaborate the correlation between the structure of Au-M and the responding activity among different reactions.

The structures of Au and other metals (*e.g.*, Pd, Pt, Ru, Cu, Sn), have been combined in many different formulations such as core–shell (A), sub cluster segregated (B), mixed (C), three-shell (D) (Fig. 1.3) by using a variety of preparation methods (*e.g.*, sol immobilization, deposition precipitation, wet impregnation).[30] Interaction between the two metals can be observed across all the preparation procedures with the resulting activity of the bimetallic catalyst not being an easy summation of each substitute metal. The origin of this phenomenon depicted as enhancement effect became the focus of investigation among many research groups worldwide.

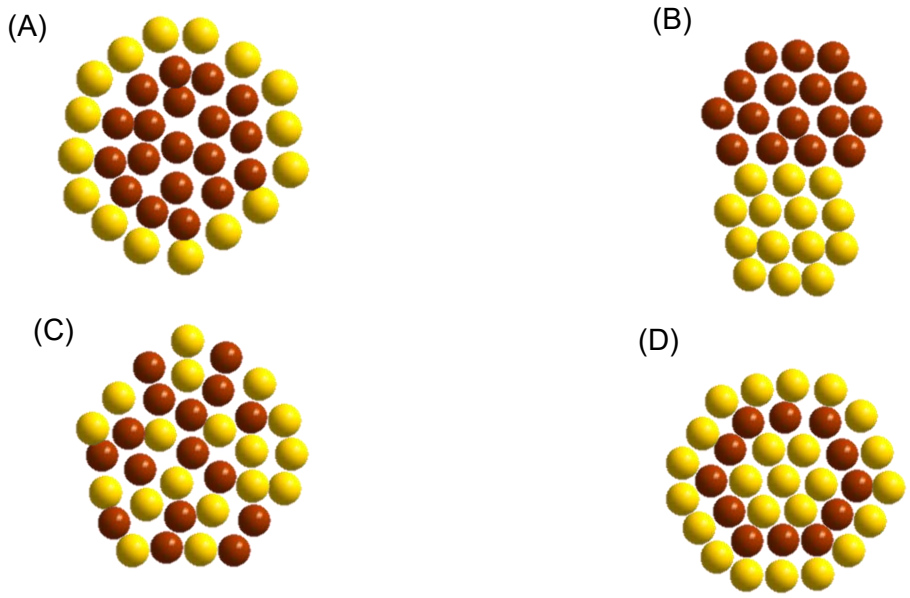

Figure 1.3. Different configurations of Au-metal nanoparticles[31]. (**A**) Core-shell. (**B**) Sub cluster segregated. (**C**) Mixture. (**D**) Three shell.

For few years, scientists have found that alloying Au with Ag showed higher activity in CO oxidation even at room temperature when compared to the monometallic catalysts. Here, Ag alone demonstrated no activity, and the enhanced behavior from bimetallic Au and Ag was not due to size effects which indicates there is strong interaction between the two metals[32,33]. Independently, an AuCu alloy was also investigated for the same reaction. By annealing the AuCu alloyed nanoparticles, the crystal structure transferred into two phases of Au and CuO, then enhanced adsorption of CO molecule on the separated phases leads to a higher activity[34].

From another study, Au itself demonstrated negligible activity for octanol oxidation in toluene. In contrast, when Au is alloyed with Ru as a bimetallic catalyst, a large increase in activity was observed without noticeable difference of selectivity[35]. This is possibly due to a dilution effect, also known as geometric effect, from the Au atoms on the surface of Ru nanoparticles as it had been reported that the surface atomic structure of metallic nanoparticles plays an important role in their physical and chemical properties, which could affect the activity[36,37].

In addition to Ag, Cu and Ru, Hensen *et al.* had reported a synergistic effect between Au and Ir which results in an improved activity in gas-phase ethanol oxidation to acetaldehyde, whereby the bimetallic catalyst shows a higher ethanol conversion than its monometallic catalysts. According to characterization of the material, the catalyst was evaluated as a metallic core and surface shell structure, where those uncovered Au atoms are the active sites for the adsorption and dissociation of ethanol molecules, meanwhile the Ir atoms on the surface of nanoparticles are oxidized to provide the oxygen atoms for the dehydration of ethanol[38]. Later, a similar rate enhancement was found in bimetallic AuCr catalysts in both ethanol and benzyl alcohol oxidation with rates again being higher than their monometallic counterparts. Using techniques of XPS and UV-vis[39,40], it was evidenced that electrons transfer in the catalyst between the Au^{3+} and the redox cycle of Cr^{3+}/Cr^{6+} in benzyl alcohol oxidation. In theory, oxygen activation takes place on the surface of Cr^{3+}, leading to the formation of Cr^{6+}, in

parallel, the electrons are transferred to reduce the Au^{3+} into Au^{0}. The alcohol activation therefore takes place on the surface of Au from the hydroxyl groups and the oxygen species in generating the Au-alcoholate[41].

Accordingly, proper bimetallic Au-M catalysts had promoted the catalytic performance due to the different kinds of interaction between the two metals within the Au based bimetallic system. However, few works have focused on catalysts present as a physical mixture in catalytic reactions. It is not known if the synergistic effect can originate from two independent parts of a catalyst mixture in one reaction. This is the primary focus of this study. In the next section, a short review is given for those reported catalytic formulations in the form of a physical mixture, with focus on Au and Pd in biomass conversion.

1.3 Catalysis over Au and Pd in a presence of physical mixture in biomass conversion

Biomass, such as starch, cellulose and fructose, is a resource derived from plant or animal feedstocks used for the production of energy and heat, and also as raw materials for conversion into high value-added products including bioplastics, biofuels, and fine chemicals[42,43]. The possibility of utilizing this renewable source for replacing the old non-renewable crude oil based feedstocks has been extensively studied in recent decades[44].

Nanoparticles of Au-Pd alloy have been largely used to catalyze various bio-derived alcohols/aldehydes with an excellent activity due to the synergistic effect between Au and Pd, compared to the monometallic catalysts[16,30,45–49]. For this reason, researchers have put numerous efforts into the study of AuPd catalysis in biomass transformation to look for the structure-activity relationship. However, investigation of catalysts as a physical mixture have rarely been reported. In this section, publications covering biomass conversion using a physical mixture catalyst are reviewed.

The use of a physical mixture catalyst of Au/AC and Pd/AC has been reported for benzyl alcohol oxidation in water (reaction route see Fig. 1.4, activity data are shown in Fig. 1.5). Both Au-Pd alloy and the corresponding mixture catalyst displayed a prominent higher activity than the corresponding monometallic Au and Pd in terms of benzyl alcohol conversion, with the Au-Pd alloy demonstrating the highest activity. It is also reported that after reaction for 0.5 h, the mixture catalyst starts to form an Au-Pd alloy structure which results in a dramatic increase in its activity[50]. The observation of the structural transition from physical mixture to alloy was characterized by aberration corrected HRTEM where the Pd nanoparticles were found to reprecipitate onto the surface of Au where Au remained stable. The migration becomes even more prominent after a reaction of 1 h. The illustration of structure-activity relation helps researchers gain a better understanding on how the Au and Pd synergistically affect each other. Compared to this work, the study of interaction between Au and Pd in this thesis were discovered an opposite trend, where the Au and Pd mixture catalyst displayed a higher activity than the corresponding Au-Pd alloy. A new explanation is going to be provided to disclose the observed rate enhancement in Au and Pd when physically mixed. This will be discussed in *Chapters 3, 4 and 5*.

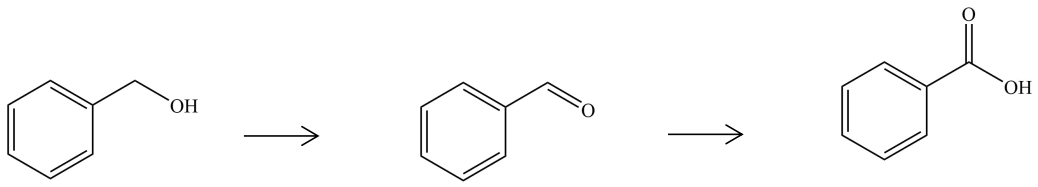

Figure 1.4. Reported reaction schemes of aqueous benzyl alcohol oxidation[51].

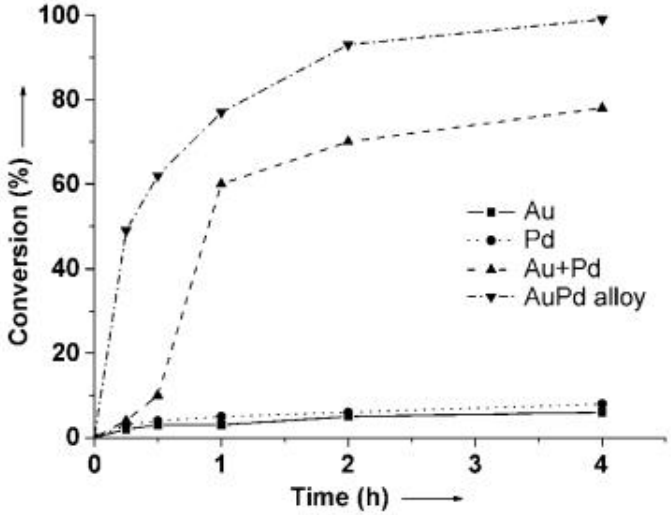

Figure 1.5. Catalytic performance of liquid-phase benzyl alcohol oxidation, conversion versus time for physically mixed Au/AC and Pd/AC, corresponding Pd/AC and Au/AC monometallic catalysts and the bimetallic 4Pd@6Au/AC (Pd/Au=4:6, mole/mole)[50].

Hydroxymethylfurfural (HMF) is another example, and is also the probe molecule used in this PhD thesis. In literature, a physical mixture catalyst of Au/AER and Pd/AER has been tested and compared with its Au-Pd alloy (Table 1.1). The AER support is a material of anion-exchange resin. This study is also analogous to the main study of this thesis, where a physical mixture of Au/C and Pd/C is investigated in HMF oxidation to look for the how Au and Pd interact with each other. However, in this example the mixture catalyst demonstrated a lower activity than the alloy in terms of the yield towards FDCA (52 % yield from mixture catalyst; 93 % yield from the alloy), despite the addition of yield from monometallic Au and Pd being less than the mixture catalyst. It suggests a synergistic effect by simply mixing two independent catalysts which can promote the oxidation reaction. With respect to the results in this thesis, the observation of enhancement effect from a physical mixture becomes even greater when a carbon support (carbon black XC-72R) is used (see *Chapter 3*). This is suggested to be the efficient process of electron transfer between the Au and Pd

through the C support, as a less conductive support, *e.g.*, TiO_2 or BN, a lower activity will be observed, See *Chapter 4, Table 4.1*.

Table 1.1. Oxidation of HMF into FDCA using AER-supported Au-Pd alloy nanoparticles. Reaction conditions: HMF (2 mM), catalyst: 200 mg, Na_2CO_3 (2 mM), O_2: 10 bar, H_2O (20 mL), 373 K, 4 h[52].

Entry	Catalyst	HMF Conversion (%)	FDCA Yield (%)
1	AER support	68.7	1.6
2	1wt.% Au/AER	100	27.6
3	1wt.% Pd/AER	80.4	5.6
4	2wt.% Au-Pd(1:1)/AER	100	93.2
5	1wt.% Au/AER + 1wt.% Pd/AER	100	52.0

Glycerol is an important byproduct in bio-diesel production and a major platform molecule for generating fine chemicals, bulk chemicals, polymers and fuels through its oxidation reaction[53]. Au and Pd are among the most popular catalysts studied and reported[54].

Davis and co-workers investigated Au and Pd catalysts supported on activated carbon for aqueous glycerol oxidation, Fig. 1.6 and, like other alcohols, the Au-Pd catalyst apparently shows a higher oxidation rate compared to the monometallic Au. An increased selectivity towards the product of glyceric acid was also observed. The added Pd was reported to decompose the *in situ* generated H_2O_2 during glycerol oxidation, which avoids the cleavage of the C-C bond in result more glyceric acid (a three carbons product) is produced in the reaction. At the same time, a physical mixture catalyst of Au and Pd was tried for the same reaction. Even though reaction rate is lower than the monometallic Au, however due to the appearance of Pd, it

displayed the same phenomenon that an enhanced selectivity to the formation of glyceric acid was observed, showing the cooperative behaviors between the two metals affects the catalytic performance. Overall, it is important to conclude that AuPd catalysts, either with a structure of alloy or physical mixture, leads to a similar trend, suggesting that the protocol of mixture catalyst has its advantage.

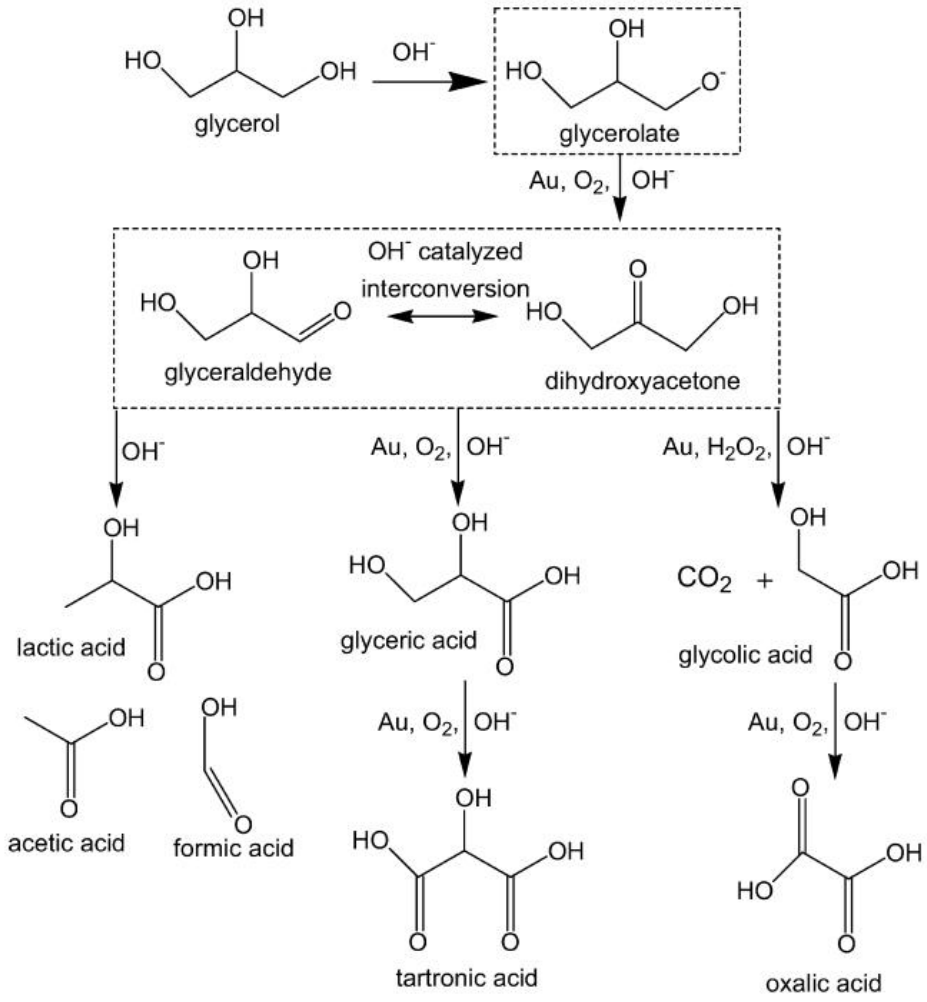

Figure 1.6. Proposed reaction network for the aqueous phase oxidation of glycerol over supported Au catalysts in the presence of a strong base[12]. Species within boxed are proposed intermediates that were never directly isolated.

Based on the review above, it seems catalysts of Au and Pd when presented as a physical mixture result in a lower activity than a presence of Au-Pd alloy. However is there any literature showing the opposite trend? Zhao *et al.* had investigated several carbon nanotube(CNT) supported AuPd catalysts, namely Au/CNT; Pd/CNT; a-Pd_3Au/CNT alloy; c-Pd_3Au/CNT core-shell; m-Pd_3Au/CNT physical mixture in oxygen reduction reaction in an alkaline condition of 1.0 M KOH saturated with O_2. As is shown in Fig. 1.7, the catalyst series follows an activity trend of AuPd physical mixtyre > Pd > AuPd core-shell > AuPd alloy > Au in terms of current density at -0.4 V *vs*. SCE (saturated calomel electrode)[55]. The physical mixture is showing 1.6 times higher in current density than the alloy, and almost doubled to the Au. Oxygen reduction to OH^- species is known as a four electrons transfer reaction for generation of one OH^-[56], the best catalytic performance of Au and Pd physical mixture indicates the highest amount of electron transfer among all the tested catalysts. In parallel, Pd alone appeared a high activity in ORR too, just close to the Au and Pd physical mixture. On the other hand, in regard to the onset potential over each catalyst in ORR, they follow an opposite trend, namely: AuPd physical mixture < Pd < AuPd alloy < AuPd core-shell < Au. Onset potential indicates the ease of reaction takes place, higher is the onset potential, larger is the driving force needed at the given electrode condition[57]. Thereby, the catalyst of Au and Pd physical mixture is overcoming less activation energy to start ORR whereas the AuPd alloy requires a higher driving force for initiating the same reaction. Actually, ORR is closely related to alcohol/aldehyde oxidation because the generated electrons from oxidized alcohol/aldehyde are scavenged by O_2, this reported phenomenon has agreed well to the observations in this thesis, where by spacial separation of the Au and Pd nanoparticles, an enhanced reaction rate compare to the corresponding AuPd alloy is observed in alcohol/aldehyde oxidation due to the effect of coupling the alcohol oxidative dehydrogenation (ODH) and ORR, thereby more electrons are transferred from one metal to the other, see *Chapter 4,* Fig. 4.3. The molecular O_2 is scavenging the

electrons generated from HMF oxidation over the Au/C, Pd/C is then the good catalyst in ORR to consume these electrons.

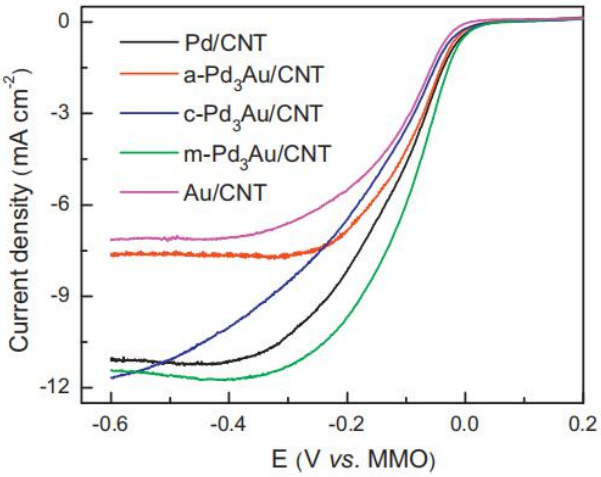

Figure 1.7. Linear sweep voltammograms (5 $mV.s^{-1}$) recorded in 1.0 M KOH solution saturated with oxygen at a rotating rate of 3600 rpm[55]. a-Pd_3Au indicates an alloyed catalyst; c-Pd_3Au indicates a core-shell catalyst; m-Pd_3Au indicates a physical mixture catalyst.

In addition to all the substrates mentioned above, oxidation of other molecules such as D-sorbitol and cyclohexane have been regarded as interesting model reactions too where bimetallic catalysts of Au and Pd shows promising activity[14,58]. In fact, the physical mixture catalyst usually demonstrated a worse performance than alloy, with the synergistic effect between Au and Pd depending on the preparation method of the catalyst.

In summary, biomass conversion using Au and Pd catalysts in many cases have led to an improvement in both activity and selectivity, especially with a structure of Au-Pd alloy. This result is often ascribed to the intimate interaction between the two metals, generally due to the physicochemical interactions. However, when the Au and Pd are presented as a physical mixture during reaction, its performance is not as active as when the two metals are alloyed. Nevertheless, the mixture catalyst still displayed an enhancement in activity compared to the monometallic counterparts. It is assumed

the physical chemical interaction in alloy is more efficient than in the profile of physical mixture. In this study, the essence of how interaction occurs between Au and Pd when present as a physical mixture in alcohol oxidation will be explained. It also provides explanations on why physical mixtures of Au and Pd exhibits higher activity than Au-Pd alloy. 5-hydroxymethylfurfural (HMF) is used as a probe molecule to investigate the intimate interaction between Au and Pd, and the different functions from each metal. In the next section, publications on HMF oxidation over Au and Pd were covered as a preliminary introduction.

1.4 Hydroxymetylfurfural (HMF) and its oxidation over catalyst of Au-Pd

1.4.1 HMF and its oxidation pathway

In 2004, HMF was recognized as one of twelve key platform molecules for valorisation by the US Department of Energy[59]. As mentioned in Section 1.3, fossil fuel derived energy and chemicals are becoming significantly pressured, due to the unsustainable nature of this feedstock. To mitigate this problem, mankind is looking for renewable substitutes, *i.e.* biomass. HMF is one of the molecules which could be synthesized from fructose, a bio-derived molecule formed through hydrothermal dehydration, reaction route in Fig. 1.8.

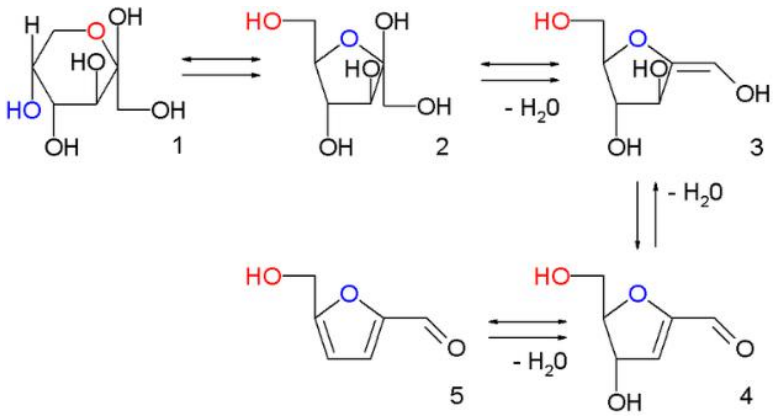

Figure 1.8. Synthesis of HMF from hydrothermal dehydration of fructose. 1: fructopyranose; 2: fructofuranose; 3,4: two intermediates; 5: HMF.

HMF can be oxidized to 5-furandicarboxylic acid (FDCA), a terminal oxidation product, which is considered to be a cost-effective component for the production of bio-based plastics that offer a green alternative to the petroleum-based terephthalate polyesters[60]. It is therefore why a great deal of effort has been made to the synthesis of different catalysts for the aerobic oxidation of HMF to FDCA[61], reaction pathways are presented in Scheme. 1.5.

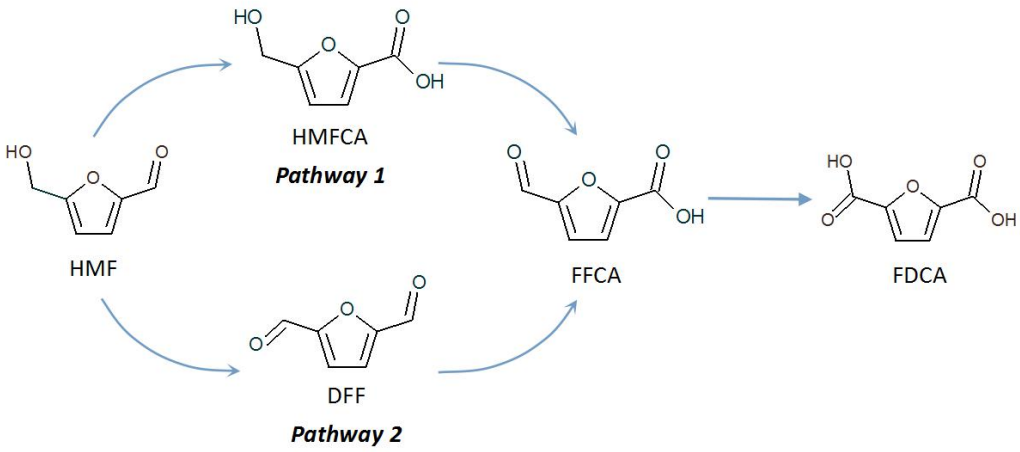

Scheme 1.5. Possible reaction routes for aqueous HMF oxidation.

As is shown in Scheme. 1.5, HMF oxidation may proceed through two different pathways. The first involves oxidation of the methyl aldehyde group in HMF forming 5-hydroxymethyl-2-furancarboxylic acid (HMFCA). This intermediate is converted *via* oxidation of the remaining alcohol group to 5-formyl-2-furan-carboxylic acid (FFCA), which subsequently oxidizes to yield the final product, FDCA. The second pathway proceeds *via* an intermediate of 2, 5-diformylfuran (DFF) which is then oxidized to FFCA and finally to the terminal product, FDCA.

1.4.2 Reported HMF oxidation mechanism over Au catalyst

Various scientists have investigated the mechanism of HMF oxidation using different catalysts. Davis *et al.* studied the mechanism over the supported Au and Pt catalyst at a high pH condition, 0.3 M NaOH and 0.15 M HMF in 5 mL H_2O. Find Fig. 1.9, HMF molecule dissolves in alkaline solution, which forms geminal diol in a reversible process. Thereafter, this geminal diol reacts with OH^- in water on the surface of Au or Pt catalyst, generating the first intermediate product HMFCA, meanwhile two electrons are liberated on the surface of Au or Pt. The formed HMFCA molecule follows the same reaction with OH^- to yield the second intermediate FFCA, with another release of two electrons. FFCA has a similar molecular structure to HMF as they both contain aldehyde functional group. Therefore, this FFCA is going through the same mechanism as HMF to its geminal diol and the final product FDCA is obtained. During all the steps, OH^- from water in the presence of Au or Pt metal catalysts promote O-H and C-H bond activation of the alcohol side chain on HMF and then add directly to aldehyde intermediates to eventually form acid products. Labeling experiments were conducted with $^{18}O_2$ and $H_2{}^{18}O$, indicating that instead of molecular oxygen, water was the source of oxygen atoms in HMF oxidation. Molecular oxygen is required to scavenge the electrons deposited on the metal catalyst surface during the reaction, thus closing the catalytic cycle. This mechanism is now well known and widely accepted[62–64].

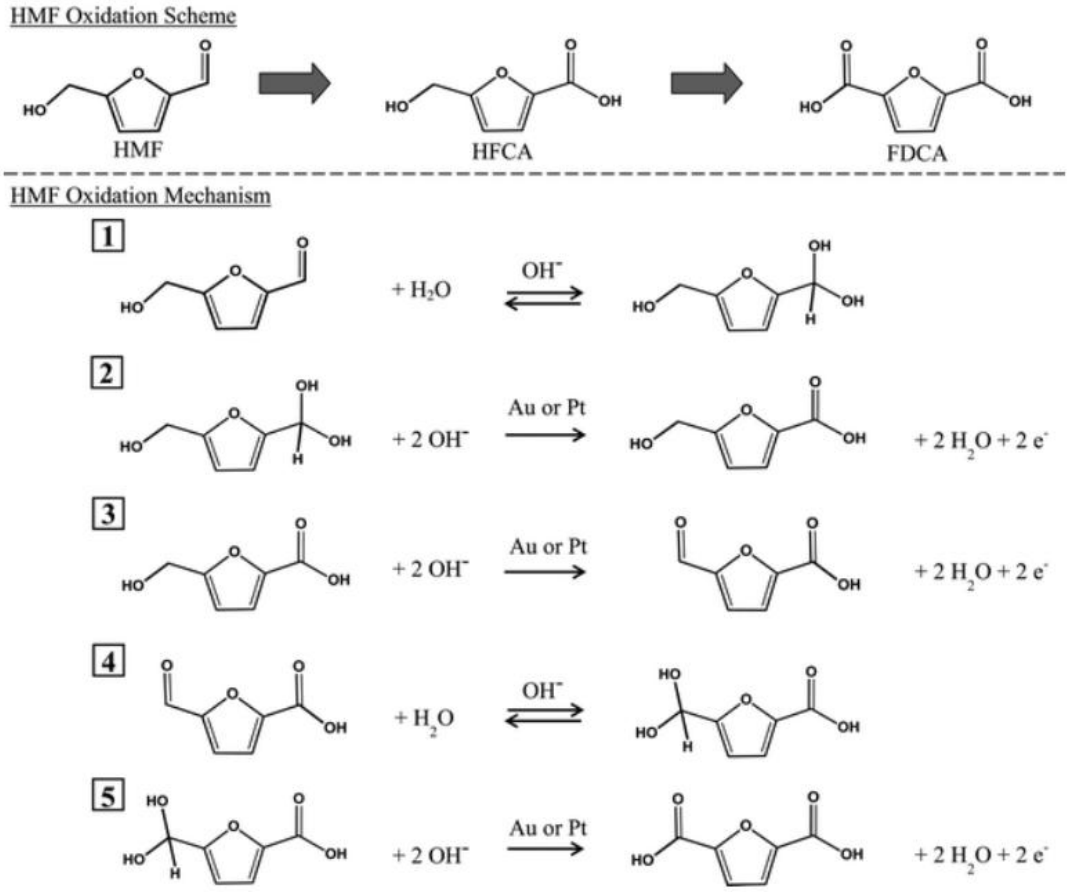

Figure 1.9. Overall reaction scheme and proposed mechanism for the oxidation of HMF in aqueous solution in the presence of excess base (OH^-) and either Pt or Au. Dioxygen (not shown) serves as a scavenger of electrons that are deposited into the metal particles during the catalytic cycle[64].

Using the above mechanism as a foundation, a large quantity of catalysts have been prepared and tested in the literature for the investigation of HMF oxidation showing good activity towards the production of FDCA. Among all, Au and Pd catalysts have triggered a big interest in terms of their high efficiency. As it was discussed in Section 1.3, bimetallic Au-Pd has demonstrated excellent behaviors in biomass conversion. However, further in-depth insight into the disclosure of interaction requires more investigation. For example, experimental data of Au and Pd catalysts with different supports are shown in the thesis to give evidence in explaining the observed

enhancement effect during HMF oxidation. Interaction between Au and Pd on different supports could provide researchers a better design for the future multi component catalyst. As such, the next section is going to introduce those published works featuring HMF oxidation using Au and Pd catalysts and demonstrate a synergistic effect between the two metals.

1.4.3 Reviews on HMF oxidation over Au/Pd catalyst in thermal catalysis

Cavani and co-workers had tried bimetallic Au-Pd and its counterpart monometallic Au and Pd supported on TiO_2, with a preparation method of sol immobilization to elucidate the mechanism of the HMF oxidation. The testing showed that catalysts of 1.5 wt.% Au/TiO_2 and Pd/TiO_2 could both obtain an intermediate product HMFCA from HMF (reaction route see Scheme 1.5). However, the monometallic Pd is less capable for the further oxidation from HMFCA into the final product FDCA than the monometallic Au. Constructing the Au and Pd into a bimetallic alloyed catalyst, it was found a higher activity in terms of selectivity to FDCA, especially for Pd_1Au_6/TiO_2 (atomic ratio of Pd/Au=1/6), which showed the highest selectivity. Calcining the Pd_1Au_6/TiO_2 at 300 °C demonstrated a rather decreased activity due to the migration of Pd to the outer surface of alloy nanoparticles, resulting in an Au core and Pd shell structure[65]. In order to compare the structure of the alloy to a core shell, catalysts with a true core shell structure were prepared using the same method but with a sequential reduction step (briefly the first reduced metal is acting as a seed for the second metal), denoted as Au@Pd (Au core, Pd shell) and Pd@Au (Pd core, Au shell). The unsupported Pd@Au indeed displayed higher activity than the Au@Pd, which confirmed the corresponding result from the calcined $Au\text{-}Pd/TiO_2$ catalyst. This paper conducts that the structure of bimetallic AuPd catalyst plays an important role in HMF oxidation as it effects the synergistic interaction between Au and Pd, the $Au_{core}Pd_{shell}$ and $Pd_{core}Au_{shell}$ have revealed different synergistic effect.

Apart from the nanoparticle structure, different catalyst supports have been studied extensively as the intrinsic nature of the support would affect the interaction in AuPd nanocatalysts too[24]. So far, TiO_2, CeO_2 and C and many other supports such as zinc hydroxycarbonate (ZOC), anion-exchange resin (AER) and hydrotalcite (HT) have been reported for the preparation of Au-Pd catalyst for the investigation of HMF oxidation. The rate enhancement in HMF oxidation using AuPd catalyst does not solely rely on the metallic nanoparticles, as the support plays a role in the observed catalysis too.

Taking ZOC as an example, researchers have reported deposition of Au-Pd nanoalloy onto ZOC with Au/Pd molar ratio of 1/1, which displayed a prominent higher activity than its counterpart monometallics of Au and Pd. ZOC was considered as a good support candidate because of its basic property, which is reported as an important factor for Au catalysis especially in alcohol/aldehyde oxidation[66]. Similar to ZOC support, the use of hydrotalcite (HT), $Mg(OH)_2$ *et al.* as supports have been widely used as the interaction between Au and Pd is promoted since the Au appears a superior activity in an alkaline condition, where this alkaline condition is given by these supports[67]. Therefore, catalyst supports seem to be important indeed in the catalytic performance of Au based bimetallic formulations. Zhou *et al.* investigated several mesoporous poly(ionic liquid) (MPIL) materials as carriers for alloyed Au-Pd nanoparticles. The nanoparticles were deposited onto the support by ion-exchange of precursors followed by a reduction process under H_2 at 300 °C. The prepared supports were named as PECN (hydrophilic) and PDCN (hydrophobic). Experimentally, the catalyst with PECN support showed a superior activity compared to PDCN support. In order to find out the reason for this difference in catalytic performance between the two supports, a zeta potential was measured. In result, PECN shows a lower zeta potential number under the same concentration of HMF solution and a higher zeta potential number under the same concentration of FDCA solution than PDCN. This suggests PECN contains a stronger affinity to the HMF molecule and an easier removal of FDCA molecules (Fig. 1.10)[68]. This work conveys

that the adsorption and desorption properties of the supports could affect the corresponding catalysis over the deposited AuPd nanoparticles in HMF oxidation. Therefore, several supports, *e.g.*, carbon black XC-72R, TiO_2 and BN were used and tested as catalyst supports in HMF oxidation (see *Chapter* 4) in this thesis, showing that support conductivity can absolutely change the activity, especially when two catalysts are presented as physical mixture. Therefore, interaction between Au and Pd is not only an issue between the metals themselves, but the influence from carriers would be accountable too.

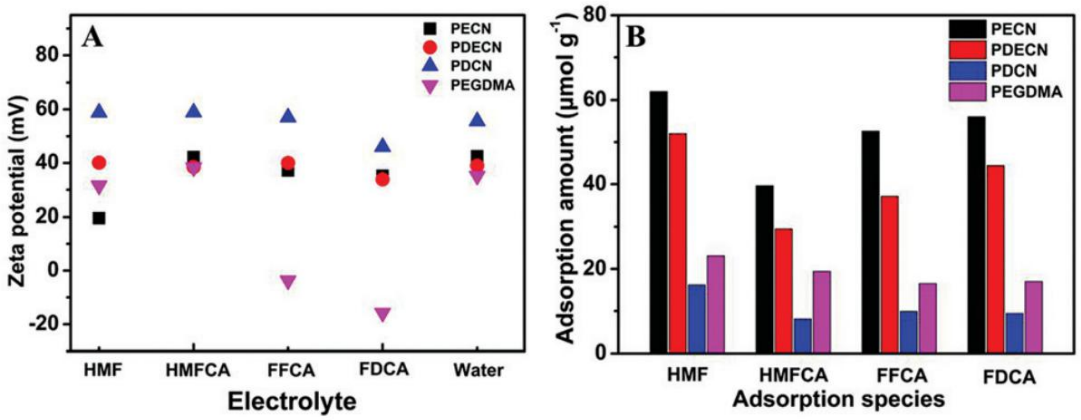

Figure 1.10. (**A**) Zeta potentials of various support colloidal particles obtained from emulsion with the same concentration of HMF, HMFCA, FFCA, and FDCA (1 mmol/L). (**B**) The reaction substrate adsorption histograms for various supports. Adsorption conditions: substrate (0.01 mmol), support: 0.1 g, H_2O (10 mL), 90 °C, 12 h[68].

Apart from different supports, the molar ratio between Au and Pd is another crucial factor in influencing the catalytic performance. As molar ratios between Au and Pd varies, a different synergistic profile in the Au-Pd alloy is observed. Looking for and understanding what the optimized ratio is between Au/Pd had been extensively investigated. For example, Wang and co-workers have focused on HMF oxidation using Au-Pd/CNT (carbon nanotube) with a wide range of molar ratios between Au to Pd (4/1, 7/3, 1/1, 3/7, 1/4)[69] in base free conditions (find in Table 1.2). The catalysts

were prepared by the sol immobilization protocol. From the activity test results, Au/Pd with a ratio of 1/1 shows the best activity towards to a full conversion of HMF and 99 % yield of FDCA at reaction conditions of 100 °C, 5 bar O_2 after 12 hours without addition of base, whereas the monometallic Au and Pd had both appeared poor catalytic behaviors. Activity results from each ratio are shown in Table 1.2. Overall, the activity profile from each Au/Pd mole ratio displayed a volcano shape in terms of FDCA yield where all the bimetallic catalysts are showing synergistic effect, namely the product yield is more than a simple summation from the monometallic, see Fig. 1.11. Similar to the publication, in this thesis the phenomena from different mole ratios in Au/Pd is studied under an alkaline condition (0.4M $NaHCO_3$, pH =8.7), see *Chapter 4*. Briefly, the Au rich Pd catalysts show generally a higher activity than the Pd rich Au catalyst. At the same time a mechanism has been proposed, where the Au and Pd nanoparticles are undertaking different roles in alcohol oxidation. The role of Au and Pd could be switched when their mole ratios change. Interestingly, this activity enhancement is observed all the way at different mole ratios which is consistent to the work from Wang *et al*.

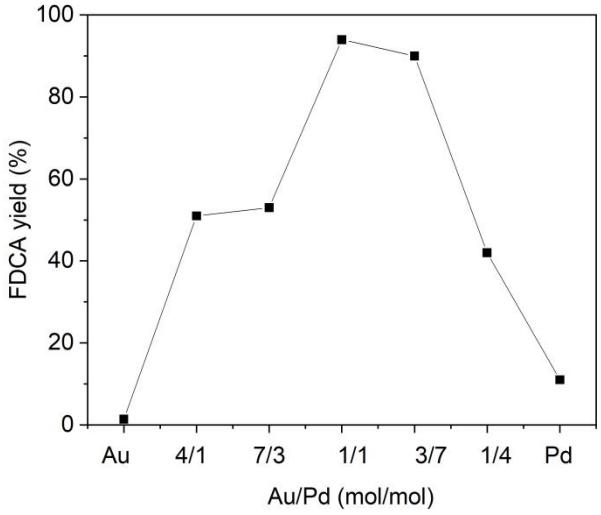

Figure 1.11. Catalytic performance of Au−Pd/CNT catalysts with a variety of Au/Pd mole ratios for aerobic oxidation of HMF[69].

Table 1.2. Catalytic Behaviors of Au−Pd/CNT Catalysts with a variety of Au/Pd Ratios for aerobic oxidation of HMF[69]. Reaction conditions: HMF (0.50 mmol); HMF/(Au + Pd) (molar ratio), 100/1; H_2O (20 mL); O_2: 0.5 MPa; temperature: 373 K; reaction time: 12 h. The number in the parentheses denotes the Au/Pd molar ratio used for preparation; loading amount of (Au + Pd) expected, 1.0 wt.%.

Catalyst	Conversion (%)	Selectivity (%)			
mol/mol		DFF	HMFCA	FFCA	FDCA
Au/CNT	78	3.8	16	8.3	1.4
Au−Pd(4/1)/CNT	75	0	0	47	51
Au−Pd(7/3)/CNT	90	3.6	0	33	53
Au−Pd(1/1)/CNT	100	0	0	1.7	94
Au−Pd(3/7)/CNT	100	0	0	5.0	90
Au−Pd(1/4)/CNT	76	16	0	39	42
Pd/CNT	63	40	0	49	11

In summary, the metallic structure, types of support and molar ratios between bimetals are all influential in the rate enhancement observed in Au/Pd catalysis in HMF oxidation. Thereby, a list of papers using relative Au and Pd catalysts in HMF oxidation had been summarized in *Table S1-S3* at appendix, involving different parameters of reaction temperature; reaction time; oxygen pressure; base type; moles ratio of substrate to metal, with compared catalytic performance in regard to FDCA productivity to results from this thesis in *Table S4*. These summarized works provide readers a more comprehensive insight into the works on HMF oxidation using series of Au and Pd catalysts, highlighting the enhanced activity over the bimetallic when compared with the monometallic. Meanwhile, the catalysts investigated in this work,

e.g., (Au + Pd)/C has achieved the second most active catalyst compare to literature in HMF oxidation in terms of FDCA productivity: 80.0 $mol_{FDCA}.mol_{metal}^{-1}.h^{-1}$ under the given reaction condition is milder (pH = 8.7). The highest FDCA productivity belongs to AuPd supported on active carbon however under a reaction condition of NaOH (pH > 13).

1.4.4 Electrocatalytic oxidation of HMF over Au/Pd catalyst

In addition to the traditional heterogeneous thermal catalysis, electro-oxidation has also been a popular area in the investigation of biomass conversion too. The replacement of high temperatures and pressures of molecular oxygen in the batch reactor system by applying a potential difference between the working and counter electrodes is one of the main advantages of electrochemistry[70]. Such potential is working as the driving force to initiate the reaction for the production of value added products at the anode, meanwhile a parallel reaction could take place at the cathode, *e.g.*, hydrogen evolution, oxygen reduction[71–73]. Electrochemical oxidation of HMF has been investigated as well[71,74–76].

Li and co-workers had focused on the electrocatalytic oxidation of HMF instead of the traditional aerobic oxidation, in which a potential is applied as the driving force for the oxidation. A flow cell reactor with an anion exchange membrane (AEM) was set up for the HMF oxidation. It was found that using Au/C as an electrode is more favorable in oxidizing HMF into its intermediate HMFCA with a relatively lower potential (0.6 V *vs.* RHE, RHE: reversible hydrogen electrode), Table 1.3. However, as the potential increases, the bimetallic electrode Au-Pd/C starts to show its higher activity for the oxidation from the first intermediate HMFCA to the second intermediate FFCA till the final product FDCA, showing that the interaction between Au and Pd is existed also in electrochemical system.

Table 1.3. HMF oxidation product analysis in the AEM-electrolysis flow cell[76].

Catalyst	Potential	Conversion (%)	Selectivity (%)		
	vs. RHE	HMF	HMFCA	FFCA	FDCA
Pd/C	0.6	75	25	64	11
Pd_2Au_1/C	0.6	87	30	62	8
Pd_1Au_2/C	0.6	100	59	16	25
Au/C	0.6	100	98	<1	1
Pd/C	0.9	97	70	<1	29
Pd_2Au_1/C	0.9	100	35	<1	64
Pd_1Au_2/C	0.9	100	16	<1	83
Au/C	0.9	100	98	<1	1
Pd/C	1.2	32	71	26	3
Pd_2Au_1/C	1.2	82	61	17	22
Pd_1Au_2/C	1.2	100	60	4	36
Au/C	1.2	99	81	5	14

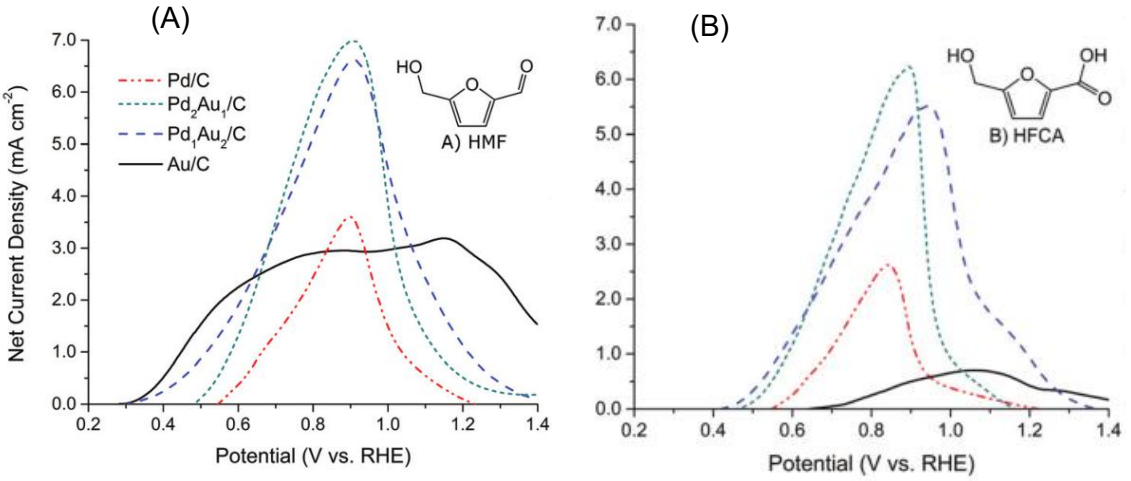

Figure 1.12. Anodic-scan from half-cell CV of 0.1 M KOH with 0.02 M of (**A**) HMF, (**B**) HFCA. Net current density is the difference between anodic-scan current density and blank current density (0.1 M KOH only test)[76]. Reaction conditions: 50 mL solution; 25 ° C; scan rate 50 mV s^{-1}.

To understand the system better, a half-cell reactor was used for detecting the onset potential and the net current density (defined as the difference between the forward-scan anodic current density and the blank current density) for each electrode (the catalyst) in different reactants. For HMF, as shown in Fig.1.12 (A), the lower onset potential on Au/C electrode than Pd/C electrode suggests that Au/C is more favored for the oxidation of the aldehyde functional group into the carboxylic acid functional group than Pd/C. In contrast for the compound of HMFCA, it appears that the bimetallic electrode demonstrated a lower onset potential than the monometallic(Fig.1.12(B)), indicating oxidation of alcohol functional groups requires the cooperation between Au and Pd, demonstrated as a synergistic effect. This result is also consistent to the heterogeneous catalysis described earlier. In terms of the generated net current density, the bimetallic electrodes all showed a higher number than monometallic Au and Pd for both HMF and HMFCA oxidation, which suggests

the turnover number is higher in the alloy, as more electrons were generated. Meanwhile from the result of blank test, cyclic voltammetry (CV) for the prepared alloyed electrode in alkaline condition(Fig. 1.13)[76], it was observed that by increasing the content of Au in the catalyst, Pd displayed a more isolated state, which resulted in Pd_1Au_2/C electrode being more active than the Pd_2Au_1/C (different molar ratios between Au and Pd). This result is also consistent with what has been reported in thermal catalysis of supported Au-Pd catalysts by different molar ratios[77]. Nevertheless, in this paper, the essence of how this interaction takes place between the two metals is still unclear and evidence is lacking.

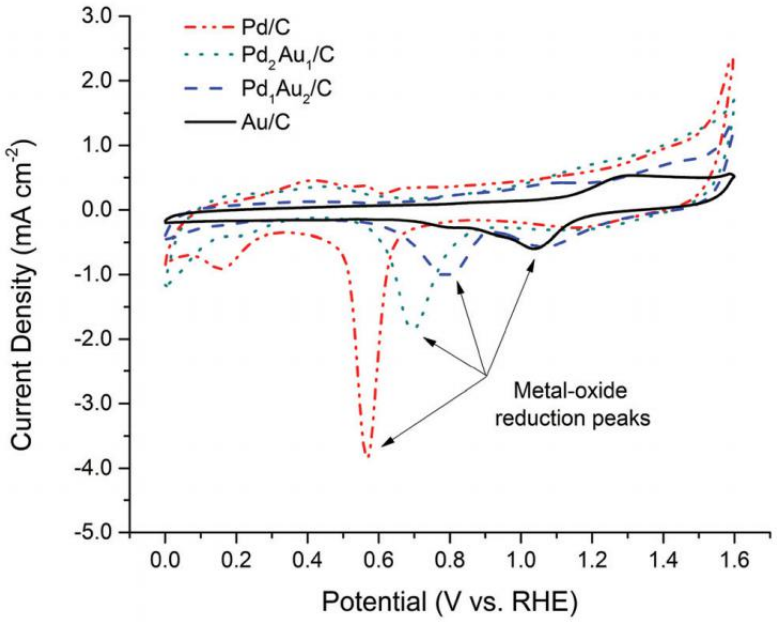

Figure 1.13. CV in 0.1 M KOH for electrochemical determination of the surface metal composition[76]. Reaction conditions: 50 mL electrolyte; 25 °C; 20 μg catalyst loading on the glassy carbon electrode; scan rate 50 mVs^{-1}.

Latsuzbaia and co-workers investigated the same reaction over Au and Pd catalyst too. Similarly, cyclic voltammetry is the same technique that Latsuzbaia used to compare the different performances between Au-Pd alloy and the monometallic Au. From Fig. 1.14, it is shown that the Au-Pd alloy displayed a higher current density in the anodic scan than the monometallic Au, and the data is presented in Table 1.4. The higher current density indicates a higher reaction rate, therefore more HMF molecules are converted at certain potential (for alloy is 0.95 V; for Au is 1.15 V or 1.25 V due to the dual peak). Furthermore, when the potential numbers (at the current density maxima) are compared, the larger number clarifies a required higher driving force for starting the reaction, while the smaller one indicates a lower driving force and thus the reaction occurs more easily[70]. Accordingly, it is concluded the Au-Pd alloy is more reactive than Au, the activity difference is attributed to the synergistic effect in the bimetallic catalyst. However, for a detailed explanation of the interaction among AuPd, more evidence is needed.

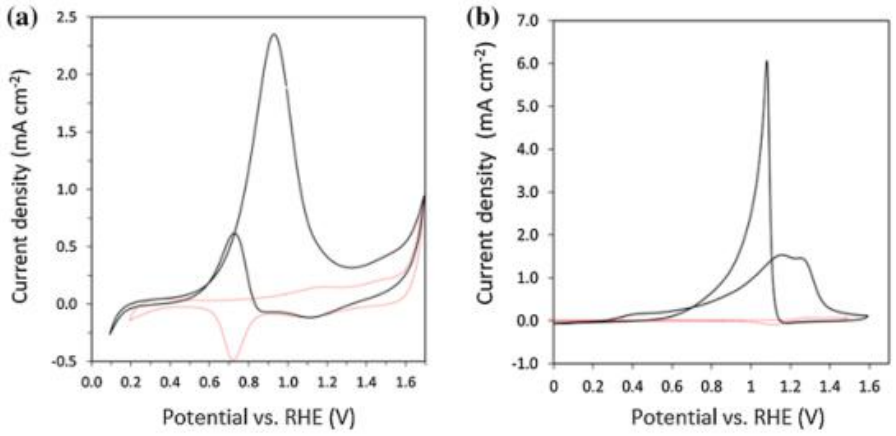

Figure 1.14. Cyclic voltammograms recorded at 50 mV/s for **(a)** Au_3Pd_2 and **(b)** Au electrode materials at pH 13 in 0.1 M NaOH + 0.3 M Na_2SO_4 (blank reaction in red curves) and 0.1 M NaOH + 0.3 M Na_2SO_4 + 50 mM HMF (black curves)[78].

Table 1.4. The net peak current densities of oxidation of 0.05 M HMF in 0.1 M NaOH + 0.3 M Na_2SO_4, pH=13[78].

Electrode	I_{P1}, mA/cm^2	E_{P1}, V	I_{P2}, mA/cm^2	E_{P2}, V	I_{P3}, mA/cm^2	E_{P3}, V
Au	1.52	1.15	1.39	1.25	6.05	1.08
Au_3Pd_2	2.28	0.95	-	-	0.59	0.73

Based on all the above reviewed works, especially for aqueous HMF oxidation using catalyst of Au and Pd either in thermal or electro catalysis, the enhancement of reaction rate is regularly observed when a bimetallic catalyst is applied, indicating an existence of intimate interaction. Various groups have attempted to explain this synergistic effect from different aspects, however this has proved to be very challenging and much remains unexplained. In this thesis, in order to provide a new explanation for the observed interaction in Au and Pd, several catalysts of Au and Pd with different structures, ***e.g.***, monometallics of Au and Pd, Au/C and Pd/C present as a physical mixture, Au-Pd alloy and Au and Pd nanoparticles deposit on a common C particle but spatially separated, have been synthesized. A newly proposed mechanism to illuminate the enhancement effect will be discussed.HMF oxidation is used as a 'model reaction', building on the mechanism proposed by Davis and co-workers[64]. Furthermore, close to the work from Li, several electrochemical experiments are provided as evidence to support the proposed mechanism, where the catalysis trend in electrochemical oxidation is consistent to what is observed in thermal catalysis.

1.5 Summary

Au nanoparticles have demonstrated excellent catalytic properties in numerous oxidation reactions. This catalytic effect is further enhanced by use of a bimetallic catalyst, particularly in the form of AuPd. Previously, synergistic interactions in Au based bimetallic catalysts have been attributed to electronic, structural and isolation effects[79–81]. In many cases, the observed enhancement effect is likely to be a combination of these factors. Works from different research groups have displayed Au with Pd shows one of the best activities in biomass conversion, however when the two metals are presented in a physical mixture less activity is achieved compared to the alloy. Specifically, in HMF oxidation to the value-added product FDCA, a rate enhancement over AuPd bimetallic catalyst is not only observed from thermal catalysis but also from electrocatalysis. However, providing conclusive evidence on the nature of this enhancement effect between Au and Pd is exceptionally challenging and has until now remained elusive.

The aim of this thesis is to elaborate the physicochemical properties of the AuPd nanoparticles with their catalytic performance. Given the current high status of HMF as a platform molecule, the synergistic relationship between physically mixed Au and Pd is studied in catalytic alcohol oxidation. In the work, a comprehensive explanation has been provided for the origin of this effect and its application into the aerobic oxidation of versatile alcohols. It is observed that the rate of a given reaction can be enhanced by improving the mobility of electrons from one metal component to the other suggesting that the enhancement effect in this case is attributable to an redox cooperation between the Au and Pd. Detailed experimental evidence is given and discussed in following *Chapters* 3, 4 and 5. It is suggested that this discovery offers a new and exciting approach for the future catalyst design and has relevance in the fuel cell area (see *Chapter* 6: future plans). A brief summary of each results chapter is given below.

Chapter 3: Preliminary works were performed on the observation of phenomena that

to physically mix the Au/C and Pd/C catalyst would overpass the activity of Au-Pd/C alloy in the aqueous oxidation reaction of HMF, whereas the monometallic catalyst from the physical mixture (PM) were relative poor catalysts for the overall chemical reaction. The used amount of metal and support were same during all the reactions. The phenomena were confirmed to be not the artifact based on running each reaction by Kai Wang (a PhD student from Cardiff University who was not involved in the same project to perform blind tests) for 3 times with calculation of error bars.

Chapter4: Mainly focus on the deviation of reaction mechanism of physical mixture (PM) in HMF oxidation based on the discussed mechanism reviewed in *Section 1.4.2*, Fig. 1.9. Several catalyst characterizations were operated to help understand the mechanism, including Transmission Electron Microscopy (TEM), X-ray photoelectron spectroscopy (XPS), Temperature programmed reduction (TPR) ***et al***. It was found that enhancement effect from Au and Pd PM catalyst was attributed to the cooperative redox cycle of Pd, which efficiently consumes the electrons generated from HMF oxidation on the surface of Au. The electron transfer from Au to Pd takes place in hypothesis during collisions between two carbon granules bearing different metal NPs suspended in an aqueous liquid phase; this could be an electron transfer but might conceivably involve ionic conduction.

Chapter 5: Based on the hypothesized mechanism, a newly designed catalyst named ‘binary mixture’ will be introduced. By depositing the different metal nanoparticles on the same carbon granule, providing the electron transfer from HMF dehydrogenation to the redox cycle of Pd does not become a rate-limiting step, resulting an even faster reaction than the PM. Meanwhile, the same series Au an Pd catalysts, denoted as (Au+Pd)/C as binary mixture; Au/C +Pd/C as physical mixture; Au-Pd/C as alloyed catalyst and rest the monometallic were applied to different reactant molecules where a same activity trend were obtained. Furthermore, electrochemical works on cyclic voltammetry (CV) were carried out, which is analogous to the content in reviewed papers in *Section 1.4.4*, showing both the binary and physical mixture catalysts can

obtain a higher current intensity than the alloyed catalyst, which aligns well to the thermal catalysis trend.

Chapter 6: Conclusions are made in this chapter with what would be the limitation in this study, following on, future works are designed.

1.6 References

1 U. H. Roger A. Sheldon, Isabel Arends, *Green Chemistry and Catalysis*, John Wiley & Sons, 2007.

2 K. Fang, D. Li, M. Lin, M. Xiang, W. Wei and Y. Sun, 2009, **147**, 133–138.

3 E. Com- and J. E. Luecke, 1972, 1–4.

4 M. Conte, A. F. Carley, G. Attard, A. A. Herzing, C. J. Kiely and G. J. Hutchings, 2008, **257**, 190–198.

5 P. Johnston, N. Carthey and G. J. Hutchings, 2015.

6 I. Chorkendorff and J. W. Niemantsverdriet, *Concepts of modern catalysis and kinetics*, John Wiley & Sons, 2017.

7 E. Sacaliuc, A. M. Beale, B. M. Weckhuysen and T. A. Nijhuis, *J. Catal.*, 2007, **248**, 235–248.

8 J. K. Edwards, B. Solsona, E. N. N, A. F. Carley, A. a Herzing, C. J. Kiely and G. J. Hutchings, *Science (80-.).*, 2009, **323**, 1037–1041.

9 J. Edwards, A. Carley, C. J. Kiely, A. Herzing and G. Hutchings, *Science (80-.).*, 2015, **351**, 6276.

10 A. S. K. Hashmi and G. J. Hutchings, *Angew. Chemie - Int. Ed.*, 2006, **45**, 7896–7936.

11 A. Venugopal and M. S. Scurrell, *Appl. Catal. A Gen.*, 2004, **258**, 241–249.

12 W. C. Ketchie, M. Murayama and R. J. Davis, *J. Catal.*, 2007, **250**, 264–273.

13 J. Long, H. Liu, S. Wu, S. Liao and Y. Li, *ACS Catal.*, 2013, **3**, 647–654.

14 N. Dimitratos, F. Porta, L. Prati and A. Villa, *Catal. Letters*, 2005, **99**, 181–185.

15 F. Moreau, G. C. Bond and A. O. Taylor, *J. Catal.*, 2005, **231**, 105–114.

16 F. Magnetism and S. Chemistry, 2015, **350**, 173–175.

17 J. K. Edwards, B. Solsona, P. Landon, A. F. Carley, A. Herzing, M. Watanabe, C. J. Kiely and G. J. Hutchings, *J. Mater. Chem.*, 2005, **15**, 4595–4600.

18 J. Pritchard, L. Kesavan, M. Piccinini, Q. He, R. Tiruvalam, N. Dimitratos, J. A. Lopez-Sanchez, A. F. Carley, J. K. Edwards, C. J. Kiely and G. J. Hutchings, *Langmuir*, 2010, **26**, 16568–16577.

19 H. Daly, A. Goguet, C. Hardacre, F. C. Meunier, R. Pilasombat and D. Thompsett, *J. Catal.*, 2010, **273**, 257–265.

20 A. Amieiro Fonseca, J. M. Fisher, D. Ozkaya, M. D. Shannon and D. Thompsett, *Top. Catal.*, 2007, **44**, 223–235.

21 Q. Chen, S. Tanaka, T. Fujita, L. Chen, T. Minato, Y. Ishikawa, M. Chen, N. Asao, Y. Yamamoto and T. Jin, *Chem. Commun.*, 2014, **50**, 3344–3346.

22 F. Gómez-Villarraga, J. Radnik, A. Martin and A. Köckritz, *J. Nanoparticle Res.*, , DOI:10.1007/s11051-016-3453-7.

23 J. Sha, S. Paul, F. Dumeignil and R. Wojcieszak, *RSC Adv.*, 2019, **9**, 29888–29901.

24 J. Li, Y. Xu, S. Wang and H. Zhang, *J. Phys. Chem. C*, 2019, **123**, 15483–15494.

25 D. Wang, A. Villa, P. Spontoni, D. S. Su and L. Prati, *Chem. - A Eur. J.*, 2010, **16**, 10007–10013.

26 L. A. Calzada, S. E. Collins, C. W. Han, V. Ortalan and R. Zanella, *Appl. Catal. B Environ.*, 2017, **207**, 79–92.

27 W. Li, A. Wang, X. Liu and T. Zhang, *Appl. Catal. A Gen.*, 2012, **433**–**434**, 146–151.

28 X. F. Chen, S. H. Liu, X. Z. You, H. K. Fun, K. Chinnakali and I. A. Razak, *Acta Crystallogr. Sect. C Cryst. Struct. Commun.*, 1999, **55**, 22–24.

29 T. Déronzier, F. Morfin, M. Lomello and J. L. Rousset, *J. Catal.*, 2014, **311**, 221–229.

30 A. Villa, D. Wang, D. S. Su and L. Prati, *Catal. Sci. Technol.*, 2015, **5**, 55–68.

31 A. Villa, D. Wang, D. S. Su and L. Prati, *Catal. Sci. Technol.*, 2015, **5**, 55–68.

32 A. Sandoval, A. Aguilar, C. Louis, A. Traverse and R. Zanella, *J. Catal.*, 2011, **281**, 40–49.

33 J. H. Liu, A. Q. Wang, Y. S. Chi, H. P. Lin and C. Y. Mou, *J. Phys. Chem. B*, 2005, **109**, 40–43.

34 W. Zhan, J. Wang, H. Wang, J. Zhang, X. Liu, P. Zhang, M. Chi, Y. Guo, Y. Guo, G. Lu, S. Sun, S. Dai and H. Zhu, *J. Am. Chem. Soc.*, 2017, **139**, 8846–8854.

35 C. Della Pina and E. Falletta, *Catal. Sci. Technol.*, 2011, **1**, 1564–1571.

36 A. K. Singh and Q. Xu, *ChemCatChem*, 2013, **5**, 652–676.

37 I. Notar Francesco, F. Fontaine-Vive and S. Antoniotti, *ChemCatChem*, 2014, **6**, 2784–2791.

38 Y. Guan and E. J. M. Hensen, *J. Catal.*, 2013, **305**, 135–145.

39 H. Tsunoyama, N. Ichikuni, H. Sakurai and T. Tsukuda, *J. Am. Chem. Soc.*, 2009, **131**, 7086–7093.

40 F. Wang, W. Ueda and J. Xu, *Angew. Chemie - Int. Ed.*, 2012, **51**, 3883–3887.

41 P. Liu, V. Degirmenci and E. J. M. Hensen, *J. Catal.*, 2014, **313**, 80–91.

42 M. Stöcker, *Angew. Chemie - Int. Ed.*, 2008, **47**, 9200–9211.

43 S. Ur-Rehman, Z. Mushtaq, T. Zahoor, A. Jamil and M. A. Murtaza, *Crit. Rev. Food Sci. Nutr.*, 2015, **55**, 1514–1528.

44 M. Hara, K. Nakajima and K. Kamata, *Sci. Technol. Adv. Mater.*, , DOI:10.1088/1468-6996/16/3/034903.

45 N. Dimitratos, J. A. Lopez-Sanchez, D. Morgan, A. F. Carley, R. Tiruvalam, C. J. Kiely, D. Bethell and G. J. Hutchings, *Phys. Chem. Chem. Phys.*, 2009, **11**, 5142–5153.

46 F. Gao and D. W. Goodman, *Chem. Soc. Rev.*, 2012, **41**, 8009–8020.

47 Y. Zhu and M. Lu, *RSC Adv.*, 2015, **5**, 85579–85585.

48 Z. Gao, R. Xie, G. Fan, L. Yang and F. Li, *ACS Sustain. Chem. Eng.*, 2017, **5**, 5852–5861.

49 M. Douthwaite, X. Huang, S. Iqbal, P. J. Miedziak, G. L. Brett, S. A. Kondrat, J. K. Edwards, M. Sankar, D. W. Knight, D. Bethell and G. J. Hutchings, *Catal. Sci. Technol.*, 2017, **7**, 5284–5293.

50 D. Wang, A. Villa, P. Spontoni, D. S. Su and L. Prati, *Chem. - A Eur. J.*, 2010, **16**, 10007–10013.

51 Dimitratos, A. Villa, D. Wang, F. Porta, D. Su and L. Prati, *J. Catal.*, 2006, **244**, 113–121.

52 C. A. Antonyraj, N. T. T. Huynh, S. K. Park, S. Shin, Y. J. Kim, S. Kim, K. Y. Lee and J. K. Cho, *Appl. Catal. A Gen.*, 2017, **547**, 230–236.

53 L. Prati, P. Spontoni and A. Gaiassi, *Top. Catal.*, 2009, **52**, 288–296.

54 A. Villa, N. Dimitratos, C. E. Chan-Thaw, C. Hammond, L. Prati and G. J. Hutchings, *Acc. Chem. Res.*, 2015, **48**, 1403–1412.

55 J. B. Xu, T. S. Zhao, Y. S. Li and W. W. Yang, *Int. J. Hydrogen Energy*, 2010, **35**, 9693–9700.

56 S. E. Davis, B. N. Zope and R. J. Davis, *Green Chem.*, 2012, **14**, 143–147.

57 R. Paul, V. Etacheri, Y. Wang and C.-T. Lin, *Carbon Based Nanomaterials for Advanced Thermal and Electrochemical Energy Storage and Conversion*, Elsevier, 2019.

58 J. Long, H. Liu, S. Wu, S. Liao and Y. Li, *ACS Catal.*, 2013, **3**, 647–654.

59 T. A. Werpy, J. E. Holladay and J. F. White, , DOI:10.2172/926125.

60 S. E. Davis, L. R. Houk, E. C. Tamargo, A. K. Datye and R. J. Davis, *Catal. Today*, 2011, **160**, 55–60.

61 S. Hameed, L. Lin, A. Wang and W. Luo, *Catalysts*, 2020, **10**, 120.

62 M. S. Ide and R. J. Davis, *Acc. Chem. Res.*, 2014, **47**, 825–833.

63 Z. Bhushan N., H. David D., N. Matthew and D. Robert J., *Science (80-.).*, 2010, **330**, 74–78.

64 S. E. Davis, B. N. Zope and R. J. Davis, *Green Chem.*, 2012, **14**, 143–147.

65 A. Lolli, S. Albonetti, L. Utili, R. Amadori, F. Ospitali, C. Lucarelli and F. Cavani, *Appl. Catal. A Gen.*, 2015, **504**, 408–419.

66 J. Yang, Y. Guan, T. Verhoeven, R. Van Santen, C. Li and E. J. M. Hensen, *Green Chem.*, 2009, **11**, 322–325.

67 J. Fu, Q. He, P. J. Miedziak, G. L. Brett, X. Huang, S. Pattisson, M. Douthwaite and G. J. Hutchings, *Chem. - A Eur. J.*, 2018, **24**, 2396–2402.

68 Q. Wang, W. Hou, S. Li, J. Xie, J. Li, Y. Zhou and J. Wang, *Green Chem.*, 2017, **19**, 3820–3830.

69 X. Wan, C. Zhou, J. Chen, W. Deng, Q. Zhang, Y. Yang and Y. Wang, *ACS Catal.*, 2014, **4**, 2175–2185.

70 R. (Rudolf) Holze, *Experimental electrochemistry : a laboratory textbook*, Wiley-VCH, Weinheim, 2009.

71 R. Latsuzbaia, R. Bisselink, A. Anastasopol, H. van der Meer, R. van Heck, M. S. Yagüe, M. Zijlstra, M. Roelands, M. Crockatt, E. Goetheer and E. Giling, *J. Appl. Electrochem.*, 2018, **48**, 611–626.

72 H. G. Cha and K. S. Choi, *Nat. Chem.*, 2015, **7**, 328–333.

73 B. A. Frontana-Uribe, R. D. Little, J. G. Ibanez, A. Palma and R. Vasquez-Medrano, *Green Chem.*, 2010, **12**, 2099–2119.

74 N. Zhang, Y. Zou, L. Tao, W. Chen, L. Zhou, Z. Liu, B. Zhou, G. Huang, H. Lin and S. Wang, *Angew. Chemie - Int. Ed.*, 2019, **58**, 15895–15903.

75 W. J. Liu, L. Dang, Z. Xu, H. Q. Yu, S. Jin and G. W. Huber, *ACS Catal.*, 2018, **8**, 5533–5541.

76 D. J. Chadderdon, L. Xin, J. Qi, Y. Qiu, P. Krishna, K. L. More and W. Li, *Green Chem.*, 2014, **16**, 3778–3786.

77 A. Villa, M. Schiavoni, S. Campisi, G. M. Veith and L. Prati, *ChemSusChem*, 2013, **6**, 609–612.

78 R. Latsuzbaia, R. Bisselink, A. Anastasopol, H. van der Meer, R. van Heck, M. S. Yagüe, M. Zijlstra, M. Roelands, M. Crockatt, E. Goetheer and E. Giling, *J.*

Appl. Electrochem., 2018, **48**, 611–626.

79 G. J. Hutchings and C. J. Kiely, *Acc. Chem. Res.*, 2013, **46**, 1759–1772.

80 A. Wang, X. Y. Liu, C. Y. Mou and T. Zhang, *J. Catal.*, 2013, **308**, 258–271.

81 D. Wang, A. Villa, F. Porta, L. Prati and D. Su, *J. Phys. Chem. C*, 2008, **112**, 8617–8622.

Experimental

2

Introduction

In this chapter, details of catalysts preparation; catalysts testing procedures and reaction conditions for different alcohol oxidation are described. Meanwhile, product analysis and quantification using high performance liquid chromatography (HPLC) and several catalyst characterization techniques are introduced.

2.1 Reagents and materials

The following chemicals and materials have been used for the purposes of catalyst preparation, catalytic testing and data analysis:

$PdCl_2$ (Johnson Matthey);

$HAuCl_4 \cdot H_2O$ (Strem Chemicals);

Poly (vinylalcohol) (PVA) (M_w = 9,000-10,000, 99 %, hydrolyzed, Sigma Aldrich);

Nafion (Sigma Aldrich, 5 wt. % in lower aliphatic alcohols and water);

Potassium chloride solution (Sigma Aldrich, ~ 3 M KCl);

$NaBH_4$ (Sigma Aldrich);

Carbon black Vulcan XC-72R (CABOT);

TiO_2 (P25 Aeroxide®, Evonik);

BN (Sigma Aldrich, powder, ~1 μm, 98 %);

HMF (5-hydroxymethylfurfural (Sigma Aldrich, > 99 %));

HMFCA (hydroxymethylfurancarboxylic acid (Carbosynth, > 97 %));

FDCA (2,5-furandicarboxylic acid (Sigma Aldrich, 97 %));

FFCA (5-Formyl-2-furoic- Acid (Tokyo Chemical Industry, > 98 %));

$NaHCO_3$ (Fisher Scientific, 99.5% for analysis);

Na_2CO_3 (Fisher Scientific, 99+ %);

NaOH (Fisher Scientific, >98.5 % for analysis);

Molecular O_2 (BOC. > 99.95%);

Distilled water millipore (18.2 MΩ.cm at 25°C);

Glycerol (Sigma Aldrich, > 99.5 %);

Ethanol (Fisher Scientific, > 99 %);

Acetic acid (Sigma Aldrich, > 99.7 %).

Glassy carbon electrode (Inner diameter 3 mm, ALS, the electrochemical company);

SCE (Saturated Calomel Electrode, ALS, the electrochemical company);

Flow meter (Cole-Parmer, 0-200 mL/min);

Potentiostat (Biologic);

Digital multimeter.

2.2 Catalyst preparation

The catalysts have all been synthesized by sol-immobilization, and protocols are comparable to the method from other papers published from Hutchings group[1–3].

2.2.1 Monometallic Au and Pd catalysts preparation

Monometallic catalyst of Au/C with target weight loading of 1.75 wt.% and Pd/C with target weight loading of 0.25 wt.% were separately made following the steps described below. The preparation procedures are shown in Fig. 2.1.

(1) Aqueous solutions of the metal precursors, $PdCl_2$ (120 μL, 10 mg/mL) or $HAuCl_4.3H_2O$ (727 μL, 12.25 mg/mL) were added to H_2O (140 mL).

(2) PVA solution (10 mg/mL) is freshly prepared and added to the solution formed in step (1) with a mass ratio of PVA/metal =1/1 (0.89 mL for Au; 0.12 mL for Pd).

(3) A freshly prepared 0.15 M $NaBH_4$ solution (1.2 mL for Au; 0.3 mL for Pd) was added into the separate precursor solution with a mole ratio of $NaBH_4$/metal =4/1, which immediately formed reddish or brownish colloidal solutions containing the colloidal Au and Pd nanoparticles, respectively.

(4) The carbon support (0.5 g) was added to the colloidal solution with stirring facilitating the immobilization of the metal nanoparticles.

(5) After 30 min, the solid catalyst was recovered by filtration and washed repeatedly with distilled water (500 mL) to remove Na^+, BH_4^- and BO_2^-. The amount of adsorbed Au or Pd were determined by MP-AES analysis of the residue metal in the mother liquid, where no Au and Pd were detected indicating all the Au or Pd are immobilized onto the C[4].

(6) Finally, the catalysts were dried at 110 °C for 16 h under static air.

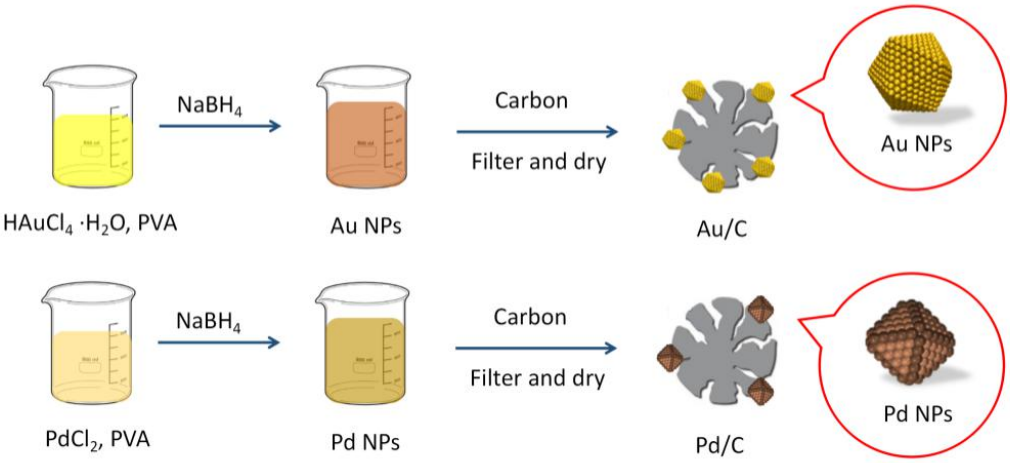

Figure 2.1. Diagrammatic representation of the sol-immobilization method used for preparing the monometallic Au/C and Pd/C catalysts.

2.2.2 Au-Pd alloy catalyst preparation

For the preparation of a 1.0 wt.% (1.0 g) alloyed catalyst (designated as Au-Pd/C), during the first step described above, the metal precursors are introduced simultaneously in the same solution, with a metal molar ratio of Au/Pd = 4/1. Steps (2) to (6) were then carried out in an identical fashion to that of the monometallic catalyst,

except that the amount of carbon added was 1.0 g, see Fig. 2.2.

(1) Aqueous solutions of the metal precursors, $PdCl_2$ (120 μL, 10 mg/mL) and $HAuCl_4.3H_2O$ (727 μL, 12.25 mg/mL) were added to H_2O (140 mL) simultaneously.

(2) PVA solution (10 mg/mL, 1.01 mL) is freshly prepared and added to the solution formed in step (1) with a mass ratio of PVA/metal =1/1.

(3) A freshly prepared $NaBH_4$ solution (1.5 mL 0.15 M) was added into the mixed precursor solution with a mole ratio of $NaBH_4$/metal =4/1, which immediately formed brownish colloidal solutions containing the colloidal Au-Pd nanoparticles.

(4) The carbon support (1.0 g) was added to the colloidal solution with stirring facilitating the immobilization of the alloyed nanoparticles.

(5) After 30 min, the solid catalyst was recovered by filtration and washed repeatedly with distilled water (500 mL) to remove Na^+, BH_4^- and BO_2^-. The amount of adsorbed Au and Pd were determined by MP-AES analysis of the residue metal in the mother liquid, where no Au and Pd were detected indicating all the Au and Pd are immobilized onto the C[4].

(6) Finally, the catalysts were dried at 110 °C for 16 h under static air.

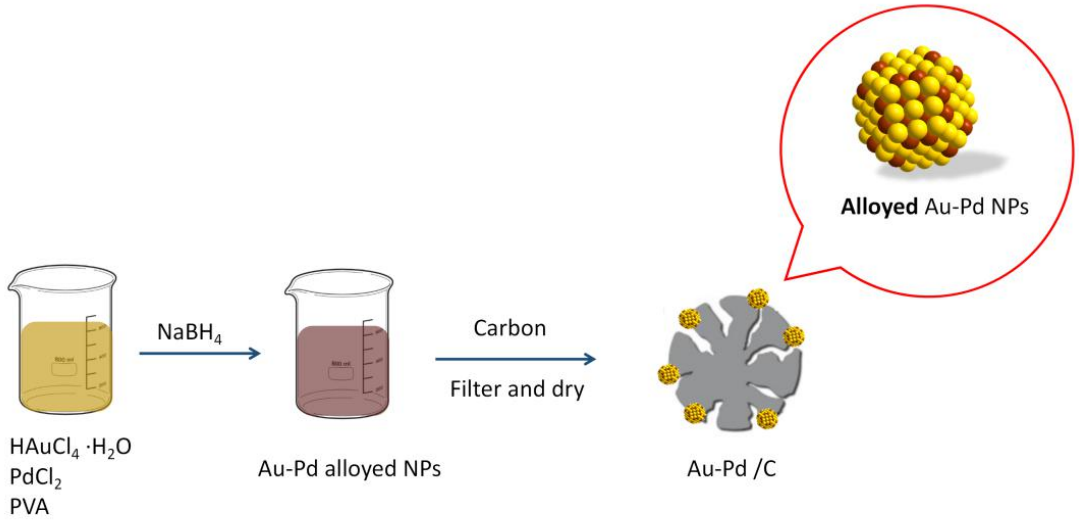

Figure 2.2. Diagrammatic representation of the sol-immobilization method used for preparing the bimetallic Au-Pd/C alloy catalyst.

2.2.3 (Au + Pd)/C binary mixture catalyst preparation

A binary mixture, designated as (Au + Pd)/C with target weight loading of 1.0 wt.%, of Au and Pd colloids have been prepared and immobilized on the carbon support to allow a close proximity between discrete gold and palladium nanoparticles on the same support grains, see Fig. 2.3. The synthesis method employed was as follows:

(1) The Au and Pd colloids were prepared separately following the steps described for the monometallic catalysts (steps 1 to 3).

(2) The prepared colloids were then combined, rapidly followed by the addition of the carbon support (1.0 g) with stirring.

The resulting mixture was aged for 30 min under stirring before filtration and washing with distilled water (500 mL) to remove Na^+, BH_4^- and BO_2^-. The amount of adsorbed Au and Pd were determined by MP-AES analysis of the residue

metal in the mother liquid, where no Au and Pd were detected, indicating all the Au and Pd are immobilized onto the C[4].

(3) The catalyst was then dried at 110 °C for 16 h under static air.

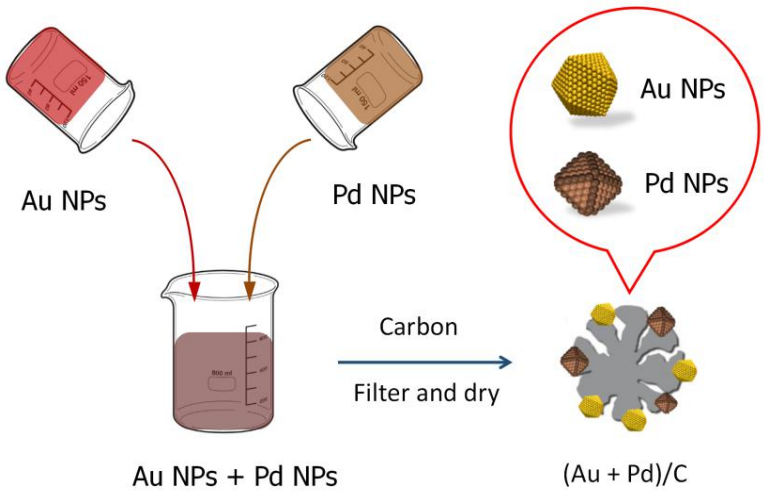

Figure 2.3. Diagrammatic representation of the sol-immobilization method used for preparing the binary mixture (Au + Pd)/C catalysts.

2.2.4 (Au + Pd)/C preparation with colloid aged for different time

For the investigation of the effect of aging time on the binary catalyst, a procedure close to *Section 2.2.3* was followed, except for the step (2). After the combination of the two prepared Au and Pd colloid, this mixed colloid was aged under vigorous stirring for a certain time, *e.g.*, 2 h, 4 h and 6 h before the addition of 1.0 g C support.

In addition, another (Au + Pd)/C was prepared through Au and Pd colloid aged in two containers separately, see Fig. 2.4. Afterward, the two colloids are combined into one common beaker with 1.0 g C support rapidly added. The rest follows the same recipe to *Section 2.2.3* as well.

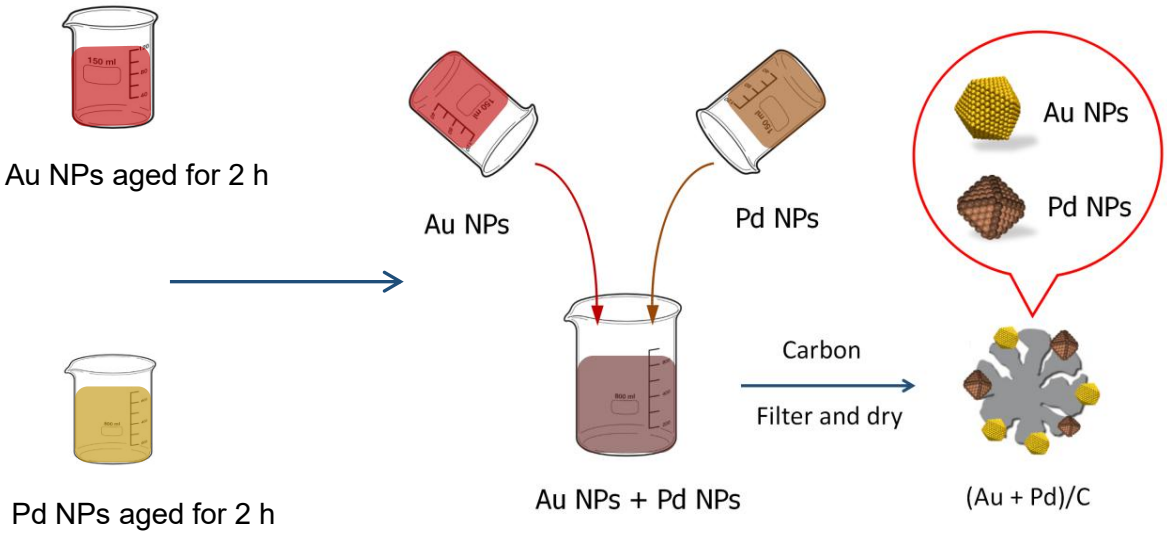

Figure 2.4. Diagrammatic representation of the sol-immobilization method used for preparing the (Au + Pd)/C catalyst with Au and Pd colloid aged for 2 h before mixing.

2.2.5 Catalysts preparation with different mole ratios

Monometallic Au and Pd nanoparticles supported on C were made with different metal loading following generally the same recipe as described in *Section 2.2.1*. Table. 2.1 lists the weight numbers. For the catalyst of physical mixture (PM), its total metal loading is calculated based on an average number of the two counterpart monometallic catalysts, see Table. 2.2.

Table 2.1. Prepared monometallic Au and Pd catalysts with different metal loading.

Entry	Au (mg)	Au metal loading (wt.%)	Pd (mg)	Pd metal loading (wt.%)
1	9.44	1.85	0.57	0.11
2	8.90	1.75	1.20	0.24
3	7.87	1.55	2.13	0.42
4	6.49	1.28	3.51	0.70
5	4.81	0.95	5.19	1.03
6	3.16	0.63	6.84	1.35
7	1.71	0.34	8.29	1.63

Table 2.2. Prepared monometallic Au and Pd catalysts and their physical mixtures (PM).

Entry	Mole ratio of Au/Pd (mol/mol)	Au/C, metal loading (wt.%)	Pd/C, metal loading (wt.%)	Total metal loading in PM (wt.%)
1	9-1	1.85	0.11	(1.85+0.11)/2 ≈ 1.0
2	4-1	1.75	0.24	(1.75+0.24)/2 ≈ 1.0
3	2-1	1.55	0.42	(1.55+0.42)/2 ≈ 1.0
4	1-1	1.28	0.70	(1.28+0.70)/2 ≈ 1.0
5	1-2	0.95	1.03	(0.95+1.03)/2 ≈ 1.0
6	1-4	0.63	1.35	(0.63+1.35)/2 ≈ 1.0
7	1-9	0.34	1.63	(0.34+1.63)/2 ≈ 1.0

2.2.6 Catalysts preparation with Polyvinylpyrrolidone (PVP) ligand and other supports

For the investigation on the effect of ligand and other supports, the same series of monometallic and bimetallic catalysts are prepared in a similar way with replacement of PVA by PVP, and replacement of C by TiO_2 or BN.

2.3 Catalyst testing

2.3.1 Protocol for testing catalysts in HMF oxidation reaction

The HMF oxidation test reaction was carried out in a glass colaver reactor (50 mL, Fig. 2.5). In a typical reaction, 0.2 M HMF (8 mL) was mixed with 0.8 M $NaHCO_3$ (8 mL) in an aqueous solution with an initial pH of 8.7. The reaction mixture was heated to

80 °C with a typical stirring speed of 1000 rpm until the required temperature was reached. Then the catalyst was added to the mixture to start the reaction (HMF/metal = 200/1, mol/mol) for 2 h. The reaction was conducted under 1000 rpm and an atmosphere of 3 bar O_2. Molecular oxygen was continually fed in a semi - batch manner to maintain a constant head pressure in the reactor. The sampled liquid was diluted in distilled water by 30-fold and filtered by syringe filter to remove any catalysts in the solution sample before injecting into HPLC. Furthermore, in order to get error bars, the same reaction was repeated for 3 times by a PhD student who was originally not involved in the project (also the catalyst was made by the student following the recipe provided in Chapter 2.2.1-2.2.3), the raw data are listed in appendix, see Table S6 - S10.

A high-performance liquid chromatography (Agilent Technologies 1200 series, Fig. 2.6) equipped with a diode array detector was used to analyse the products. A Hi-Plex H (300 x 7.7 mm) column was used to separate the products with 5 mM aqueous H_2SO_4 solution as the mobile phase, at a flow rate of 0.7 mL/min. The conversion of HMF and the yield of each product were obtained directly using calibration curves of known concentrations, see Fig. S1 in appendix.

Calculations for substrate conversion, product selectivity and yield, carbon balance.

1. HMF conversion (%) = (moles of HMF before reaction – moles of HMF after reaction)/ moles of HMF before reaction x 100 %.

2. Product selectivity (%) = moles of product after reaction / moles of total products after reaction x 100%.

3. Product yield (%) = HMF conversion x product selectivity / 100 %

4. Carbon balance (%) = total moles of carbon in products after reaction / (total moles of carbon in HMF before reaction – total moles of carbon in HMF after reaction) x 100 %.

Figure 2.5. 50 mL colaver glass reactor, used in aqueous HMF, glycerol and ethanol oxidation.

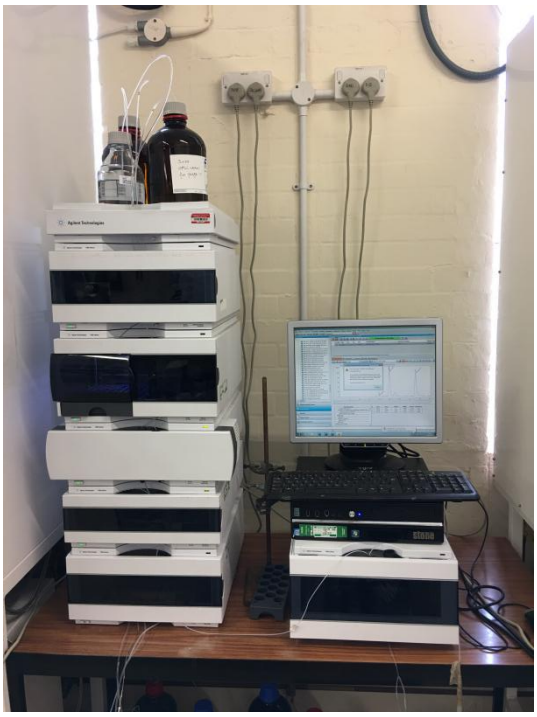

Figure 2.6. High performance liquid chromatography (HPLC) system, for analyzing conversion and products selectivity in HMF, glycerol and ethanol oxidation.

2.3.2 Protocol for testing catalysts in glycerol oxidation reaction

Glycerol oxidation was performed following a similar method as described for HMF oxidation. 1.2 M glycerol (8 mL) was mixed with 2.4 M Na_2CO_3 (8 mL) in an aqueous solution with an initial pH of 12.0. The reaction mixture was heated to 60 °C with a typical stirring speed of 1000 rpm until the required temperature was reached. The catalyst was then added to the mixture to start the reaction (glycerol/metal = 1200/1, mol/mol) for 2 h. The reaction was conducted under an atmosphere of 3 bar O_2. Molecular oxygen was continually fed in a semi - batch manner to maintain a constant head pressure in the reactor. The sampled liquid was diluted in distilled water by 30-fold and filtered by syringe filter to remove the catalysts before injecting into HPLC.

An Agilent HPLC (Agilent Technologies 1200 series) equipped with a diode array detector and refractive index detector was used to analyse the products. A MetaCarb 67H column was used to separate the products with 0.01 M aqueous H_3PO_4 solution as a mobile phase, at a flow rate of 0.8 mL/min. The conversion of glycerol and the yield of each product were obtained directly using calibration curves of known concentrations, see Fig. S2 in appendix.

Calculations for substrate conversion, product selectivity and yield, carbon balance.

1. Glycerol conversion (%) = (moles of glycerol before reaction – moles of glycerol after reaction)/ moles of glycerol before reaction x 100 %.

2. Product selectivity (%) = moles of product after reaction / moles of total products after reaction x 100%.

3. Product yield (%) = glycerol conversion x product selectivity / 100 %

4. Carbon balance (%) = total moles of carbon in products after reaction / (total moles of carbon in glycerol before reaction – total moles of carbon in glycerol after reaction) x 100 %.

2.3.3 Protocol for testing catalysts in ethanol oxidation reaction

Ethanol oxidation was performed following a similar method as described for both HMF and glycerol oxidation except that the catalyst was added to the reaction solution before the reactor was submerged inside the oil bath at 60°C. The reaction proceeded under a typical stirring speed of 1000 rpm, 3 bar O_2, ethanol/metal = 1600/1, mol / mol for 2 h. Molecular oxygen was continually fed in a semi - batch manner to maintain a constant head pressure in the reactor. The reaction was cooled down in ice after 2 h for 15 min. The sampled liquid was diluted in distilled water by 30 folders and filtered by syringe filter to remove the catalysts before injecting into HPLC.

An Agilent HPLC (Agilent Technologies 1200 series) equipped with a diode array detector and refractive index detector was used to analyse the products. A Metacarb 67H column was used to separate the products with 0.01 M aqueous H_3PO_4 solution as a mobile phase, at a flow rate of 0.5 mL/min. The conversion of ethanol and the yield of acetic acid were obtained directly using calibration curves of known concentrations, see Fig. S3 in appendix. However, it is known that acetaldehyde has a low boiling point (around 20.2 °C), therefore there are difficulties associated with determination of the exact yield of the acetaldehyde. Analysis *via* HPLC, conducted at temperature in excess of 20 °C, can lead to loss of the analyte due to evaporation.

<u>Calculations for substrate conversion, product selectivity and yield, carbon balance.</u>

1. Ethanol conversion (%) = (moles of ethanol before reaction – moles of ethanol after reaction)/ moles of ethanol before reaction x 100 %.

2. Product selectivity (%) = moles of product after reaction / moles of total products after reaction x 100%.

3. Product yield (%) = conversion x product selectivity / 100 %

4. Carbon balance (%) = total moles of carbon in products after reaction / (total moles of carbon in ethanol before reaction – total moles of carbon in ethanol after reaction) x 100 %.

2.3.4 Protocol for testing catalysts in cyclic voltammetry (CV)

Theory

To measure the potential of the working electrode, a reference electrode is used which is to maintain a constant potential, and the resulting applied potential produces an excitation signal as is shown in Fig. 2.7[5]. In the forward scan, the potential is negative first, then starts from a greater potential a and ends at a lower potential d. The potential extrema d is regarded as the switching potential where the voltage is sufficient enough to make either an oxidation or reduction of an analyte. Besides, the reverse scan occurs from d to g, where the potential scans positively. Overall in Fig. 2.7, it displays a typical reduction occurring from a to d and an oxidation occurring from d to g. It is also noted that some analytes can undergo oxidation first. Such cycle can be repeated with a varied scan rate. The slope of the excitation signal represents the used scan rate.

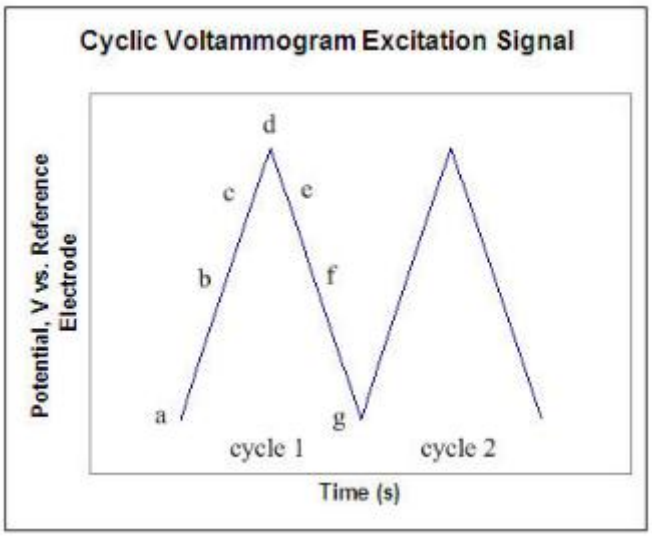

Figure 2.7. Cyclic voltammetry excitation signal.

Cyclic voltammogram is obtained through measuring the current at the working electrode during the potential scans[5]. In Fig. 2.8 below, it shows a cyclic voltammogram from reduction and oxidation of a single electron. See equation (1) below:

$$M^+ + e^- \rightleftharpoons M \qquad \text{eq. (1)}$$

As is shown in Fig. 2.8, the reduction process starts from a (the initial potential) to d (the switching potential). In this process, the potential is scanning negatively to cause a reduction reaction. Therefore the resulting current is called cathodic current (ipc), the corresponding peak potential occurs at region of c is called the cathodic peak potential Epc. The Epc is reached till all the substrates on the electrode surface have been reduced. After reaching the switching potential, *e.g.*, d, the potential will scan positively from d to g. This leads to an anodic current (Ipa) and an oxidation reaction to occur. Accordingly, the peak potential at f is called the anodic peak potential (Epa), and can be reached when all the substrates on electrode surface have been oxidized.

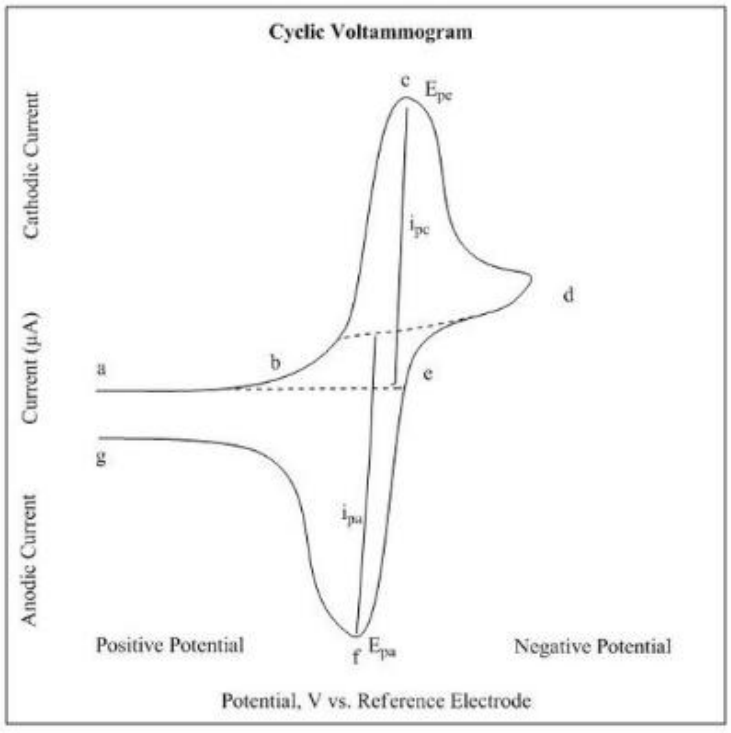

Figure 2.8. Voltammogram of a single electron oxidation-reduction reaction.

Experiment

To prepare the working electrode, a catalyst ink was made by adding 7 mg of the monometallic or 14 mg of the bimetallic catalysts into 1 mL DI H_2O mixed with 100 µL nafion solution, followed by sonification for 150 s. Afterward, the ink (20 µL) was dropped onto the surface of the glassy carbon electrode and dried overnight. See Fig. 2.9 below.

Figure 2.9. The prepared electrode of Au/C or Pd/C on glassy carbon electrode.

Cyclic voltammetry (CV) was performed with potentiostat (Biologic) under an inert environment with N_2 pre bubbled in the solution for 20 min. Pt wire was used as the counter electrode with a saturated calomel electrode working as the reference electrode, see Fig. 2.10. The working electrode was firstly reduced at a fixed negative potential (-1.0 V) for 10 s in order to clean the surface. CV was then recorded for 3 loops as a background. Afterward, HMF solution was added into the background solution with another CV recorded for 3 loops. All the experiments were conducted at a scan rate of 50 mV/s under room temperature and vigorous stirring.

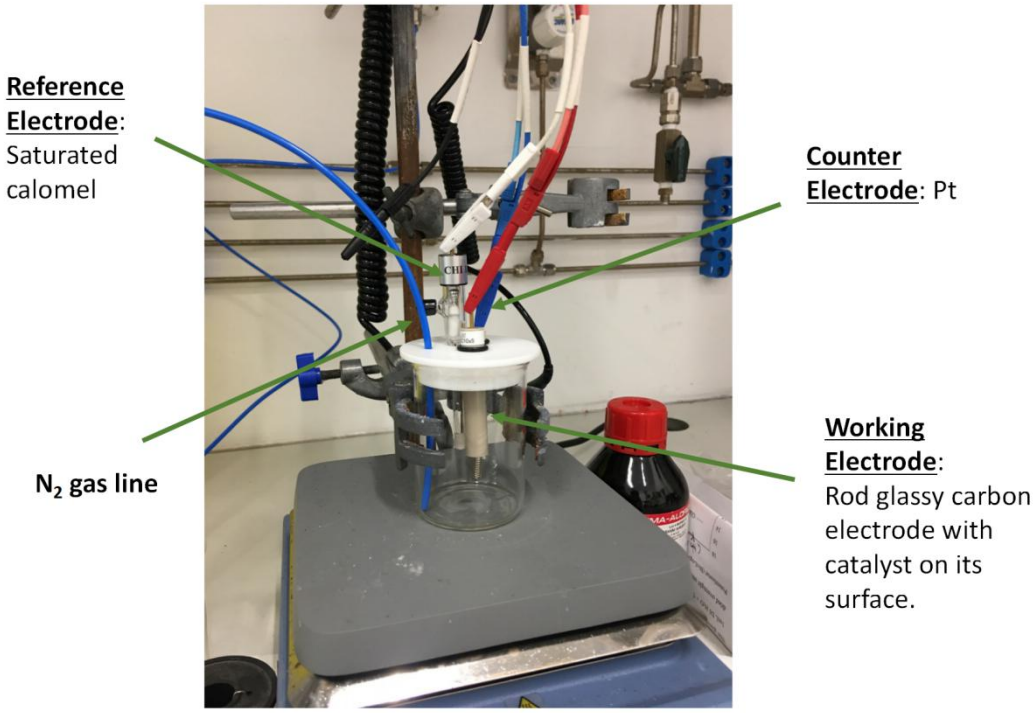

Figure 2.10. The setup for experimental work on cyclic voltammetry.

2.4 Characterization techniques

2.4.1 Scanning Transmission Electron Microscopy (STEM)

Theory

Electron microscopes is one of the most important techniques in catalysis as it can observe the catalyst surface. Therefore, it is fine to determine the size distribution and morphologies of supported particles. In transmission electron microscopy (TEM), an electron beam between 100-400 KeV is directed on the material, for the transmitted electrons will form a 2D image of the catalyst surface which is magnified to generate a bright field image, while the electrons which are diffracted by the sample particles will generate a dark field image.

For scanning electron microscopy (SEM), a narrow beam of electrons are rastered

over the catalyst surface. Part of the surface electrons are displaced by the electron beam, which are recognized as secondary electrons and contains lower energy, these are detected for providing the images of catalyst surface. Some of the incident electrons can be backscattered through atomic nuclei and give information of the elemental composition of the material, since the amount of scattering relies on atomic weight.

Scanning transmission electron microscopy (STEM) combines both techniques as mentioned above. Besides, elemental analysis is commonly affiliated with STEM due to the emission of X-rays from the material when it is bombarded with electron beam. These X-rays are analyzed by energy dispersive analysis of X-rays, namely EDX.

Experiment

In this work, samples for examination by scanning transmission electron microscopy (STEM) were prepared by dry dispersing the catalyst powder onto a holey carbon film supported by a 300 - mesh copper TEM grid. Bright field (BF) and high angle annular dark field (HAADF) STEM images were taken using aberration corrected JEOL JEM ARM-200CF microscopes operating at 200 kV. The microscope in Lehigh University (USA) was also equipped with a JEOL Centurio silicon drift detector for X-ray energy dispersive spectroscopy (XEDS). One sample was analyzed in the JEM ARM - 200CF microscope equipped with dual Centurio silicon drift XEDS detectors in the in ePSiC facility at the Diamond Light Source (UK). Particle size distribution histograms were generated by analysis of representative HAADF electron micrographs using Image J.

The STEM were performed and analyzed in Lehigh University, US, with contributions from Professor Christopher J. Kiely and Dr. Sultan M. Althahban and Dr. Qian He.

2.4.2 X-ray photoelectron spectroscopy (XPS)

Theory

XPS is a important and commonly used characterization technique in the field of catalysis for the determination of elemental composition of catalyst surface and furthermore the oxidation state of the elements found. Because of the short mean free path of electrons with kinetic energies between 15 and 1000 eV, XPS can just be used to probe a short distance into the surface (less than 2 nm), however depth selective information could be obtained by altering the angle of the flat sample to the electron energy analyzer. Thereby XPS can also be used in some cases to identify where one phase may be covered by another.

XPS is based on the principles of the photo-electric effect while atoms that are irradiated with light will absorb photon energy then emit electrons. These photoelectrons possess kinetic energy which represents characteristic of the wavelength of irradiating light and the binding energy of the electron.

$$Ek= hv-Eb$$

In which:

Ek = kinetic energy of the photoelectron

h = planck's constant

v= frequency of radiation

Eb= binding energy of the photoelectron or ionisation energy

The basic set up for XPS, shown in Fig. 2.11 includes an X-ray source, a variable angle sample stage for depth dependant analysis and an electron energy analyser.

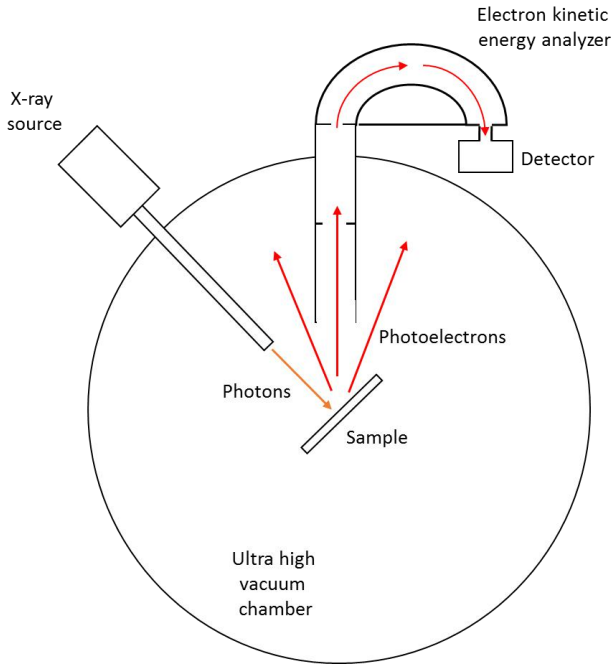

Figure 2.11. Schematic of an X-ray photoelectron spectrometer

Experiment

In this work, XPS measurements were performed using a Kratos Axis Ultra-DLD photoelectron spectrometer employing a monochromatic aluminium Kα source operating at 144 W (10 mA × 14 kV emission). Analysis was performed in the Hybrid mode with a slot aperture affording greater sensitivity, over a sample area of approximately 700 x 300 μm at pass energies of 40 eV and 160 eV for high resolution and survey scans respectively, using step sizes of 0.1 and 1.0 eV respectively. Catalyst powders were pressed into carbon tape attached to a glass slide to ensure each sample was electrically isolated from the spectrometer. Charge compensation was achieved using low energy electrons and an immersion lens system. All data were subsequently calibrated to the C (1s) core-level taken to be 284.5 eV, typical for graphitic/graphitic-like carbons. All binding energies are quoted with an accuracy of ±0.2 eV. Due to the propensity for cationic Au and Pd species to undergo photoreduction, both Au (4f) and Pd (3d) spectra were collected first and then again

with all other regions of interest to minimise this effect. Data analysis was performed using CasaXPS using sensitivity factors supplied by the manufacturer after removal of a Shirley background.

This XPS works were performed and analysed by Dr. David J. Morgan from Cardiff University.

2.4.3 UV-vis spectroscopy

Theory

UV-visible (UV-Vis) spectroscopy, the visible region of the electromagnetic radiation, is conventionally divided into three sub-domains: (i) near UV (185-400 nm); (ii) visible (400-700 nm) and (iii) very near infrared (700-1100 nm). The nature of absorption is the interaction of photons with ions or the sample molecules, including excitation of rotational, vibrational, and electronic levels. Due to the certain energy transitions, they will occur at defined wavelengths. The rotational and vibrational levels will be affected when there is a change in the electronic energy , leads to a collection of possible transitions obtained in the three domains.

Spectrophotometers consists a source of continuous radiation over the certain wavelengths, a monochromator (prisms, diffraction gratings, optical filters) for the selection of a narrow wavelength band, and a detector for converting the radiant energy into electric energy. After measurement, we could get a plot representing the transmittance (or the absorbance) as a function of wavelength, normally presented in nanometers. Transmittance (T) and absorbance (A) are interdependent, where T is the measurement of the beam attenuation of a monochromatic light, see the relationship below:

$$T = I / I_0$$

In which, I and I_0 are the intensities of the transmitted and the incident light respectively, and the second one related to this by the following equation:

$$A = - \log T$$

The absorbance (or transmittance) is proportional to the concentration, see Lambert-Beer equation:

$$A = \varepsilon * l * C$$

In which, ε is the molar absorptivity (L/cm·g), l represents the cell path way (cm) and C represents the concentration in g/L.

Furthermore for solid materials, diffuse reflection (DR) spectroscopy is widely employed. The DR spectra is from the radiation incident on the solid sample which is absorbed as it refracts through the particles, and is scattered by a combined process of reflection, refraction, and diffraction.

Experiment

In this study, the optical absorption properties of the individual monometallic Au and Pd colloids, the Au - Pd alloy colloid, and the homogeneous mixture of individual monometallic Au and Pd colloids, were analyzed using a Cary 60 UV/vis spectrophotometer. Scans were collected across the 400 to 800 nm wavelength range, at a scan rate of 24,000 $nm.min^{-1}$.

2.4.4 Microwave plasma atomic emission spectroscopy (MP-AES)

Theory

MP-AES is a technique for elemental analysis based on the principles of atomic emission. This technique relies on a microwave and magnetically excited nitrogen plasma heated to *ca* 5000 K and is formed within a quartz torch. Samples are in liquid phase or fully digested into solution and thereby energy from the torch is used for sample atomisation and excitation. However MP-AES limits samples to soluble or digestible materials though inductively coupled plasma optical emission

spectrometers can analyse solid samples through a laser ablation system too.

Sample atomisation is facilitated by the high temperatures from plasma source which results in a high population of excited states too. This allows MP-AES a higher sensitivity over those lower temperature techniques such as flame atomic absorption spectrometers. Fig. 2.12 below presents the basic principles behind MP-AES from the introduction of a liquid sample to the nitrogen plasma. Electrons relax into lower quantised energy levels releasing photons of defined energies after excitation and wavelengths which are characteristic for each element. One of the main advantages of this type of technique is the function to analyse each wavelength individually and sequentially using a monochromator detector and mirror grating. Along with the high intensities observed, result in a high sensitivity and low interference for each element.

It is plausible to use multiple emission wavelengths for each element, especially when analysis solution comprising versatile elements, as interference from nearby wavelengths can occur, resulting in false positives and concentrations.

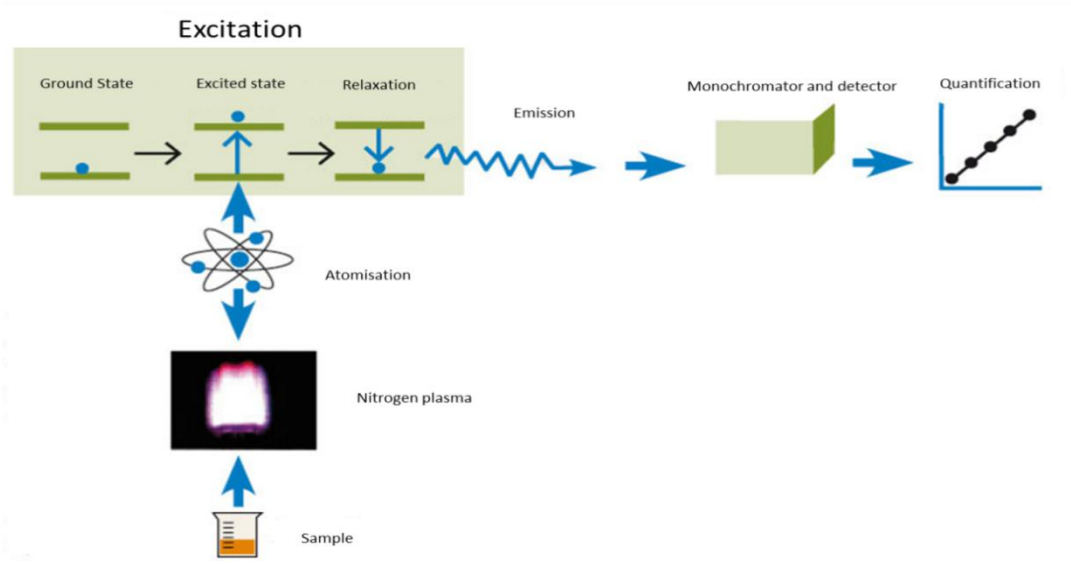

Figure 2.12. Flowchart showing basic principles of microwave plasma atomic emission spectroscopy

Experiment

In this study, post reaction solutions or catalyst filtration solution during preparation were first filtered to remove heterogeneous catalyst from the sample. Further filtration was carried out using PTFE syringe filters (0.456 µm). The samples were then analysed using an Agilent MP-AES 4100 spectrometer. Samples were investigated for the presence of precious metals (Au and Pd) using multiple wavelength calibrations for each individual element.

There are significant difficulties associated with the digestion of carbon supported nanoparticles, due to the inability of the prepared aqua regia to fully leach the metals from the support or indeed dissolve the carbon black unless with boiling, but still it only dissolves partially the carbon[6]. Alternatively, the only way to do this reliably would be to use HF however we do not have that facility. Therefore, the determination of metal loading of all the catalysts were based on the MP-AES results from the post filtration solution during catalyst preparation where no metal leaching was detected.This MP-AES work was performed and analyzed by Dr. Samuel Pattisson from Cardiff University. It was also reported for C supported nanoparticle catalysts prepared through sol immobilization, target loading, *e.g.*, 1.0 wt.% are frequently obtained without the need for acidification unlike other supports[7], and the immobilization period lasts only for 10 min if the C was carbon black XC-72R[8].

2.4.5 Temperature programmed reduction (TPR)

Solid catalyst after reaction was washed by DI water (500 mL) and acetone (250 mL) and dried for 16 h overnight. 50 mg catalyst (25 mg Au/C and 25 mg Pd/C for physical mixture) was deposited in quartz tube for temperature programmed reduction following two steps: degassing step under argon with an ramp rate of 10 °C/min to 110 °C and maintained at 110 °C for 60 min; reduction step under 5 % H_2 in argon with an ramp rate of 5 °C/min till 700 °C then cooled naturally.

2.4.6 Short circuit current (SCC)

Au/C and Pd/C catalyst were deposited onto glassy carbon electrode respectively, same recipe as it was in Section 2.3.4. The two electrodes submerged in reaction solution (0.1 M HMF, 0.02 M NaOH, 50 mL DI H_2O) were connected by ampere, forming a short circuit. Before the circuit is formed, O_2 gas was introduced into the reaction solution for 20 min with a flow rate of 150 mL/min till saturated, during reaction, the O_2 flow was turned down to 50 mL/min in avoid of any caused noise or catalyst drop off from the surface of electrode. A camera was used to record the current change for a 3 h reaction.

This SCC work was assisted by Dr. Ouardia Akdim and Kai Wang from Cardiff University.

2.4.7 BET surface area

Theory

BET (Brunauer, Emmett andTeller) is commonplace in catalysis for the measurement of surface area of a given catalyst. The BET equation can be explained as an adaption of the Langmuir isotherm which states that:

$$\theta = \frac{K_p}{1 + K_p} \; where \; K = \frac{k_a}{k_d}$$

Above Langmuir isotherm only considers monolayer formation *ie*, θ<1 however the BET equation expands on this to multilayer formation *ie*, θ>1. Not required for a full monolayer to be formed before multilayer formation can proceed. So the BET equation, as an expansion of the Langmuir can be provided as:

$$v = \frac{\left(\frac{v_m c}{p_0} p\right)}{\left(1 + \frac{c}{p_0} p\right)}$$

When rearranged it is fine to obtain the following form which can form a plot of y=mx+c:

$$\frac{p}{v(v_0 - p)} = \frac{1}{v_m c} + \left(\frac{c-1}{v_m c}\right)\left(\frac{p}{p_0}\right) \; and \; c = exp\left(\frac{E_{1-}E_L}{RT}\right)$$

Where:

p = pressure of adsorbate gas in pascals, v =volume of adsorbed gas at standard temperature and pressure, p_0=saturation pressure in pascals,, v_m= molar volume of gas to form monolayer, E_1=heat of adsorption for monolayer formation, E_2=heat of adsorption for multilayer formation, R=gas constant, T=Temperature(K).

Thereby, by plotting $\frac{p}{v(v_0-p)}$ against $\left(\frac{p}{p_0}\right)$ can yield a straight line graph with intercept $\frac{1}{v_m c}$ and a gradient of $\left(\frac{c-1}{v_m c}\right)$. Through obtaining v_m it is plausible to calculate the specific surface area using the following equation:

$$S = (N_a)(v_m)(A)$$

Where S =specific surface area, N_a=Avogadro's number, v_m= molar volume of gas to form a complete monolayer, A=cross sectional area of adsorbent gas. For nitrogen this is 16 $Å^2$.

Experiment

In this work, catalysts' surface areas were measured by multi-point N_2 adsorption at 77 K on a Micromeretics Gemini 2360 according to the Brauner– Emmet–Teller (BET) method. Before analysis, samples were degassed at 120 °C for 2 h under N_2 flow[9], results are listed in Appendix. Also this work of BET was assisted by Dr. Nia Richards from Cardiff University.

2.5 Summary

A series of C supported catalysts, namely monometallic Au and Pd, bimetallic Au-Pd alloy, physical mixture Au/C + Pd/C and binary mixture (Au + Pd)/C were prepared through the method of sol-immobilization, in which PVA and PVP were used as ligand. Protocols for aqueous HMF, glycerol and ethanol oxidation in testing the catalysts' activity were described, involving cyclic voltammetry. Meanwhile catalyst characterisations, *e.g.*, STEM, XPS, UV-vis, MP-AES, TPR, BET and SCC were performed in order to investigate the chemical and physical properties of the prepared catalysts.

2.6 References

1 J. Pritchard, L. Kesavan, M. Piccinini, Q. He, R. Tiruvalam, N. Dimitratos, J. A. Lopez-Sanchez, A. F. Carley, J. K. Edwards, C. J. Kiely and G. J. Hutchings, *Langmuir*, 2010, **26**, 16568–16577.

2 N. Dimitratos, J. A. Lopez-Sanchez, D. Morgan, A. Carley, L. Prati and G. J. Hutchings, *Catal. Today*, 2007, **122**, 317–324.

3 V. Peneau, Q. He, G. Shaw, S. A. Kondrat, T. E. Davies, P. Miedziak, M. Forde, N. Dimitratos, C. J. Kiely and G. J. Hutchings, *Phys. Chem. Chem. Phys.*, 2013, **15**, 10636–10644.

4 M. Comotti, C. Della Pina, R. Matarrese, M. Rossi and A. Siani, *Appl. Catal. A Gen.*, 2005, **291**, 204–209.

5 P. T. Kissinger and W. R. Heineman, *J. Chem. Educ.*, 1983, **60**, 702.

6 G. Norwitz and M. Galan, *Carbon N. Y.*, 1967, **5**, 287–289.

7 A. Villa, D. Wang, G. M. Veith and L. Prati, *J. Catal.*, 2012, **292**, 73–80.

8 J. Fu, Q. He, P. J. Miedziak, G. L. Brett, X. Huang, S. Pattisson, M. Douthwaite and G. J. Hutchings, *Chem. - A Eur. J.*, 2018, **24**, 2396–2402.

9 I. Orlowski, M. Douthwaite, S. Iqbal, J. S. Hayward, T. E. Davies, J. K. Bartley, P. J. Miedziak, J. Hirayama, D. J. Morgan, D. J. Willock and G. J. Hutchings, *J. Energy Chem.*, 2019, **36**, 15–24.

Preliminary research on physical mixture of Au/C + Pd/C

3

Introduction

This chapter describes the experimental behaviors of series of monometallic Au and Pd, bimetallic Au-Pd alloy and physical mixtures of Au and Pd all supported on carbon black type XC-72R for aqueous 5-hydroxymethylfurfural (HMF) oxidation. All the catalysts were characterized by Scanning Transmission Electron Microscopy (STEM) and Ultraviolet–visible Spectroscopy (UV-vis). No leaching was detected by Microwave Plasma-Atomic Emission Spectrometer (MP-AES) from the post reaction solution. Same as HMF oxidation, reactions started from corresponding intermediate products, *e.g.*, HMFCA and FFCA were tested showing that HMF oxidation using a physical mixture catalyst of Au/C and Pd/C is not a simple two step reaction. Finally, the corresponding reaction rate and rate constant are calculated and analyzed.

3.1 Performances of bimetallic AuPd in HMF oxidation

The Au based bimetallic catalysts were reviewed in *Chapter 1* showing an enhanced reaction rate when compared to its monometallic counterparts in a variety of reactions, *e.g.*, alcohol, aldehyde oxidation[1–7]. Among which, the catalyst of Au-Pd has been widely reported as displaying an exceptionally good activity in the conversion of biomass deviations in particular. Therefore, the catalyst of Au and Pd was chosen as a model catalyst in this study to investigate the different performances among bimetallic in the presence of Au-Pd alloy and Au/C + Pd/C as physical mixture; monometallic of Au and Pd in HMF oxidation. Given the results from Prati *et al.* on the work of HMF oxidation, reported AuPd supported on active carbon with a mole ratio of 4 to 1 exhibits the highest activity (productivity towards FDCA of 99 $mol_{FDCA}.mol_{metal}^{-1}.h^{-1}$, see Appendix)[8]. Due to which, the ratio of 4 to 1 between Au and Pd was picked as a starting point for exploring the bimetallic catalyst in this study.

Bimetallic alloy (denoted as Au-Pd) was prepared through a method of sol immobilization, the nanoparticles were protected with a stabilizer of polyvinyl alcohol (PVA), carbon black type XC-72R was used as the catalyst support (a full preparation recipe was given in *Chapter 2*). Analogously, a catalyst of physical mixture was prepared in the same way, briefly each the Au/C and Pd/C was prepared separately, each contains same moles of Au and Pd to the alloy. The alloy was characterized to be a true Au-Pd nanoalloy by UV-vis spectroscopy and STEM, as shown in Fig. 3.1 and Fig. 3.2. The monometallic Au colloid shows a characteristic surface plasmon resonance (SPR) peak centred around 520 nm[9]. No surface plasmon resonance peak was observed for the monometallic Pd colloid[10]. The spectrum from a physical mixture of Au and Pd colloids shows a relatively smaller Au SPR peak due to the diluted Au colloids present compared to the monometallic Au system, however no Au SPR band was found for the Au-Pd colloids confirming that both metallic components are intimately alloyed. Furthermore, the Energy Dispersive X-ray (EDX) spectrum measured for the same nanoparticle (from the solid catalyst), both signals of Au (2.2

keV) and Pd (3.0 keV)[8,11,12] were detected showing Au and Pd are alloyed after immobilization onto the C.

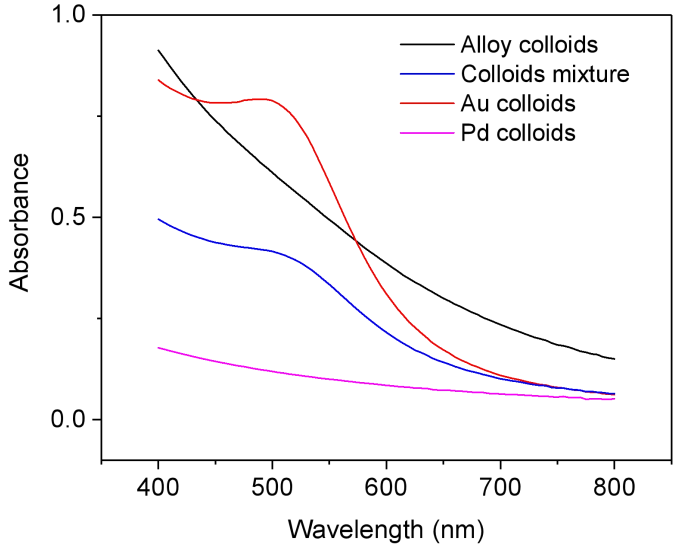

Figure 3.1. Ultraviolet-visible (UV-vis) spectrophotometry of the four different colloids: namely: (i) the Au-Pd nanoalloy, (ii) a physical mixture of Au and Pd (iii) Au only, and (iv) Pd only.

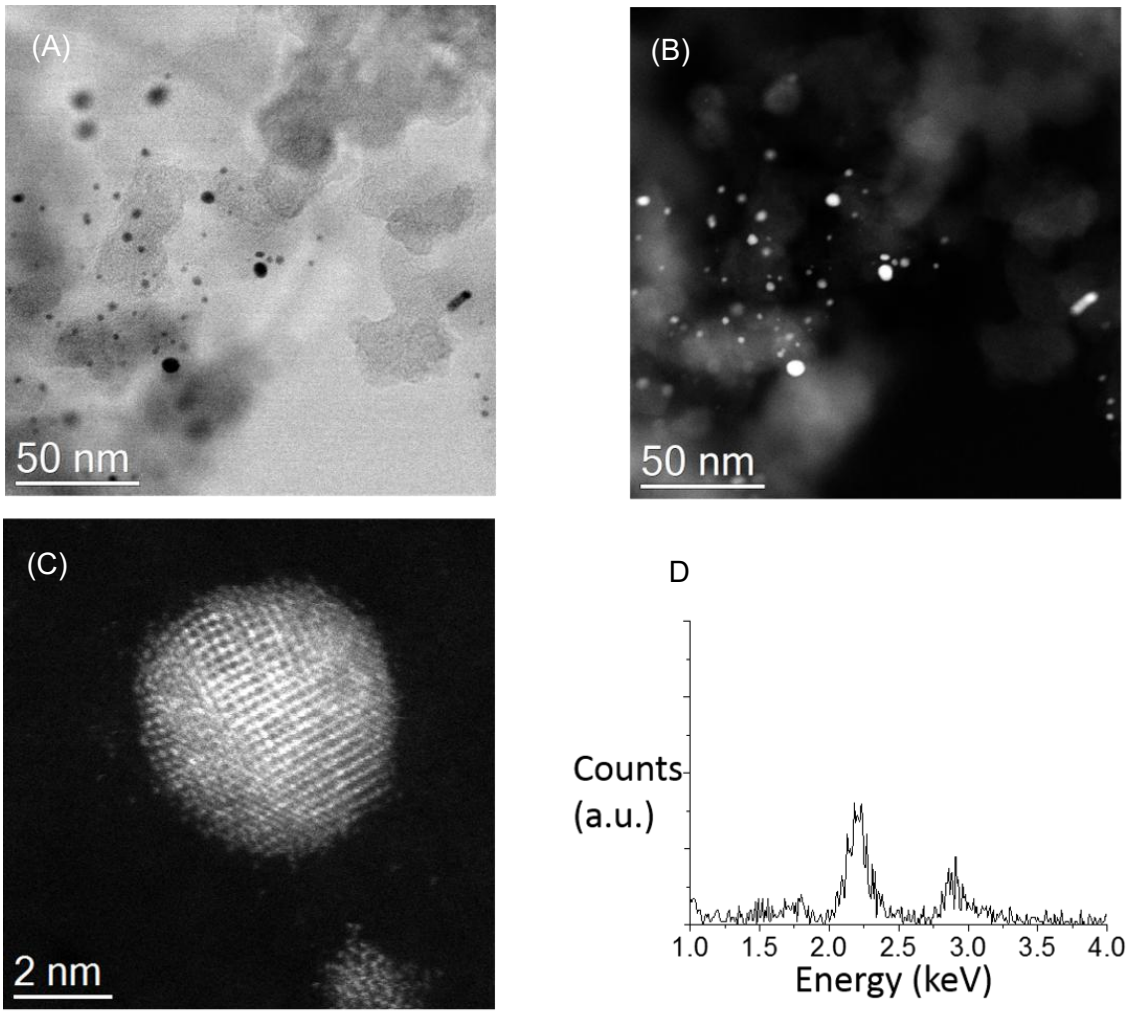

Figure 3.2. Electron microscopy analysis of Au-Pd/C alloy sample before use as a catalyst: (**A**) and (**B**) are complementary low magnification BF-and HAADF-STEM images showing nanoparticle size and spatial distribution; (**C**) is a higher magnification HAADF-STEM image of a typical particle and (**D**) is the corresponding X-EDS spectrum showing the nanoparticles in (C) is an Au-Pd alloy. All Images were obtained by Dr. Qian He from National University of Singapore.

After catalysts synthesis, the aqueous HMF oxidation was conducted in a colaver reactor at temperature of 80°C under 3 bar O_2 for 2 hours, the possible reaction route is exhibited in Scheme 3.1. The result of activity test for Au-Pd alloy is shown in Fig.

3.3, HMF gets a full conversion by a reaction time of 90 min, one of its intermediate products HMFCA which is the first product generated from HMF oxidation reached the highest yield *ca* 60% at 90 min. No significant amount of the final product FDCA was obtained at the end of reaction, less than 20%. To compare with the alloy, a physical mixture of Au/C and Pd/C was examined for the same reaction. To the best of our knowledge, alloy is commonly known as a more active catalyst than physical mixture due to its stronger interaction between Au and Pd[4], which has been also reviewed in *Chapter 1*. For example, scientists had tried a mixture catalyst of Au/AER and Pd/AER in HMF oxidation. AER is a polymer material abbreviated for anion-exchange resin. In result, the mixture catalyst shows a lower activity (52% yield of FDCA after a 4 hours reaction) than the corresponding Au-Pd/AER alloy (93% yield of FDCA after a 4 hours reaction)[13]. Apart from HMF oxidation, the mixture catalyst of Au/AC and Pd/AC (AC: active carbon) was tested in benzyl alcohol oxidation too. In this case, the mixture catalyst is about 20% less active than the corresponding Au-Pd/AC alloy towards benzyl alcohol conversion. Meanwhile, based on the microscopy analysis, this physical mixture could transfer its structure into alloy structure during the reaction so an enhanced activity was obtained[4]. All the literature reviewed in *Chapter 1* show the alloy catalyst is usually known as the highly active catalyst than a simple mixture catalyst. However, in this study, from the results shown in Fig. 3.4, the moles of HMF decreased more quickly for the physical mixture of Au/C + Pd/C than the alloy Au-Pd/C in this study (Fig. 3.3). Instead of spending 90 min, HMF was totally consumed at *ca* 60 min over the mixture catalyst, which is more efficient than the alloy. From the physical mixture of Au/C + Pd/C, yield of both intermediates HMFCA and FFCA start to decrease notably from 60 min (for the alloy, 90 min) due to the formation of FDCA, at the end of reaction about 40 % yield of FDCA is achieved over the physical mixture while the alloy has only 16 %. To compare with literature, though scientists had achieved a 100% HMF conversion after a 2 hours reaction over Au-Pd alloy catalyst with a same mole ratio of HMF/metal = 200 (productivity of 99 $mol_{FDCA}.mol_{metal}^{-1}.h^{-1}$ towards FDCA , see Table S1 in *Appendix*), but use of 2 eq

NaOH strong base, which makes the condition less environmentally friendly[8]. In this work, $NaHCO_3$ is used, leading to a milder reaction condition and the physical mixture catalyst is showing a relatively good activity (productivity towards FDCA of 55 $mol_{FDCA}.mol_{metal}^{-1}.h^{-1}$ see Table S4 in *Appendix*). In parallel, around 4 % carbon balance were missing at the start of the reactions which are probably due to the chemical or physical adsorptions of HMF molecules from the carbon support[14,15] or might be the base catalyzed aldol condensation reactions leading to humin formation, reported from literature[16]. As reaction time goes longer, the carbon balance is getting closer to 100 %, which could be attributed to any evaporated water from the reaction solution during experiment, thereby the carbon balance has increased slightly. To confirm what observed is not an artifact, all the reactions over both alloy and mixture were repeated for 3 times to calculate error bars (performed by Kai Wang, who was initially not involved in the project). For this, He used my experimental protocols to synthesize the catalysts and run the oxidation experiments. Each catalyst system was synthesized three times and tested. Carbon balances were all calculated to be around 95% during the entire reaction.

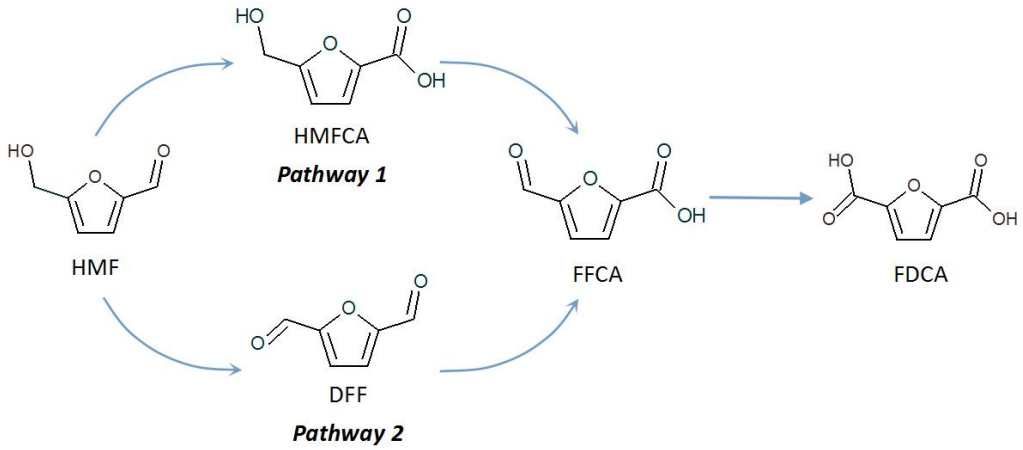

Scheme 3.1. Possible reaction routes for aqueous HMF oxidation.

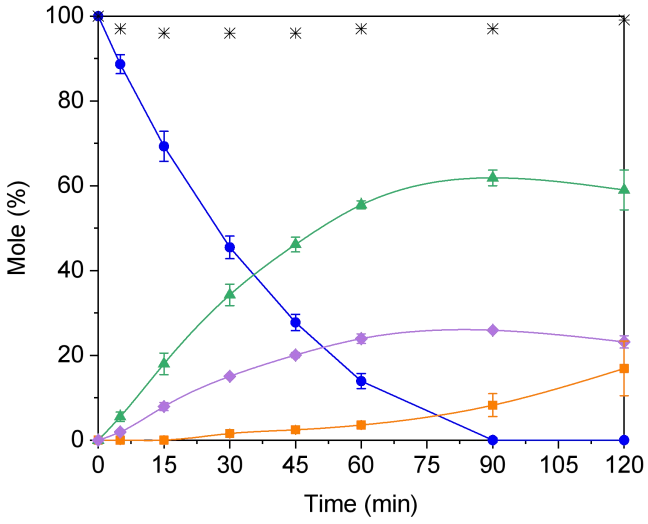

Figure 3.3. Time-on-line data of aqueous HMF oxidation over the alloyed Au-Pd/C catalyst. *Reaction conditions*: HMF (0.1 M), $NaHCO_3$ (0.4 M), H_2O (16 mL), Au-Pd/C: 143.1 mg, 80 °C, pO_2 = 3 bar, 160 min. *Key*: FDCA (■), FFCA (♦), HMFCA (▲), HMF (●), mass balance (*). Error bars were provided by Kai Wang from Cardiff University.

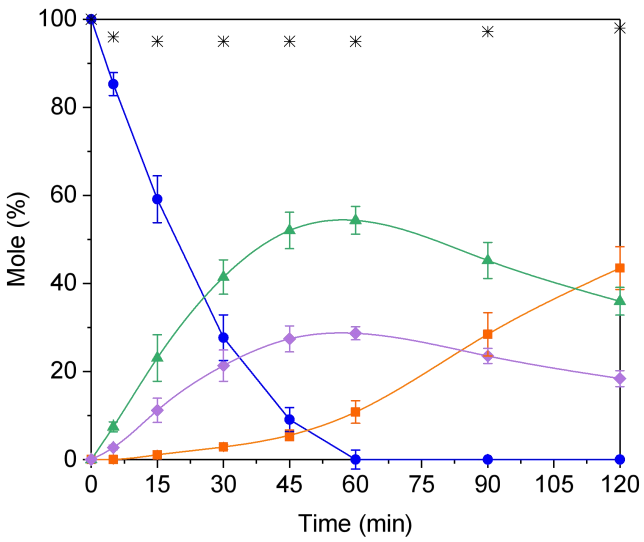

Figure 3.4. Time-on-line data of aqueous HMF oxidation over a physical mixture of the Au/C and Pd/C catalysts. *Reaction conditions*: HMF (0.1 M), $NaHCO_3$ (0.4 M), H_2O (16 mL), Au/ C: 72.1 mg, Pd/C: 71 mg, 80 °C, pO_2 = 3 bar, 160 min. *Key*: FDCA (■), FFCA (♦), HMFCA (▲), HMF (●), mass balance (*). Error bars were provided by Kai Wang at Cardiff University.

At present, we have found the phenomenon that physically mixed of Au/C and Pd/C shows a better performance than Au-Pd/C alloy in aqueous HMF oxidation, the two catalysts were prepared with the same amount of metal, PVA and C, and tested under identical reaction conditions. In order to know the reason why mixture catalyst is unexpectedly more efficient than alloy, its counterparts, namely the monometallic Au/C and Pd/C were separately evaluated in the same reaction, which is beneficial to explain the mechanism.

3.2 Catalytic behaviors of monometallic Au and Pd in HMF oxidation

As has been reviewed in *Chapter 1*, monometallic Au nanoparticles displayed good catalytic activity in alcohol and aldehyde oxidation[17–25]. Here in this study, considering HMF molecule contains both alcohol and aldehyde groups and the experimental data shows that the presence of a physical mixture of Au/C + Pd/C is more active than the alloy in HMF oxidation, it is therefore necessary to explore the activity of the monometallic Au/C and Pd/C in the same reaction.

Fig. 3.5 shows Au/C is able to oxidize the HMF molecule in alkaline conditions, after a reaction of 120 min, most of the HMF molecules (blue line) are consumed into its first intermediate product HMFCA (green line), which is less efficient compare to the Au-Pd alloy catalyst, in Fig. 3.3. Over the reaction course of the first 60 min, HMF conversion and HMFCA yield *vs*. time showed a quite linear correlation, meaning that the reaction rate (around 0.085 mol· L^{-1}·h^{-1}) keeps almost constant. However, its subsequent reaction from HMFCA to the second intermediate FFCA appears to be not as easy as the first step, negligible amounts of FFCA are yielded during the whole reaction over Au/C, which leads to less production of the final product FDCA. The performance from the monometallic Au in HMF oxidation is quite similar to those reported results from literature[26–29]. For example, Au nanoparticles supported on active carbon or carbon nanofiber can reach a full HMF conversion with a 98% selectivity to HMFCA after a 2 hours reaction in an alkaline condition, but only 2 % yield of the FDCA was detected[8].

On the other hand, monometallic Pd/C, which is the other counterpart from the physical mixture, was evaluated in the same reaction. In this case, the conversion number was found to be very low, less than 10% of HMF was converted during an entire 120 min reaction as shown in Fig. 3.6. Comparing to Au however, the Pd displayed a much lower activity, which is consistent to reports in literature. If you find in Table S3 and Table S2 in appendix, supported Au catalysts displayed overall a higher activity than supported Pd catalysts. Furthermore, the activity of physical mixture Au/C + Pd/C in HMF oxidation is much higher than a simple addition of monometallic Au/C and Pd/C, the series of turnover numbers after 5 min reaction for each catalyst were compared and displayed in Table 3.1, following an order of Au/C + Pd/C > Au-Pd/C > Au/C >> Pd/C. Therefore, the observed performance from the physical mixture is ascribed to the synergy taking place between Au and Pd, in addition, this synergistic effect is even stronger than the one originates from the alloy.

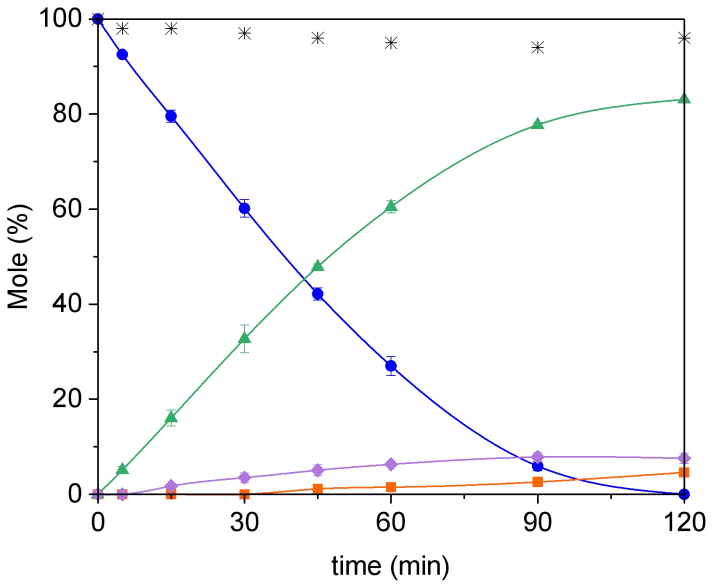

Figure 3.5. Time-on-line data of aqueous HMF oxidation using the monometallic Au/C catalyst. *Reaction conditions*: HMF (0.1 M), $NaHCO_3$ (0.4 M), H_2O (16 mL), Au/C: 72.1 mg, 80 °C, pO_2 = 3 bar, 120 min. *Key*: FDCA (■), FFCA (♦), HMFCA (▲), HMF (●), mass balance (*). Error bars were provided by Kai Wang at Cardiff University.

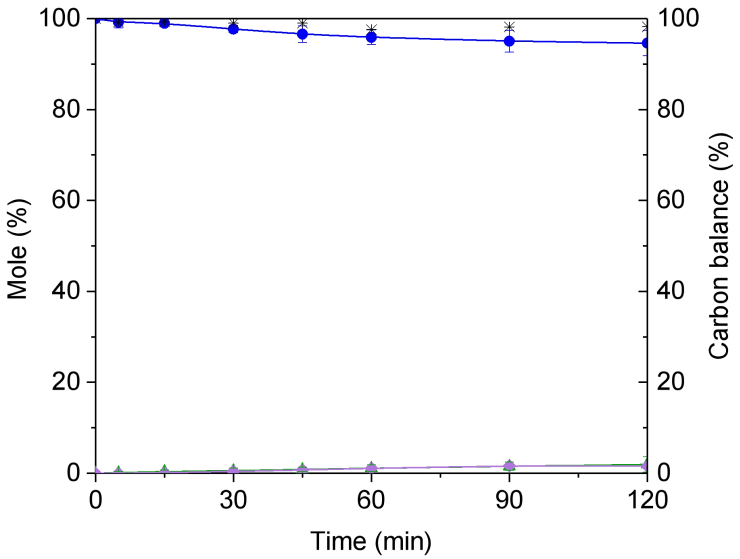

Figure 3.6. Time-on-line data of aqueous HMF oxidation using the monometallic Pd/C catalyst. *Reaction conditions*: HMF (0.1 M), $NaHCO_3$ (0.4 M), H_2O (16 mL), Pd/C: 71 mg, 80 °C, pO_2 = 3 bar, 120 min. *Key*: FFCA (♦), HMFCA (▲), HMF (●), mass balance (*). Error bars were provided by Kai Wang at Cardiff University.

Each of the catalysts was subsequently characterized by STEM ensuring that the differences in performance were not attributable to particle size effects. The mean particle sizes for the Au/C, Pd/C and Au-Pd/C catalysts were determined to be 3.12 nm, 3.40 nm and 2.80 nm respectively, shown from Fig 3.7 to 3.9. The particle size distribution (PSD) analysis provided further evidence that the enhanced activity for the physically mixed Au/C + Pd/C sample was not attributed to the differences of particle size. Also, the post-reaction samples were analyzed by MP-AES whereby no metal was observed in reaction solution. All these evidence are showing that the noticeable difference between the catalytic behavior of physical mixture and alloy is not a coincidence, investigation on the mechanism providing explanation on this observation triggers attention, which would be beneficial for multi component heterogeneous catalyst design.

Table 3.1. Estimated TOFs for each of the catalytic systems in the aerobic oxidation of HMF. The total active sites available in each catalyst was estimated using the Mackay model[30] (see appendix, Table S11), based on the particle size distributions presented in Fig. 3.9. Initial rates measurements used in these calculations were after 5 minutes of reaction.

Entry	Catalyst	Conversion (%)	Initial Rate ($M \cdot s^{-1}$)	Mean Particle Size (nm)	TOF (s^{-1})
1	Au/C	7.5	2.5×10^{-5}	3.12	0.169
2	Pd/C	0.8	2.7×10^{-6}	3.40	0.068
3	Au-Pd/C	11.3	3.8×10^{-5}	2.80	0.228
4	Au/C +Pd/C	14.7	4.9×10^{-5}	See entries 1 and 3	0.262

Reaction conditions: HMF (0.1 M), $NaHCO_3$ (0.4 M), H_2O (16 mL), 80 °C, pO_2 = 3 bar, 5 min, catalyst amount for Au/C: 72.1 mg; Pd/C: 71 mg; Au-Pd/C:143.1 mg.

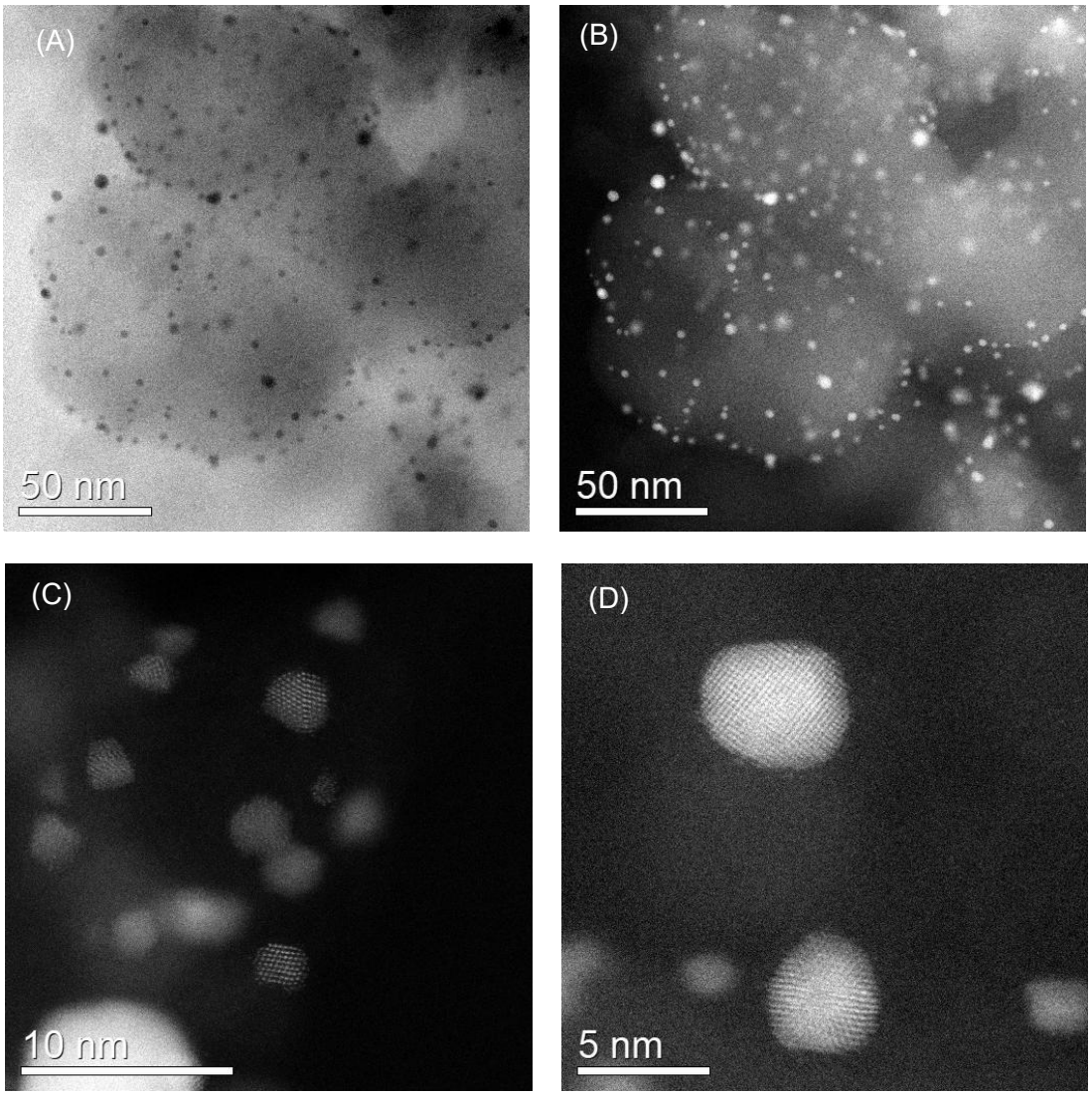

Figure 3.7. Electron microscopy analysis of Au/C sample before use as a catalyst: (**A**) and (**B**) complementary pair of BF- and HAADF STEM images showing Au size and spatial distribution; (**C**) and (**D**) Atomic resolution HAADF-STEM images showing that the Au particles a mixture of cub-octahedral and icosahedral morphologies. All the images were obtained by Dr. Sultan M. Althahban from Lehigh University.

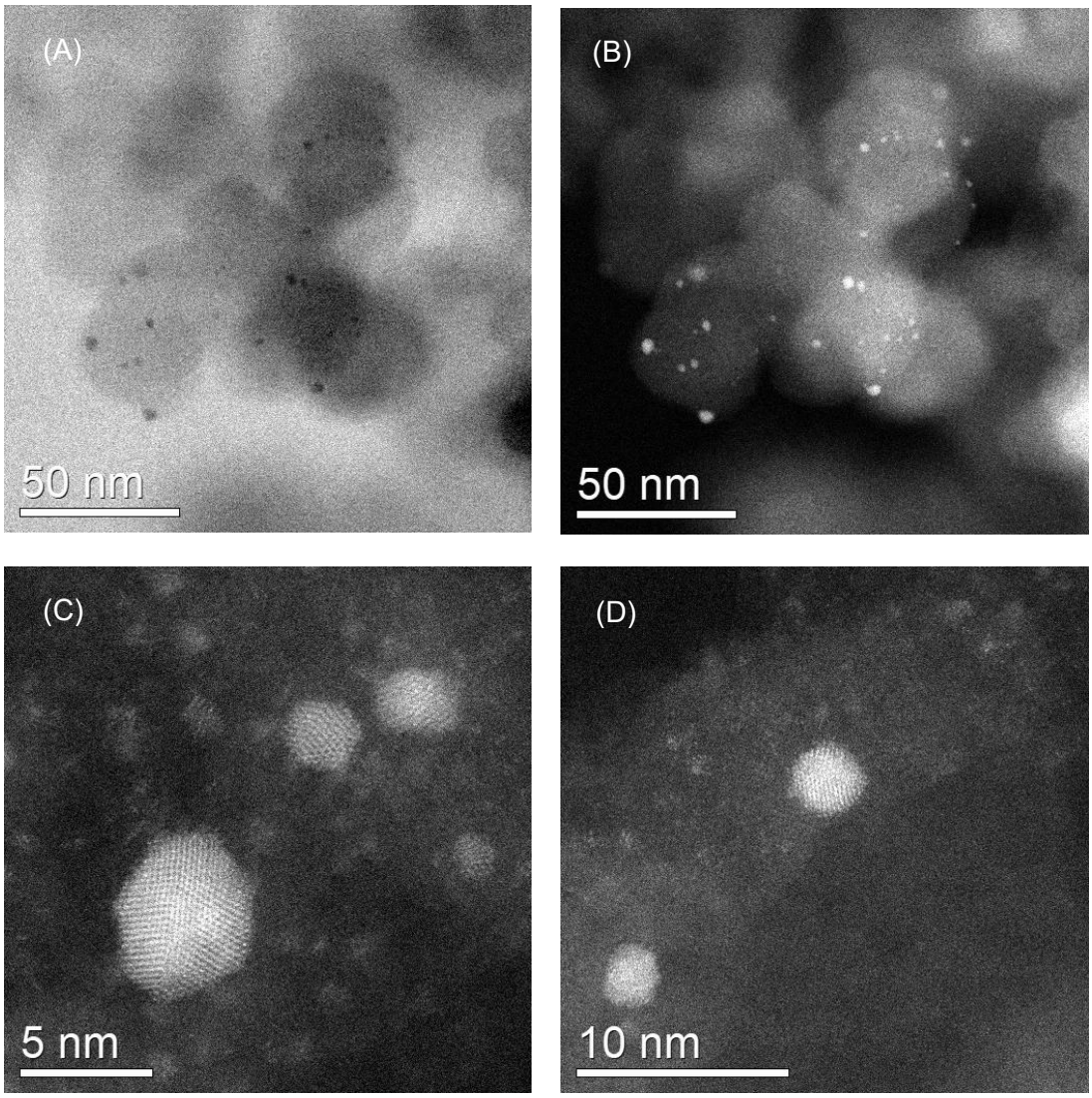

Figure 3.8. Electron microscopy analysis of Pd/C sample before use as a catalyst: (**A**) and (**B**) Complementary pair of BF- and HAADF-STEM images showing Pd size and spatial distribution; (**C**) and (**D**) Atomic resolution HAADF STEM images showing that the Pd exists as a mixture of cub-octahedral particles and sub-nm clusters. All the images were obtained by Dr. Sultan M. Althahban from Lehigh University.

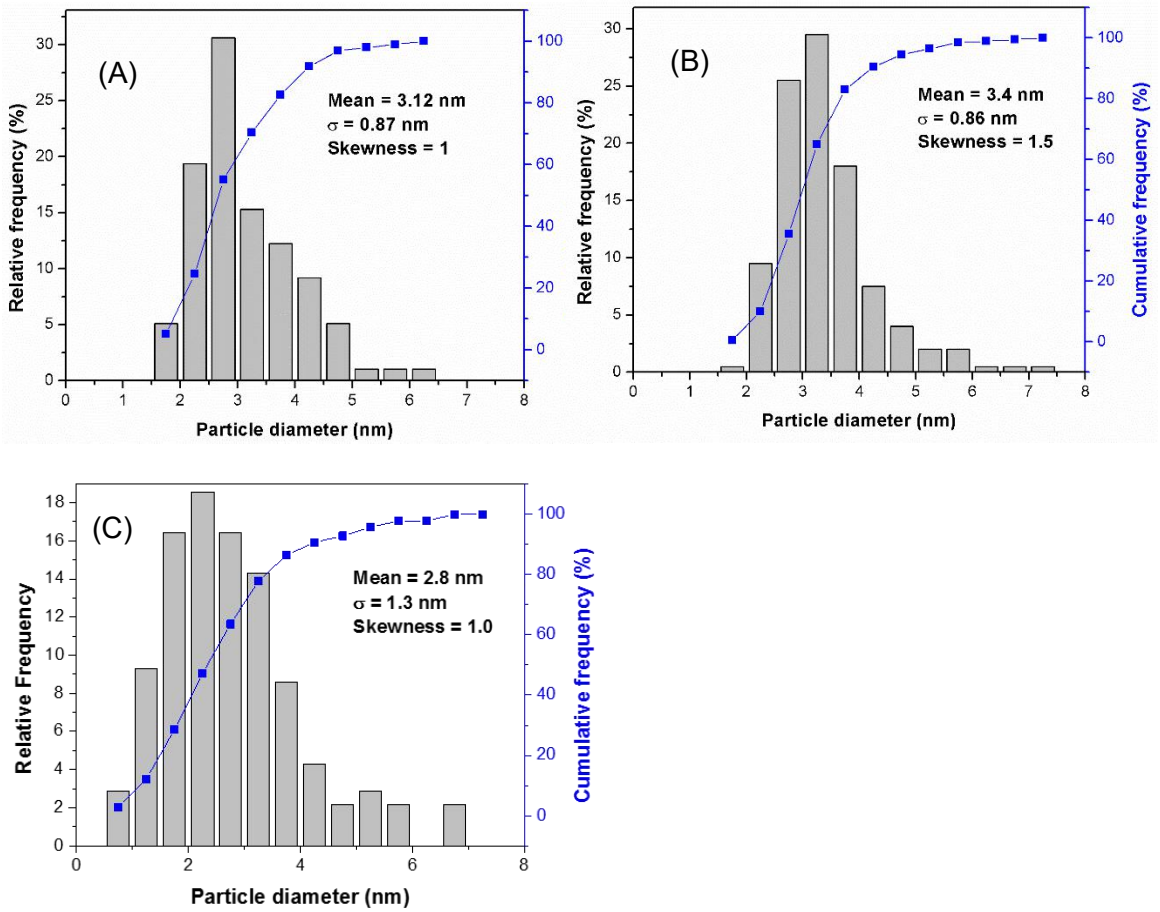

Figure 3.9. Measured particle size distributions for (**A**) Au/C sample before use as a catalyst; (**B**) Pd/C sample before use as a catalyst; (**C**) Au-Pd/C alloy sample before use as a catalyst. σ refers the deviation of mean particle size(calculation methodology see appendix eq. (1)), skewness is a measure of the asymmetry of the probability distribution of a real-valued random variable about its mean. All the bar charts were provided by Dr. Sultan M. Althahban from Lehigh University.

Previously, a Mechanistic study of this reaction was well developed by Robert Davis *et al*. they found during HMF oxidation in basic conditions, over Au or Pt catalyst, the oxidants come from OH^- in water, rather than the molecular oxygen[31]. This mechanism has been widely accepted. In order to confirm this conclusion, based on

the experimental results obtained, additional HMF oxidation reactions using Au/C under different oxygen pressures, with the other parameters kept identical were performed. As is shown in Fig 3.10, apart from 3 bar O_2 which is set to be the standard reaction condition, reactions under 1.5 bar, 0.6 bar O_2 and 3 bar pure N_2 are tested in parallel. The conversion of HMF gets correspondingly lower when there is less oxygen content and pressure. Furthermore, the linear correlation between HMF conversion and time concludes an unchanged reaction rate during the reaction under each O_2 pressure(0.085 mol· L^{-1}·h^{-1} for 3.0 bar; 0.068 mol· L^{-1}·h^{-1} for 1.5 bar; 0.048 mol· L^{-1}·h^{-1} for 0.6 bar O_2). When the reaction was under pure N_2, there is almost no activity over the Au/C. Therefore, HMF oxidation over Au requires the participation of molecular oxygen, which is playing an important role in this reaction, presumably that the oxygen reduction reaction (ORR) was taking place on the surface of Au nanoparticles[32]. From the literature it is known that for conversion of every HMF molecule, two electrons are correspondingly formed on the surface of Au nanoparticles in solution[31], see equations from (1) to (5) below. Therefore the *in-situ* ORR process is possibly working as a scavenger for consuming the generated electrons from HMF and its intermediates oxidation[33].

(1) $C_6H_6O_3$ (HMF) + H_2O → $C_6H_8O_4$ (geminal diol)

(2) $C_6H_8O_4$ (geminal diol) + $2OH^-$ → $C_6H_6O_4$ (HMFCA) + $2H_2O$ + $2e^-$

(3) $C_6H_6O_4$ (HMFCA) + $2OH^-$ → $C_6H_4O_4$ (FFCA) + $2H_2O$ + $2e^-$

(4) $C_6H_4O_4$ (FFCA) + H_2O → $C_6H_6O_5$ (another geminal diol)

(5) $C_6H_6O_5$ (geminal diol) + $2OH^-$ → $C_6H_4O_5$ (FDCA) + $2H_2O$ + $2e^-$

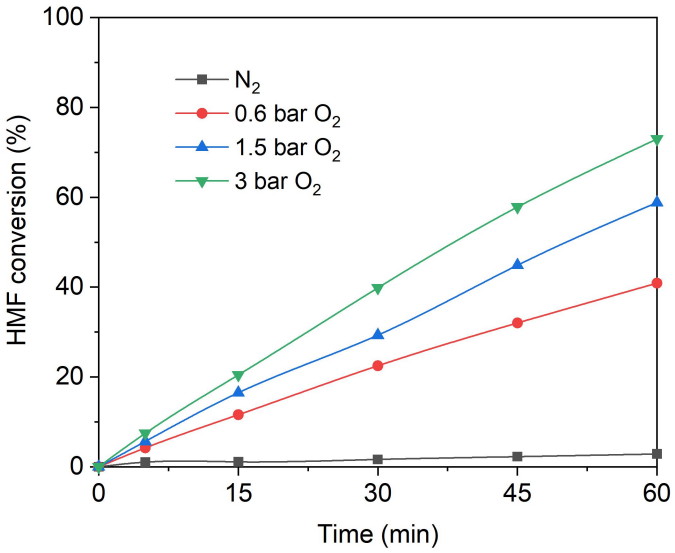

Figure 3.10. Aqueous HMF oxidation over the monometallic Au/C catalyst under varying O_2 and N_2 partial pressures. *Reaction conditions*: aqueous HMF (0.1 M), $NaHCO_3$ (0.4 M), H_2O (16 mL), 80 °C, 60 min, Au/C: 72.1 mg.

To summary what it has been discovered so far, Au/C is active in converting HMF into HMFCA in an alkaline reaction condition, whilst the Pd/C is not able to. Oxygen is important to the process without which, there is no activity over Au/C. A specific synergy must take place between Au/C and Pd/C which promotes the catalysis higher when two catalysts were in the presence of physical mixture in HMF oxidation, instead of a simple add up of activity from each counterpart. To further elucidate the nature of this synergistic effect in the physical mixture, several other reactions ran by Au/C with the addition of Pd/C at half way were designed and operated.

3.3 Two step method using Au/C and Pd/C

According to the experimental performances of each catalyst depicted above, it is known the monometallic Pd/C appeared to have the lowest activity in HMF oxidation, however when it is physically combined to the Au/C, the Pd is greatly contributing, in

another way, by accelerating the Au catalysis. In order to understand how the Pd/C catalyst works cooperatively with the Au/C, series of two step procedures were designed to run the reaction over Au/C for a period of time, followed by the addition of Pd/C to the same reactor for the rest of the reaction. As shown in Fig.3.11, the addition of Pd/C had a big effect on both the HMF consumption and its products distribution, with no discernible change in activity observed for an analogous experiment where no Pd was added. To ensure that this enhancement was not attributable to the addition of carbon black XC-72R, a control experiment was conducted which replaced the addition of Pd/C by adding just carbon after 30 min (Fig. 3.12). Upon the addition of carbon, no change was observed to the reaction profile, which underlines the importance of Pd in the catalysis. A similar phenomenon was also observed when Pd/C was added to the reaction over Au/C after 120 min (Fig. 3.13). Au/C is able to convert HMF into HMFCA and a full conversion is obtained after reaction time of 120 min. However, this generated HMFCA is difficult to be further oxidized into FDCA over Au alone, as it was discussed in Fig. 3.5. By the addition of Pd into the same reaction as a physical mixture at 120 min has made HMFCA decreased sharply. Seemingly, that the Pd/C is doing the job of converting the intermediate product HMFCA into the final product FDCA, suggesting this HMF oxidation in the presence of a physical mixture might be a two step reaction, where Au/C is working on HMF transformation to HMFCA firstly, then Pd/C is working on the following reaction from HMFCA to FDCA. From all these two step reactions, assuming that synergy is taking place between Au and Pd not only in oxidizing the HMF but also in its intermediates. In order to prove either this hypothesis is correct or false, reactions starting from intermediates, *e.g.*, HMFCA, FFCA are then performed.

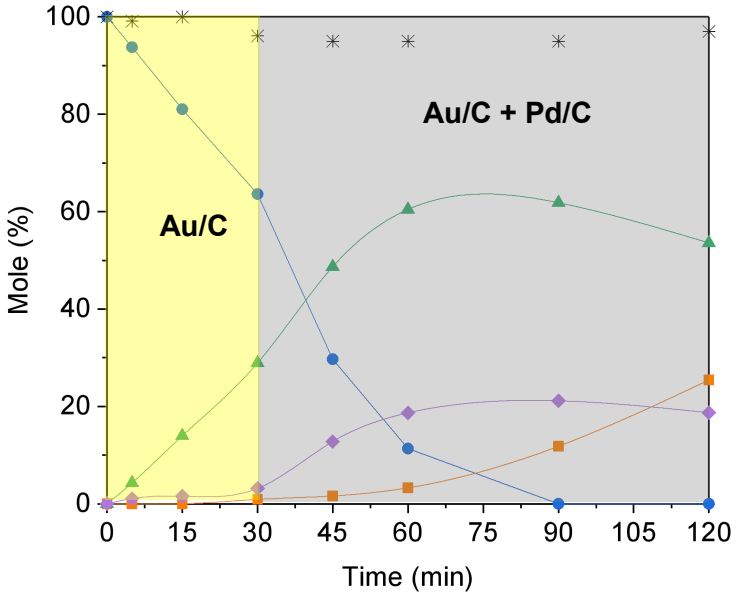

Figure 3.11. Aqueous HMF oxidation using Au/C followed by addition of Pd/C after 30 min, *Key*: FDCA (■), FFCA (♦), HMFCA (▲), HMF (●), mass balance (*). *Reaction conditions*: HMF (0.1 M); $NaHCO_3$ (0.4 M); H_2O (16 mL); 80 °C; pO_2 = 3 bar; catalyst amounts for Au/C: 72.1 mg; Pd/C: 71 mg.

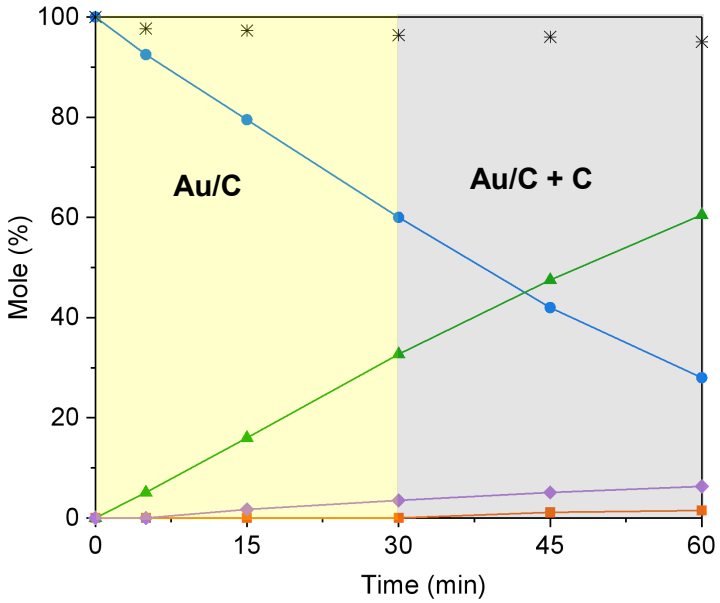

Figure 3.12. Aqueous HMF oxidation using Au/C followed by addition of C after 30 min, *Key*: FDCA (■), FFCA (♦), HMFCA (▲), HMF (●), mass balance (*). *Reaction conditions*: HMF (0.1 M); $NaHCO_3$ (0.4 M); H_2O (16 mL); 80 °C; pO_2 = 3 bar; catalyst amounts for Au/C: 72.1 mg; C: 71 mg.

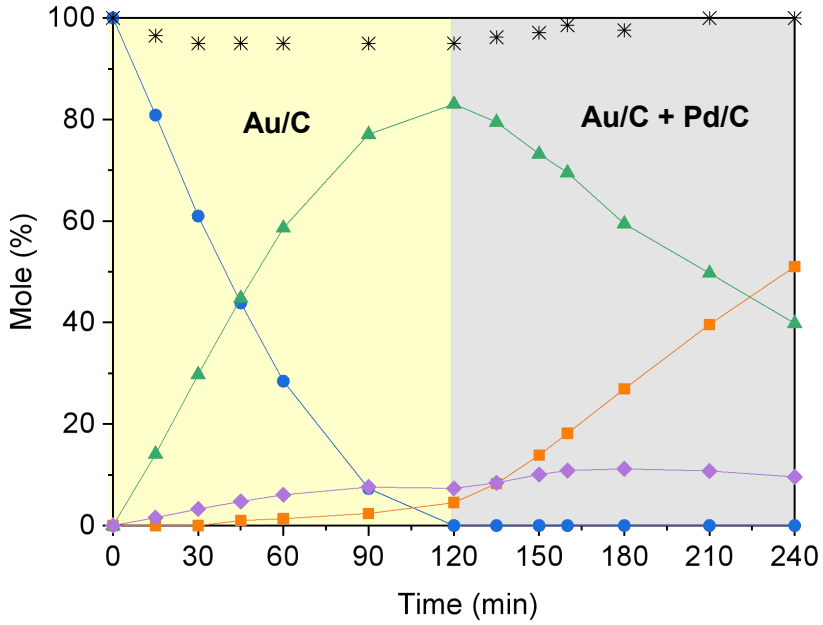

Figure 3.13. Aqueous HMF oxidation using the Au/C catalyst followed by the addition of the Pd/C catalyst after 120 min. *Reaction conditions*: HMF (0.1 M), $NaHCO_3$ (0.4 M), H_2O (16 mL), Au/C: 72.1 mg, Pd/C: 71 mg, 80 °C, pO_2 = 3 bar, 240 min. *Key*: FDCA (■), FFCA (♦), HMFCA (▲), HMF (●), mass balance (*).

3.4 Oxidation of intermediate products using Au and Pd

To understand on the mechanism how the physical mixture catalyst works in HMF oxidation, reactions start from each intermediate product are performed. Based on all these experiments done so far in alkaline conditions, no intermediate product of 2, 5-diformylfuran (DFF) was observed (see the reaction pathway in Scheme 3.1), which is consistent to what other scientists had reported[34]. Therefore, oxidation of intermediate products 5-hydroxymethylfuroicacid (HMFCA) and 5-Formyl-2-furancarboxylic acid (FFCA) were operated to evaluate the behaviors of physical mixture; alloy and monometallics.

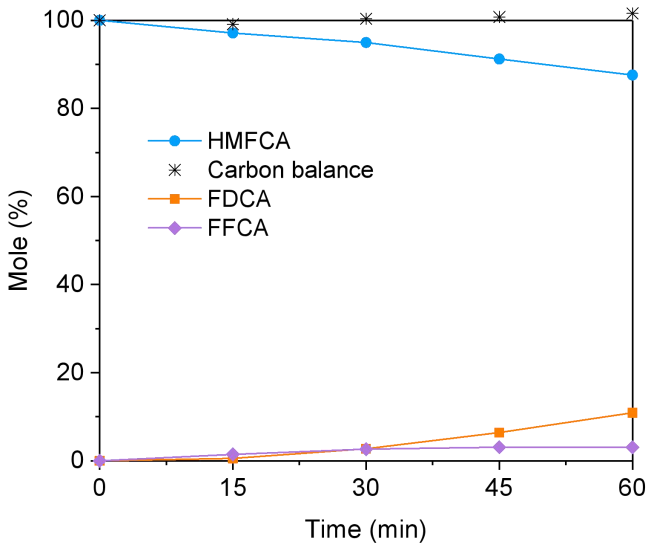

Figure 3.14. Time-on-line data of aqueous HMFCA oxidation using mono metallic Au/C catalyst. *Reaction conditions*: HMFCA (0.1 M), $NaHCO_3$ (0.4 M), H_2O (16 mL), Au/C: 72.1 mg, 80 °C, pO_2 = 3 bar, 60 min, catalyst amount: 72.1 mg.

The molecule of HMFCA contains one carbonyl alcohol group (-CH_2OH) and one carboxylic acid group (-CHOOH). Essentially to oxidize HMFCA is merely the process of transforming the alcohol into aldehyde or acid. As shown in Fig 3.14, oxidation of aqueous HMFCA using Au/C seems to be possible but not easy as a small quantity of HMFCA were converted and yield of products were obtained (by 60 min only 10 % HMFCA were consumed). This result is consistent to Fig. 3.5, when HMF is fully converted, the generated HMFCA remained in a high concentration in solution, which is hard to be further catalyzed by Au/C. At present, it has been confirmed that Au alone is not highly active in oxidizing the intermediate HMFCA. Next, the performance of Pd/C alone in HMFCA oxidation is assessed to determine if HMF oxidation is with a two steps mechanism in which Au is working on HMF oxidation to HMFCA, followed by Pd in working on HMFCA oxidation to the final products.

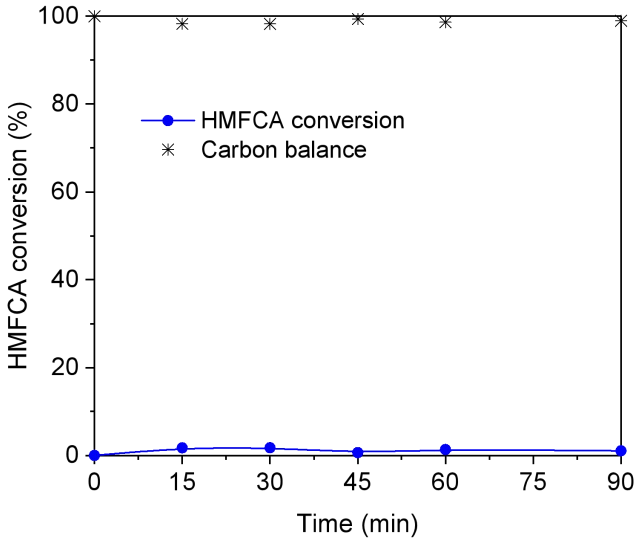

Figure 3.15. Time-on-line data of aqueous HMFCA oxidation using a monometallic Pd/C catalyst. *Reaction conditions*: HMFCA (0.1 M), $NaHCO_3$ (0.4 M), H_2O (16 mL), Pd/C: 71 mg, 80 °C, pO_2 = 3 bar, 90 min, catalyst amount: 71 mg.

Interestingly, compared to Au/C, the Pd/C alone exhibits an even lower activity in HMFCA oxidation, where there is almost no conversion throughout the entire reaction, not any products were detected, as shown in Fig. 3.15. Based on all these results from the monometallic Au/C and Pd/C, it appears neither of them are active to oxidize the HMFCA, suggesting that HMF oxidation in the presence of Au/C + Pd/C does not follow a two step mechanism, Pd/C in the physical mixture is not doing the subsequent conversion of HMFCA. Therefore, it is necessary to find other evidences in looking for the right explanation for the mechanism. Subsequently, performance of the bimetallic mixture and alloy catalysts are tested in the HMFCA oxidation reactions.

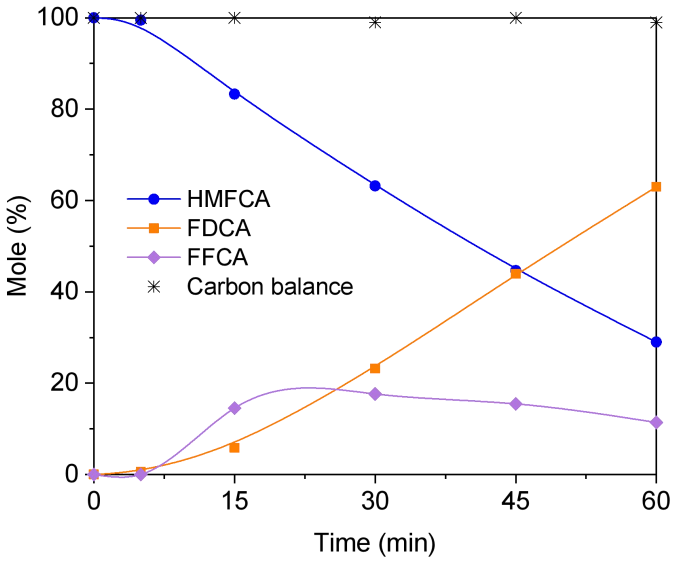

Figure 3.16. Time-on-line data of aqueous HMFCA oxidation using alloy Au-Pd/C catalyst. *Reaction conditions*: HMFCA (0.1 M), $NaHCO_3$ (0.4 M), H_2O (16 mL), 80 °C, pO_2 = 3 bar, 60 min, catalyst amount: 143.1 mg.

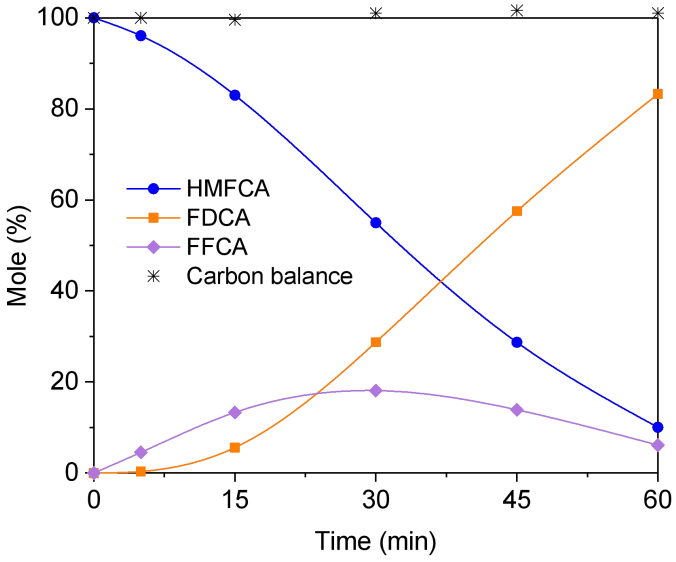

Figure 3.17. Time-on-line data of aqueous HMFCA oxidation in the presence of physical mixture Au/C + Pd/C. *Reaction conditions*: HMFCA (0.1 M), $NaHCO_3$ (0.4 M), H_2O (16 mL), 80 °C, pO_2 = 3 bar, 60 min, catalyst amount for Au/C: 72.1mg; Pd/C: 71mg.

In contrast to the monometallic Au/C and Pd/C, both showed little activity in catalyzing the intermediate product HMFCA, their bimetallic catalyst of alloyed Au-Pd/C and physical mixture Au/C + Pd/C exhibit good behaviors in converting the HMFCA to FFCA and FDCA, as shown in Fig.3.16 and Fig.3.17. Approximately 90% of HMFCA is converted after 60 min over the mixture catalyst while a 70% conversion for the alloy. Similar to literature, scientists had observed that both Au-Pd and Au can catalyze the HMFCA oxidation but not the Pd[28]. It is therefore concluded that synergy exist between the Au and Pd in the oxidation of intermediate HMFCA both in the presence of alloy and physical mixture too. Close to HMF oxidation, this synergy is manifested stronger in the presence of physical mixture than alloy, as compared in Fig. 3.18, in which the mixture catalyst displayed the highest HMFCA conversion than any other alloy or monometallics during the whole reaction.

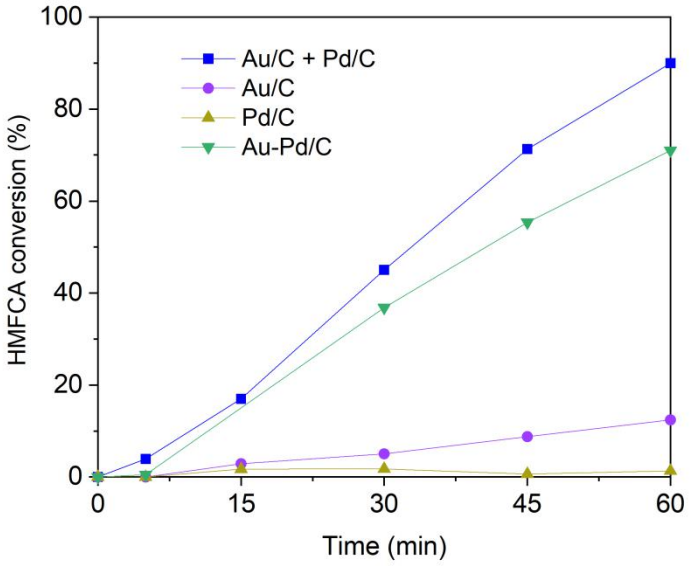

Figure 3.18. Compared data of aqueous HMFCA oxidation in the presence of physical mixture Au/C + Pd/C, Au-Pd/C alloy and monometallics. *Reaction conditions*: HMFCA (0.1 M), $NaHCO_3$ (0.4 M), H_2O (16 mL), 80 °C, pO_2 = 3 bar, 60 min, catalyst amount for Au/C: 72.1mg; Pd/C: 71mg; Au-Pd/C: 143.1 mg.

It is surprising to observe a promoted activity in HMFCA oxidation when the Au and Pd were in the presence of physical mixture as well as synergy were observed in HMF oxidation previously. It concludes that the catalysis from physical mixture is not restricted to only one molecule but to different ones.

Analogous to the oxidation of intermediate product HMFCA, the second intermediate product FFCA was tested over bimetallic and monometallic of Au and Pd in the same way. Fig. 3.19 shows that Pd is not able to make the conversion of FFCA to FDCA, whereas Au can do this job (an over 50% FDCA yield is achieved by 60 min). This result is under expectation since previously observed that Au is a good catalyst in oxidizing the aldehyde group in HMF into HMFCA, therefore it is rational to observe a high activity using Au in FFCA oxidation as FFCA molecule has aldehyde functional group as well. The alloy Au-Pd/C catalyst has close to the performance to Au and Pd in the presence of physical mixture, though the physical mixture is still showing a bit higher activity than the alloy.

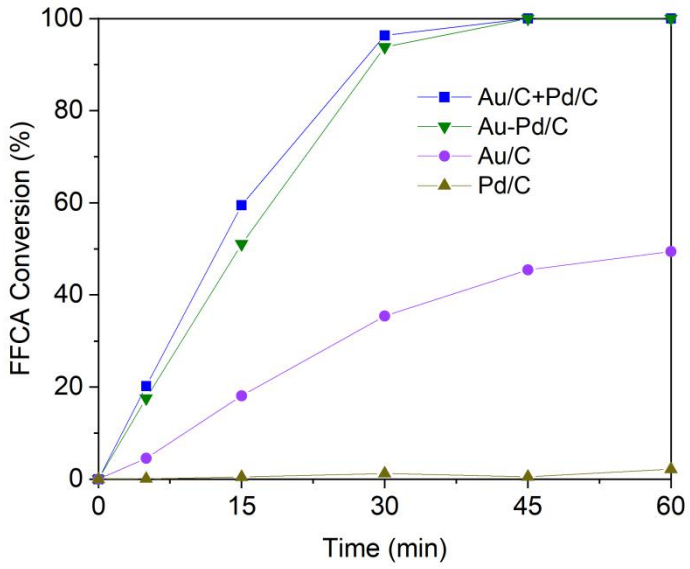

Figure 3.19. Time-on-line data of aqueous FFCA oxidation using Pd/C. *Reaction conditions*: FFCA (0.1 M), $NaHCO_3$ (0.4 M), H_2O (16 mL), Pd/C: 71 mg, 80 °C, pO_2 = 3 bar, 60 min, catalyst amount for Au/C: 72.1mg; Pd/C: 71mg; Au-Pd/C: 143.1 mg.

According to all these experimental results from intermediate product oxidation, the same catalysis trend is observed from catalysts series tested, namely: Au/C + Pd/C > Au-Pd/C > Au/C >> Pd/C. As a result, it is able to draw Scheme 3.2, where activity from each catalyst is displayed on each step of HMF oxidation. It is displayed that Au/C is preferentially able to convert products of HMF and FFCA, during process the aldehyde group is transformed into carboxylic acid group, however to convert the first intermediate product HMFCA seems hard, presumably because this step contains a higher energy barrier[32,35]. In contrast, HMFCA could be efficiently converted over catalyst of Au and Pd bimetallics presumably due to the synergistic effect in catalysis. Overall, the Pd alone is not working efficiently through all the steps in HMF oxidation, nevertheless without Pd, Au cannot convert HMFCA rapidly. Therefore, it is assumed that Pd must play a specific role in the bimetallic catalysis, promoting the Au for converting each compound in HMF oxidation to a higher activity. To understand deep further of HMF oxidation, kinetic analysis were therefore operated, the reaction rate *v* and its rate constant *k* from each step of HMF oxidation were calculated and exhibited in Table 3.2 and Table 3.3, the calculation is based on a first order reaction to the concentration of base in aqueous oxidation of HMF and FFCA, and a zero order reaction in aqueous oxidation of HMFCA[27]. Rate of HMFCA and FFCA oxidation were estimated from fittings in Fig. 3.20, where the rate constant number *k* follows a same trend as the activity trend, namely: Au/C + Pd/C > Au-Pd/C > Au/C > Pd/C, see Table 3.3. Meanwhile, the definite value follows $k_1 \approx k_3 >> k_2$, indicating oxidation of HMF and FFCA contain similar numbers of activation energies (k_1 and k_3), however oxidation of HMFCA is harder (k_2) with a higher activation energy.

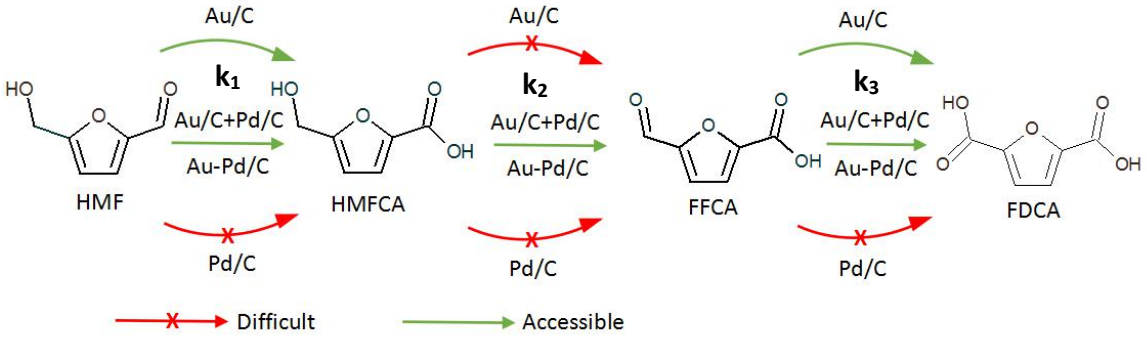

Scheme 3.2. Performances of mono and bimetallic Au and Pd catalysts in each step of aqueous HMF oxidation and its rate constant k.

Reaction rate equations:

$$V_{\text{HMF to HMFCA}} = k_1\,[NaHCO_3] \rightarrow k_1 = V_{\text{HMF to HMFCA}} / [NaHCO_3];$$

$$V_{\text{HMFCA to FFCA}} = k_2 \rightarrow k_2 = V_{\text{HMFCA to FFCA}};$$

$$V_{\text{FFCA to FDCA}} = k_3\,[NaHCO_3] \rightarrow k_3 = V_{\text{FFCA to FDCA}} / [NaHCO_3].$$

Based on the measured pH number of the reaction solution before and after reaction, pH=8.7, it is known that $[NaHCO_3] = 10^{-5.3}$ mol.L^{-1}. Each reaction rate (v) over different catalysts were calculated based on linear fitting in Fig. 3.20 below, followed by the calculation of rate constant k, see Table 3.3.

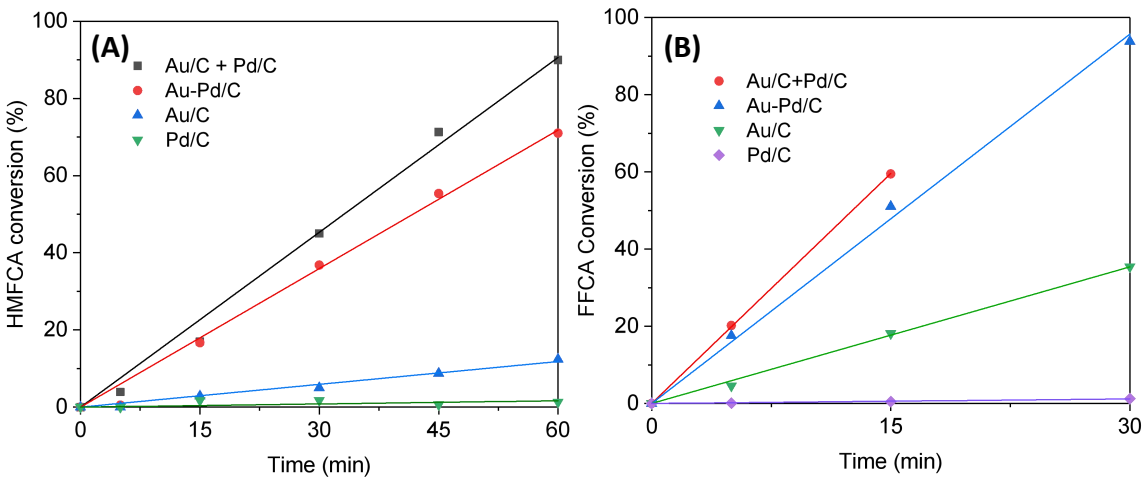

Figure 3.20. Linear fitting of conversion *vs*. time in aqueous (**A**) HMFCA oxidation; (**B**) FFCA oxidation over catalysts of physical mixture, alloy, monometallic Au and Pd.

Table 3.2. Reaction rate for each step in aqueous HMF oxidation over series of AuPd catalysts.

Catalyst	Reaction rate V, $mol.L^{-1}.s^{-1}$		
	V^a HMF to HMFCA	V^b HMFCA to FFCA	V^c FFCA to FDCA
Au/C + Pd/C	4.7×10^{-5}	2.4×10^{-5}	5.4×10^{-5}
Au-Pd/C	3.4×10^{-5}	1.9×10^{-5}	5.1×10^{-5}
Au/C	2.4×10^{-5}	3.2×10^{-6}	1.9×10^{-5}
Pd/C	1.2×10^{-6}	8.4×10^{-7}	8.4×10^{-7}

Note:

a: Reaction rate in HMF oxidation were calculated based on Fig. 3.3-3.6

b: Reaction rate in HMFCA oxidation were calculated based on the slop in Fig. 3.20(A)

c: Reaction rate in FFCA oxidation were calculated based on the slop in Fig. 3.20(B)

Table 3.3. Reaction rate constant for each step in aqueous HMF oxidation over series of AuPd catalysts.

Catalyst	Rate constant, k		
	k_1, s^{-1}	k_2, $mol.L^{-1}.s^{-1}$	k_3, s^{-1}
Au/C + Pd/C	9.3	2.4×10^{-5}	10.8
Au-Pd/C	6.7	1.9×10^{-5}	10.2
Au/C	4.7	3.2×10^{-6}	3.8
Pd/C	0.2	8.4×10^{-7}	0.1

From the comparison of rate constant number and reaction rate, it is clearly observed that Pd is working inefficiently in both alcohol and aldehyde oxidation. To consider the role of Pd/C in catalysis of the bimetallics, specifically in the physical mixture, another hypothesis was raised, that the superior performance from physical mixture in HMF oxidation may originate from a new alloy structure formed during the reaction because of the nanoparticles migration under the given reaction condition (80°C, 3 bar O_2, pH = 8.7). In the next section, the characterization of the mixed catalyst by microscopy with EDX is performed, to identify if there is any metal migration among Au and Pd nanoparticles. Furthermore, the catalyst is recycled in the same reaction and under same reaction conditions for 3 times to confirm the effect from the metal migration in the physical mixture if there is any.

3.5 Re-usability of physical mixture Au/C + Pd/C

The physical mixture Au/C + Pd/C catalyst was reused for 3 cycles, see Fig. 3.21 and after each cycle the catalyst was washed with 500 mL distilled water followed by 250 mL acetone and then dried at 110 °C for 16 h[36]. No noticeable catalytic deactivation was observed over three usage cycles, indicating the catalyst is stable in reaction. In fact the HMF conversion was enhanced slightly in the second and third cycle, which is possibly due to the gradual removal of PVA ligands during the reaction[37,38].

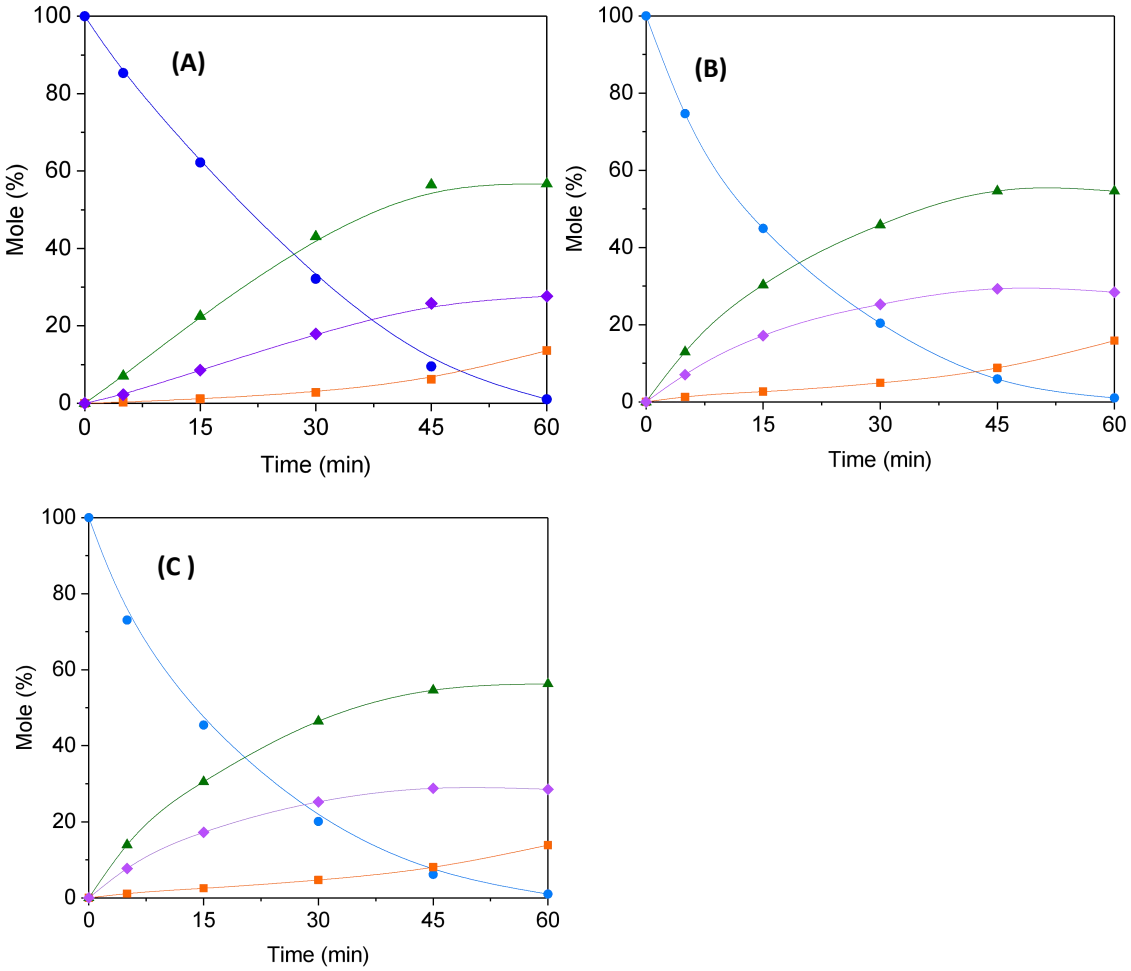

Figure 3.21. Re-usability data for the physically mixed Au/C + Pd/C catalyst in (**A**) first cycle; (**B**) second cycle; (**C**) third cycle. *Reaction conditions:* HMF (0.1 M), $NaHCO_3$ (0.4 M), H_2O (16 mL), Au/C: 72.1 mg, Pd/C: 71 mg, 80 °C, pO_2 = 3 bar, 60 min. *Key*: HMF (●); HMFCA (▲); FFCA (♦); FDCA (■).

At the same time, post-reaction samples from the recycle test were all analyzed by MP-AES whereby no metal was observed in solution, suggesting the high catalyst stability was due not to migration of the metals. Furthermore, STEM-EDX analysis for the physically mixed Au/C + Pd/C sample after use confirms no identification of metal migration for alloying (Fig. 3.22). This result is consistent to the lack of any observed deactivation and loss of FDCA yield over three uses of the mixture catalyst.

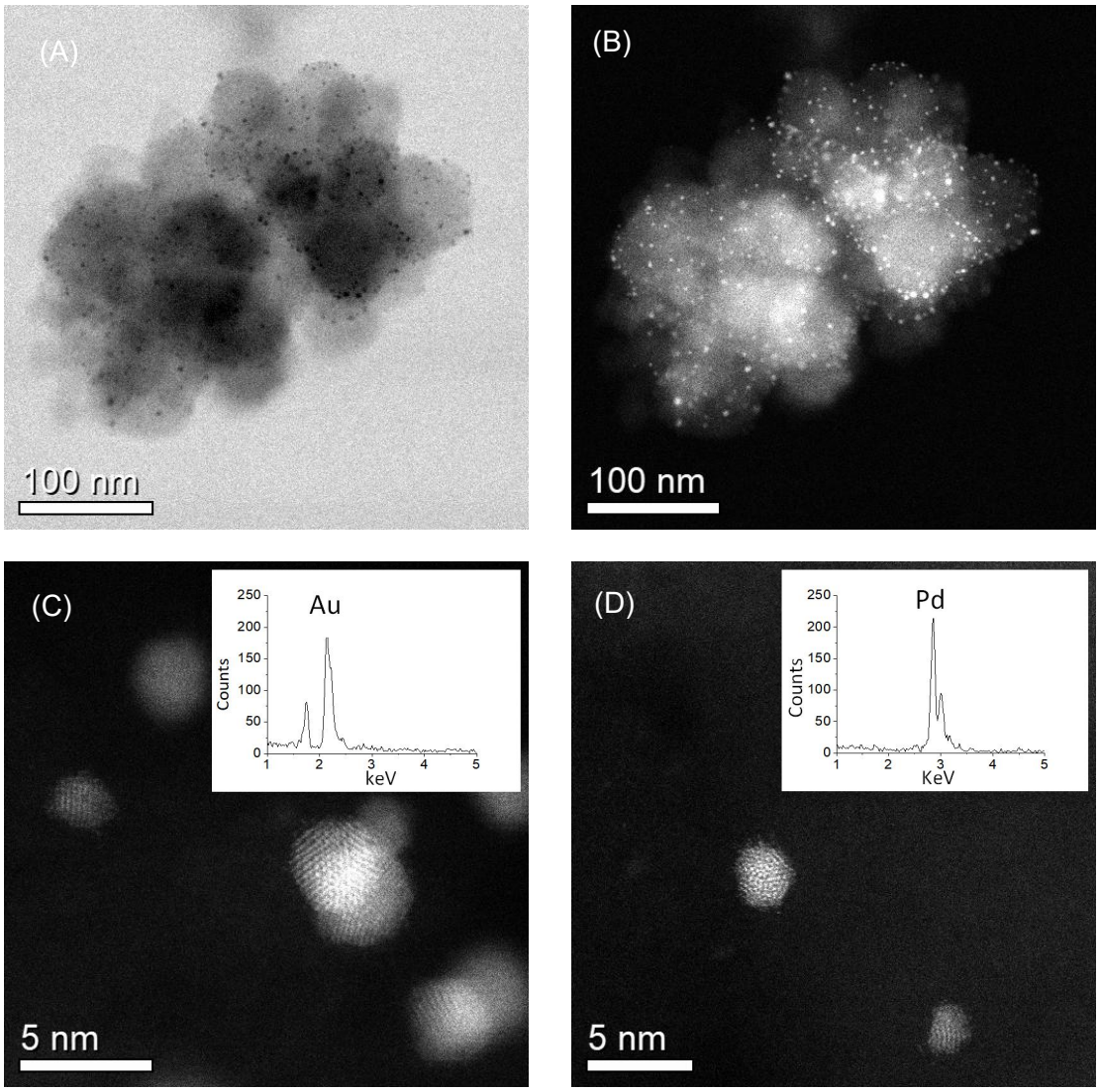

Figure 3.22. Electron microscopy and EDX analysis of Au/C + Pd/C (physical mixture) sample after use as a catalyst: (**A**) and (**B**) Complementary pair of BF- and HAADF-STEM images showing metal nanoparticle size and spatial distribution; Atomic resolution HAADF-STEM images of (**C**) a C grain supporting Au particles and (**D**) a C grain supporting Pd particles confirming that the Au and Pd essentially remain separated. All the images were obtained by Dr. Sultan M. Althahban from Lehigh University.

In an effort to explain the slight increase of activity from the physical mixture in the second recycle, a fresh catalyst was placed into hot water (80 °C) for 1 h to remove the PVA ligands. This experiment was operated in the same manner as HMF oxidation, except for the absence of HMF molecules. Afterward, the catalyst was washed with water and acetone for a recycle test. From the result presented in Fig. 3.23, it is found this treated catalyst of physical mixture has indeed exhibited an enhanced activity in terms of HMF consumption compared to the fresh catalyst, presumably it is a result from the removal of some PVA ligands.

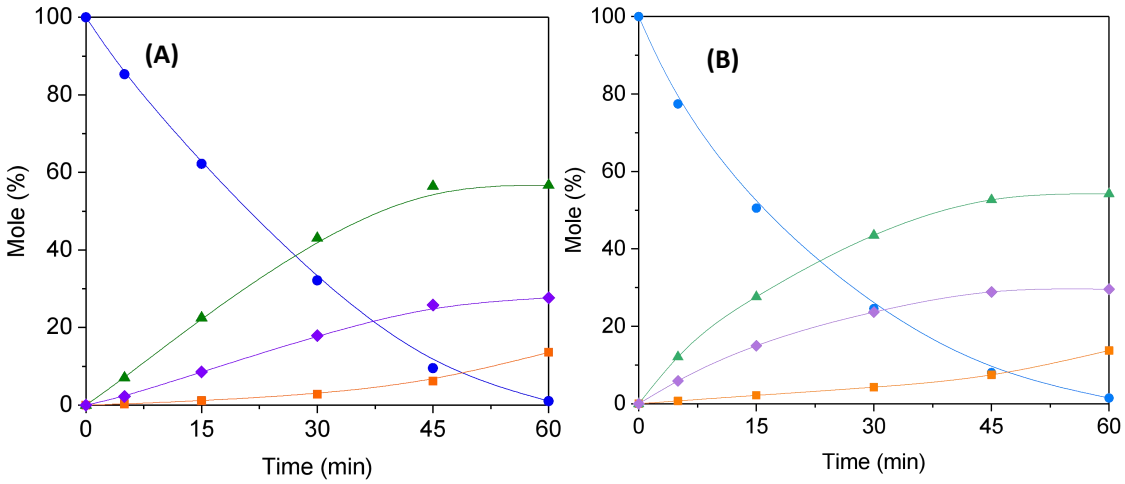

Figure 3.23. Catalytic performance of (**A**) a freshly made of Au/C + Pd/C catalyst without and (**B**) Au/C + Pd/C catalyst with pretreatment. *Reaction conditions*: HMF (0.1 M), $NaHCO_3$ (0.4 M), H_2O (16 mL), Au/C: 72.1 mg, Pd/C: 71 mg, 80 °C, pO_2 = 3 bar, 60 min. *Key*: HMF conversion (●); HMFCA yield (▲); FFCA yield (♦); FDCA yield (■).

Based on all the evaluations of catalyst reusability and microscopy characterization for the used catalyst, the superior catalysis from physical mixture over alloy in HMF oxidation can't be ascribed to the structure change during the reaction. Instead, the mixture of Au/C and Pd/C in reaction stays quite stable where there is no metal

migration between the counterparts observed, neither metal leaching in the post reaction solution. In compare to literature, researchers find the physical mixture of Au and Pd nanoparticles supported on active carbon G60 start to be alloyed after a 30 min reaction in benzyl alcohol oxidation and the metal migration become more prominent after 1 hour (See Fig. 1.5 in *Chapter 1*). The reason why there is a change of structure in catalyst however there is not in this work could be that the G60 carbon has a much smaller surface area (60 m^2/g) than the carbon black XC-72R (324 m^2/g, see Table S5 in *Appendix*) we use, allowing a higher chance for the meet up of Au and Pd.

3.6 Summary

As a preliminary conclusion of all these experiments, bimetallic AuPd supported on C was discovered to be a more active catalyst in the presence of physical mixture than alloy. Counterparts from the mixture catalyst showed a much lower reaction rate, indicating the catalysis from mixture is not a simple addition from Au/C and Pd/C. The synergistic effect that exists between Au and Pd significantly improves the catalytic behavior. HMF oxidation is a consecutive oxidation since it has two intermediates before reaching the final product FDCA. Reactions start from each intermediate over the same series of catalysts draw the conclusion that Au alone is active in oxidizing the aldehyde group into carboxylic acid, *e.g.*, HMF to HMFCA; FFCA to FDCA. However, to catalyze the alcohol group, cooperation between Au and Pd seems to be necessary, the estimation of rate constant k shows a consistent result, the alcohol oxidation from intermediate HMFCA to FDCA is the rate limiting step. The two step reaction in *Section 3.3* shows the participation of Pd/C is crucial for the catalysis, though the Pd/C alone exhibited low activity in every step of HMF oxidation. Finally, the physical mixture catalyst was found to be quite stable after being reused for 3 cycles, during which no metal migration was observed from the characterization of microscopy and elemental analysis.

3.7 References

1 W. C. Ketchie, M. Murayama and R. J. Davis, *J. Catal.*, 2007, **250**, 264–273.

2 N. Dimitratos, F. Porta, L. Prati and A. Villa, *Catal. Letters*, 2005, **99**, 181–185.

3 H. Daly, A. Goguet, C. Hardacre, F. C. Meunier, R. Pilasombat and D. Thompsett, *J. Catal.*, 2010, **273**, 257–265.

4 D. Wang, A. Villa, P. Spontoni, D. S. Su and L. Prati, *Chem. - A Eur. J.*, 2010, **16**, 10007–10013.

5 W. Li, A. Wang, X. Liu and T. Zhang, *Appl. Catal. A Gen.*, 2012, **433**–**434**, 146–151.

6 T. Déronzier, F. Morfin, M. Lomello and J. L. Rousset, *J. Catal.*, 2014, **311**, 221–229.

7 J. Long, H. Liu, S. Wu, S. Liao and Y. Li, *ACS Catal.*, 2013, **3**, 647–654.

8 A. Villa, M. Schiavoni, S. Campisi, G. M. Veith and L. Prati, *ChemSusChem*, 2013, **6**, 609–612.

9 M. Doyen, K. Bartik and G. Bruylants, *J. Colloid Interface Sci.*, 2013, **399**, 1–5.

10 E. Giorgetti, P. Marsili, S. Cicchi, L. Lascialfari, M. Albiani, M. Severi, S. Caporali, M. Muniz-Miranda, A. Pistone and F. Giammanco, *J. Colloid Interface Sci.*, 2015, **442**, 89–96.

11 J. K. Edwards, J. Pritchard, M. Piccinini, G. Shaw, Q. He, A. F. Carley, C. J. Kiely and G. J. Hutchings, *J. Catal.*, 2012, **292**, 227–238.

12 Z. Hasan, N. Ullah, S. Ullah and A. Kakar, *J. Anim. Plant Sci.*, 2015, **25**, 532–535.

13 C. A. Antonyraj, N. T. T. Huynh, S. K. Park, S. Shin, Y. J. Kim, S. Kim, K. Y. Lee and J. K. Cho, *Appl. Catal. A Gen.*, 2017, **547**, 230–236.

14 A. Tiwari, H. K. Patra and X. Wang, *Advanced Materials Interfaces*, John Wiley & Sons, 2016.

15 K. H. J. Buschow, R. W. Cahn, M. C. Flemings, B. Ilschner, E. J. Kramer and S. Mahajan, *Sci. Technol.*

16 O. Casanova, S. Iborra and A. Corma, *ChemSusChem*, 2009, **2**, 1138–1144.

17 A. Sandoval, A. Aguilar, C. Louis, A. Traverse and R. Zanella, *J. Catal.*, 2011, **281**, 40–49.

18 A. K. Sinha, S. Seelan, S. Tsubota and M. Haruta, *Top. Catal.*, 2004, **29**, 95–102.

19 R. J. Chimentão, F. Medina, J. L. G. Fierro, J. Llorca, J. E. Sueiras, Y. Cesteros and P. Salagre, *J. Mol. Catal. A Chem.*, 2007, **274**, 159–168.

20 A. S. K. Hashmi and G. J. Hutchings, *Angew. Chemie - Int. Ed.*, 2006, **45**, 7896–7936.

21 O. Casanova, S. Iborra and A. Corma, *ChemSusChem*, 2009, **2**, 1138–1144.

22 B. P. C. Hereijgers and B. M. Weckhuysen, *J. Catal.*, 2010, **270**, 16–25.

23 M. J. Climent, A. Corma, J. C. Hernández, A. B. Hungría, S. Iborra and S. Martínez-Silvestre, *J. Catal.*, 2012, **292**, 118–129.

24 Y. Guan and E. J. M. Hensen, *J. Catal.*, 2013, **305**, 135–145.

25 S. Kanungo, D. M. Perez Ferrandez, F. Neira D'Angelo, J. C. Schouten and T. A. Nijhuis, *J. Catal.*, 2016, **338**, 284–294.

26 S. E. Davis, L. R. Houk, E. C. Tamargo, A. K. Datye and R. J. Davis, *Catal. Today*, 2011, **160**, 55–60.

27 S. E. Davis, A. D. Benavidez, R. W. Gosselink, J. H. Bitter, K. P. De Jong, A. K. Datye and R. J. Davis, *J. Mol. Catal. A Chem.*, 2014, **388**–**389**, 123–132.

28 A. Lolli, S. Albonetti, L. Utili, R. Amadori, F. Ospitali, C. Lucarelli and F. Cavani, *Appl. Catal. A Gen.*, 2015, **504**, 408–419.

29 S. Albonetti, A. Lolli, V. Morandi, A. Migliori, C. Lucarelli and F. Cavani, *Appl. Catal. B Environ.*, 2015, **163**, 520–530.

30 Q. He, S. J. Freakley, J. K. Edwards, A. F. Carley, A. Y. Borisevich, Y. Mineo, M. Haruta, G. J. Hutchings and C. J. Kiely, *Nat. Commun.*

31 S. E. Davis, B. N. Zope and R. J. Davis, *Green Chem.*, 2012, **14**, 143–147.

32 S. E. Davis, A. D. Benavidez, R. W. Gosselink, J. H. Bitter, K. P. De Jong, A. K. Datye and R. J. Davis, *J. Mol. Catal. A Chem.*, 2014, **388**–**389**, 123–132.

33 M. S. Ide and R. J. Davis, *Acc. Chem. Res.*, 2014, **47**, 825–833.

34 H. Ait Rass, N. Essayem and M. Besson, *ChemSusChem*, 2015, **8**, 1206–1217.

35 D. Lei, K. Yu, M. R. Li, Y. Wang, Q. Wang, T. Liu, P. Liu, L. L. Lou, G. Wang and S. Liu, *ACS Catal.*, 2017, **7**, 421–432.

36 M. Douthwaite, X. Huang, S. Iqbal, P. J. Miedziak, G. L. Brett, S. A. Kondrat, J. K. Edwards, M. Sankar, D. W. Knight, D. Bethell and G. J. Hutchings, *Catal. Sci. Technol.*, 2017, **7**, 5284–5293.

37 L. Abis, S. J. Freakley, G. Dodekatos, D. J. Morgan, M. Sankar, N. Dimitratos, Q. He, C. J. Kiely and G. J. Hutchings, *ChemCatChem*, 2017, **9**, 2914–2918.

38 N. Dimitratos, A. Villa, L. Prati, C. Hammond, C. E. Chan-Thaw, J. Cookson and P. T. Bishop, *Appl. Catal. A Gen.*, 2016, **514**, 267–27.

Derivation of the reaction mechanism over the Au/C + Pd/C physical mixture

4

Introduction

This primary aim of this chapter is to derive an explanation for the rate enhancements observed in the oxidation of HMF over the Au/C and Pd/C physical mixture (PM), compared to the Au-Pd/C alloy catalyst. The activity data corresponding to each of these catalytic systems was presented in *Chapter 3*. It is proposed that the rate of reaction is enhanced by facilitating electron transfer from one metal component to the other. This occurs *via* the catalyst support and therefore, the conductivity of this material is important. The enhancement is proposed to be a result of redox cooperation between Au and Pd active sites. The experimental evidence which led to these conclusions is presented herein.

4.1 Proposed mechanism for HMF oxidation over Au/C + Pd/C

The identification of any changes to the chemical states of Au and Pd during the reaction is important, as this information can be used to gain insight on the catalytic active sites. XPS is a highly versatile surface sensitive technique, commonly used to probe the elemental composition and electronic surface species in heterogeneous catalysts[1–3]. It was therefore important that the Au and Pd supported monometallic catalysts were probed by XPS, before and after the reaction with HMF.

Fig. 4.1 (A) and (B), show the survey scan of the fresh Au/C sample and its corresponding Au (4f) region, respectively, exhibiting peaks centered at binding energies (BE) of 83.6 eV and 87.4 eV, which are characteristic of spin-orbit split peaks for metallic Au[4]. Similar to Au, Fig 4.1 (C) and (D) demonstrate the survey scan of the fresh Pd/C before use and the corresponding Pd (3d) region. Analysis of the Pd (3d) region is complicated due to overlap of the region with a loss-structure of the carbon support, therefore the background has been modelled using a series of broad constrained peaks fitted from the untreated support. It is assumed that no significant change to this loss structure occurs between catalysts. Peaks centered at BE 335.6 eV and 341.0 eV are observed, both are the characteristic metallic Pd[5]. Meanwhile, a small quantity of PdO was observed; a peak centered at BE 337 eV is observed, which may be attributed to air exposure, during the handling of the Pd material. Therefore, it is conclusive that Au is present as Au (0) and Pd, predominantly exists as Pd (0) prior to the catalytic reaction.

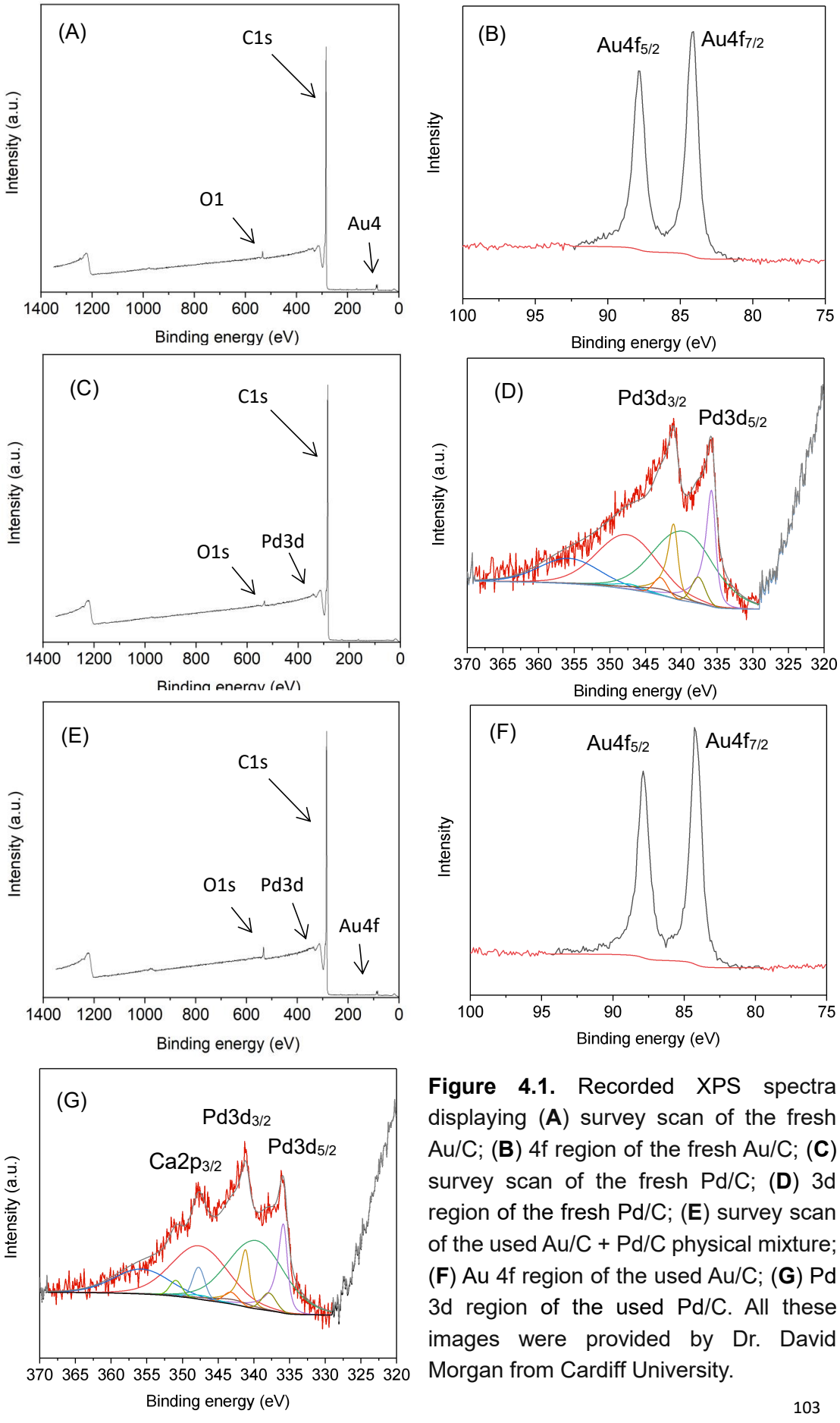

Figure 4.1. Recorded XPS spectra displaying (**A**) survey scan of the fresh Au/C; (**B**) 4f region of the fresh Au/C; (**C**) survey scan of the fresh Pd/C; (**D**) 3d region of the fresh Pd/C; (**E**) survey scan of the used Au/C + Pd/C physical mixture; (**F**) Au 4f region of the used Au/C; (**G**) Pd 3d region of the used Pd/C. All these images were provided by Dr. David Morgan from Cardiff University.

Analysis of the used catalyst are shown in Fig. 4.1 (E to G), there is no notable change to the Au spectra indicating that it remains in its metallic state during the reaction. The same can be conducted for the state of Pd in these materials; there is no evidence to suggest that an increased quantity of PdO is observed in the used catalyst, see Fig. 4.1 (G). The same peaks, indicative of Pd $3d_{5/2}$ and Pd $3d_{3/2}$ are present for both Pd (0) and Pd (2) however, the overall data envelope is changed. Another peak located at a BE of 347.2 eV is observed, which is likely to be attributed to Ca(2p)[6]. The presence of Ca is attributed to deposition from the water, The incorporation of Ca likely arises from the reactions being conducted in water, which has been observed previously and often, *e.g.*, in liquid phase reactions with H_2O_2. Here, it is not considered as one of the important factors affecting the catalysis effect.

Overall, the accurate deconvolution of Pd (3d) region is remaining inconclusive because such low levels of Pd signal (0.24 wt.% metal loading) which are swamped by the carbon loss at BE 284.8 eV. It is known that PdO can readily reduce during the analytical procedure[7]. Based on this, and the low Pd metal loading, it is difficult to conclude whether any changes in the oxidation state of the Pd occur during the reaction. For this reason, TPR was conducted on the fresh and used samples to establish whether any evidence of PdO in the used Pd/C could be obtained. The results from the TPR experiments are displayed in Fig. 4.2.

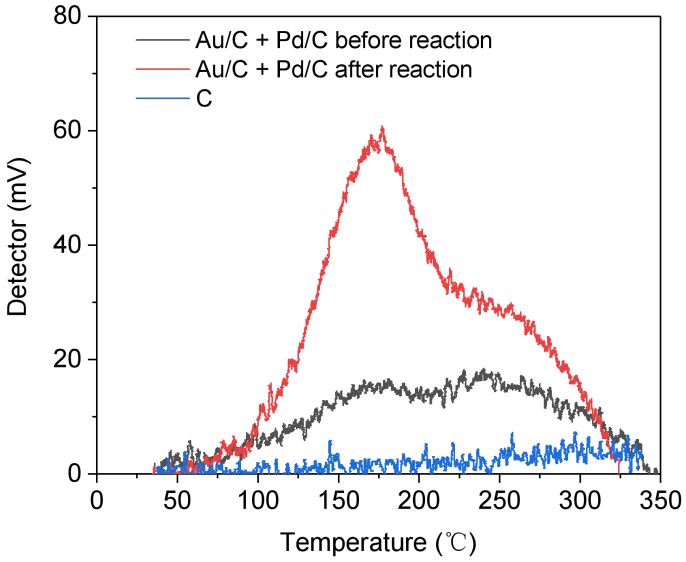

Figure 4.2. H_2 temperature programmed reduction data for a physical mixture of Au/C and Pd/C before (black) and after (red) a standard HMF oxidation reaction. An experiment with the bare C support was also conducted as a control.

In literature, it is generally known the reduction of PdO takes place at a relative low temperature, for example, PdO with support of CeO_2 can be reduced at 180°C and when it is supported on active carbon has a reduction temperature of 120 and 200°C[8], therefore PdO could be easily reduced by H_2 to form metallic Pd[9,10], however this is not absolute because the reduction process is heavily related to different support materials. From the TPR results, presented in Fig. 4.2, it is evident that there is a significantly higher TCD response observed at 170°C which may be attributed to the reduction of surface PdO in the used catalyst[11]. In the corresponding fresh catalyst, less TCD response is observed, this is likely due to the PdO over layer formed from exposure of the reduced catalyst to air. Additionally, there appears another peak at 250 °C for both the fresh and used catalysts, which was reported to be the different metal loading effect, when the metal loading is low, *e.g.*, 0.5 wt.%, two reduction peaks are going to be observed whereas only a broad peak can be found when the

loading of Pd becomes high[8], *e.g.*, 5 wt.%. In this study, the metal loading of Pd is 0.27 wt.%. A corresponding control experiment was performed on the bare C support after treatment with PVA. Tiny TCD signal is observed which could be attributed to any H_2 consumption of the functional groups on the surface of carbon. Previous studies have demonstrates that there exists, *e.g.*, lactone, phenol, quinone and other different groups on the surface of carbon, which might react under such reaction conditions in TPR measurement[12]. Given that the TCD signal is relatively small from the bare support, suggesting that the peaks observed in experiments over the fresh and used Pd/C cannot be attributed to the reactions from those surface functional groups on carbon. All these results evidence that metallic Pd nanoparticles are oxidized to PdO during aqueous HMF oxidation.

To recap from *Chapter 3*, the reaction rate over the monometallic Pd/C was significantly lower than that exhibited by the Au/C catalyst for the oxidation of HMF and each of the reaction intermediates. However, when the supported Au and Pd monometallic catalysts are combined as a physical mixture, a much higher activity was observed. Based on this and results acquired from the XPS and TPR data (Fig. 4.1 and Fig. 4.2), a mechanism can be proposed, see Fig. 4.3, detailing the role of Pd and Au sites in the reaction.

When the reaction occurs over a physical mixture of Au/C and Pd/C, it is proposed that the Au and Pd sites catalyze different reactions. Pd nanoparticles predominantly catalyze an oxygen reduction reaction (ORR), which involves the consumption of electrons. In the contrary, metallic Au nanoparticles catalyze the oxidative dehydrogenation of alcohol and aldehyde functional groups. According to previous work, the oxidation of each HMF or intermediate molecule leads to the generation of 2 electrons[13]. As such, oxidation of HMF to FDCA results in the production of 6 electrons in total, see Scheme 4.1. Given that Pd can readily undergo oxidation from Pd^0 to Pd^{2+} under aerobic conditions[14,15] it is plausible to suggest that over the physical mixture, Pd^{2+} behaves as the electron acceptor. Hence, it catalyzes the

oxygen reduction reaction with water; a process which involves the consumption of electrons and reduction of Pd^{2+} to Pd^{0}. Due to the abundant supply of oxygen and the continuous generation of electrons from the simultaneous oxidation reactions occurring on the Au sites, it is proposed that the Pd sites are engaged in a continuous redox cycle (Pd^{2+}/Pd^{0}). The role of the carbon support is equivalent important. XC72R is a highly conductive material[16], which serves as an electron transfer mediator through collisions between carbon particles in these reactions. The catalyst quantity used in these reactions amounts to 143 mg, in a volume of 16 mL reaction solution (see *Chapter 2*, reaction protocol) which may contribute to the quantity of collisions which occur.

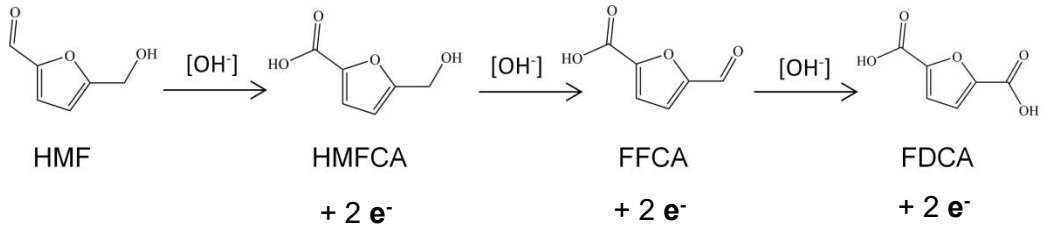

Scheme 4.1. Reaction route of aqueous HMF oxidation to terminal product FDCA.

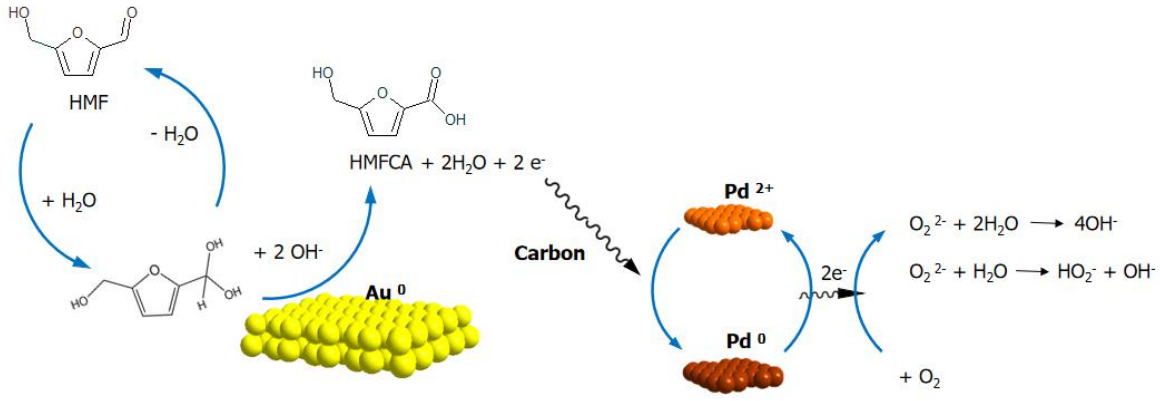

Figure 4.3. Proposed mechanism for the aqueous oxidation of HMF to HMFCA over a physical mixture of Au/C and Pd/C.

Based on this theory, an illustrative representation is presented for HMF oxidation to HMFCA, see Fig. 4.3. Over metallic Au, oxidation of HMF to HMFCA proceeds *via* a dehydrogenation reaction on the Au surface, where two protons are generated and neutralized in solution, this process was well studied and known from literature[13]. Furthermore, these electrons generated in this process are transferred to a PdO site, where they are consumed in an ORR leading to the liberation of the Au active site. The oxidation mechanism of HMFCA and FFCA proceeds through similar steps, generating electrons and protons until the terminal reaction product (FDCA) is produced. As such, the rate of alcohol/aldehyde oxidation over supported Au catalysts was suggested to be largely dependent on the rate of the simultaneous ORR occurring on the Pd. However, the lower activity observed over the Au-Pd alloy catalyst compared to the physical mixture, is explained by the change in the redox properties of Pd when it is alloyed with Au[17]. This change slows down the redox cycle rate of Pd and the consumption rate of the electrons generated by the oxidation of HMF over Au. To further highlight this process, a more detailed representation is provided (Fig. 4.4.)[5].

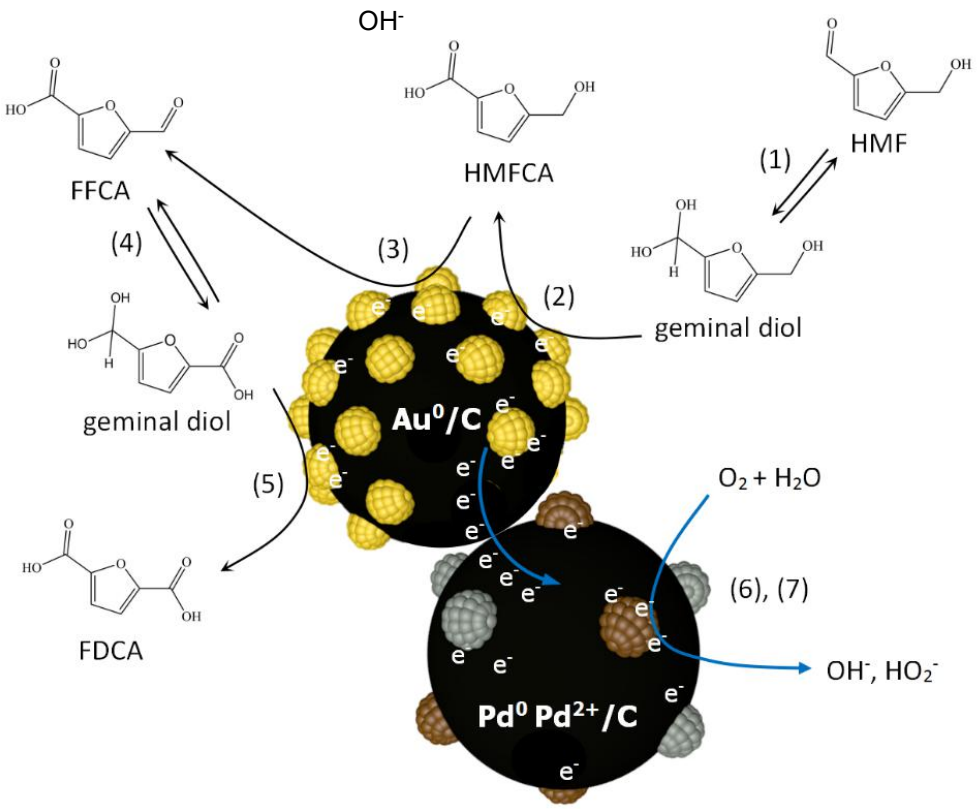

Figure 4.4. A proposed mechanism for aqueous HMF oxidation to FDCA over a physical mixture of Au/C and Pd/C. This figure highlights the significance of collisions between C grains, which is proposed to facilitate electron transfer. Corresponding reaction steps (1) - (7) are listed below.

Step (1): $C_6H_6O_3$ (HMF) + H_2O $\rightleftharpoons$ $C_6H_8O_4$ (*gem*-diol)

Step (2): $C_6H_8O_4$ (*gem*-diol) + 2 OH^- $\xrightarrow{Au^0}$ $C_6H_6O_4$ (HMFCA) + 2 H_2O + 2 e^-

Step (3): $C_6H_6O_4$ (HMFCA) + 2 OH^- $\xrightarrow{Au^0}$ $C_6H_4O_4$ (FFCA) + 2 H_2O + 2 e^-

Step (4): $C_6H_4O_4$ (FFCA) + H_2O $\overset{OH^-}{\rightleftharpoons}$ $C_6H_6O_5$ (*gem*-diol)

Step (5): $C_6H_6O_5$ (*gem*-diol) + 2 OH^- $\xrightarrow{Au^0}$ $C_6H_4O_5$ (FDCA) + 2 H_2O + 2 e^-

Step (6): O_2 + 2 H_2O + 4 e^- $\xrightarrow{Pd^0/Pd^{2+}}$ 4 OH^-

Step (7): O_2 + H_2O + 2 e^- $\xrightarrow{Pd^0/Pd^{2+}}$ HO_2^- + OH^-

Fig. 4.4 illustrates how electrons generated from substrate dehydrogenation on the surface of Au are shuttled from one C grain to another through collisions. Herein, it is therefore hypothesized that the C support, due to the high conductivity, plays an important role to facilitate the electron transfer; the carbon used as a support in these reactions, the carbon XC72R, is usually applied in fuel cell materials due to its chemical physical properties[18]. To further investigate the importance of this electron transfer, next, the reactivity of physical mixtures of Au and Pd catalysts with different supports were investigated, to establish whether the rate of reaction is suppressed when C is replaced by other non- or less conductive supports.

4.2 Catalysis by combination of different supports

As discussed, the carbon (Vulcan XC-72R) is proposed to have an important role in the enhancement observed in reactions over a mixture of monometallic Au/C and Pd/C. This highly conductive support is proposed to serve as a medium to transport electrons generated from Au to Pd. To acquire further evidence for this hypothesis, a series of additional experiments were conducted. These involved synthesizing and testing different combinations of monometallic Au and Pd catalysts supported on C, TiO_2 and boron nitrite (BN). TiO_2 and BN were selected as the additional supports, as they are considered to be semi-conductive and non-conductive, respectively[19,20]. As shown in Fig.4.5, each of the monometallic Pd catalysts exhibited very little activity, when they were tested for HMF oxidation in the absence of Au (product yield < 2%). Interestingly, when Au/C was combined with Pd/BN in a physical mixture, the yield of products was comparable to the sum of products produced in the reactions using the Au/C and Pd/BN independently. This indicates that it is unlikely that this co-operative effect is prevalent in the reactions with Au/C and Pd/BN. Given, that BN is considered to be non-conductive, it provides evidence for the hypothesis discussed in *Section 4.1*.

An analogous experiment was subsequently conducted using a physical mixture of Au/C and Pd/TiO_2. In this case, the yields of the products formed were notably greater than a simple sum of the products produced in the corresponding reaction over monometallic Au/C and Pd/TiO_2 catalysts independently. It is possible that the enhancement observed is attributed to the semi-conductive nature of TiO_2. It is therefore plausible to suggest that the rate of reaction on the Au-supported component is promoted by electron transfer to the Pd/TiO_2. Among all the tested mixtures in Fig. 4.5, Au/C + Pd/C remained the most active. All the various combinations and control experiments conducted are presented in Table 4.1. All these results provide further evidence that the electronic properties of the material used as support for Au and Pd nanoparticles has a significant impact to the initial rate of reaction.

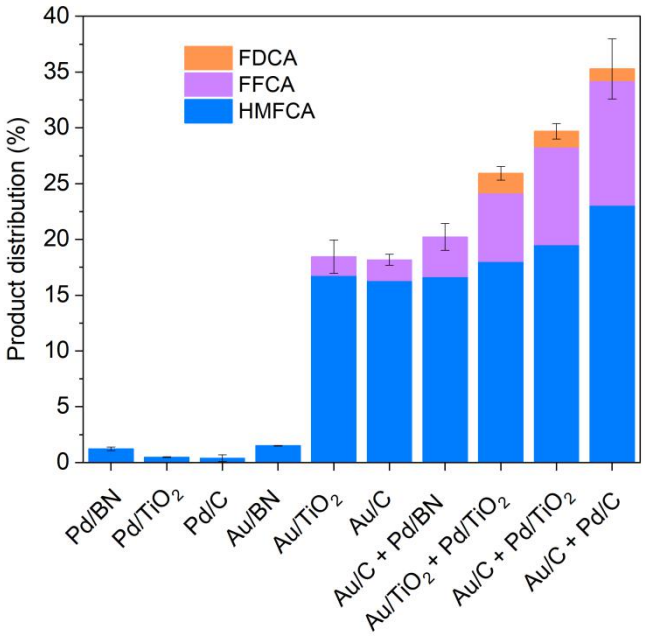

Figure 4.5. Product yield distribution for aqueous oxidation of HMF over physical mixtures of different catalysts or supports. *Reaction conditions*: HMF (0.1M); $NaHCO_3$ (0.4 M); H_2O (16 mL); 80 °C; pO_2 = 3 bar; supported Au catalyst (72.1mg); supported Pd catalyst (71 mg), 15 min.

Table 4.1. Conversion and activity of various catalysts for the aqueous phase aerobic oxidation of HMF, after 15 min of reaction. Error bars are calculated by standard deviation of results from each reaction. *Reaction conditions*: HMF (0.1M); $NaHCO_3$ (0.4 M); H_2O (16 mL); 80 °C; pO_2 = 3 bar; supported Au catalyst (72.1mg); supported Pd catalyst (71 mg), 15 min.

Entry	Catalyst	HMF conversion (%)	Error bar	Rate ($mmol.L^{-1}.h^{-1}$)
1	Au/C	20.5	±0.5	82.0
2	Au/TiO_2	19.1	±1.3	76.4
3	Au/BN	1.2	±0.03	4.8
4	Pd/C	1.0	±0.37	4.0
5	Pd/TiO_2	1.4	±0.03	5.6
6	Pd/BN	2.8	±0.16	11.2
7	Au-Pd/C	30.7	±3.5	122.8
8	$Au\text{-}Pd/TiO_2$	38.3	±2.1	153.2
9	Au/C + Pd/C	40.9	±2.7	163.6
10	Au/TiO_2 + Pd/TiO_2	26.8	±0.6	107.2
11	Au/C + Pd/TiO_2	35.0	±0.7	140.0
12	Au/TiO_2 + Pd/C	29.4	±1.67	117.6
13	Au/BN + Pd/C	18.8	±0.4	75.2
14	Au/C + Pd/BN	24	±1.2	96.0
15	Au/BN + Pd/BN	3.7	±0.19	14.8

The results listed in Table 4.1 are for short reactions, lasting for 15 min. This is important to effectively compare each of the catalytic systems as an initial rate. To further explore the enhancements observed over physical mixtures of monometallic reactions, a series of additional experiments were conducted where one component of each mixture was added during the reaction. For these reactions, sampling was conducted to accurately monitor how the rates of HMF conversion and products produced are influenced over time. The reaction rate was compared with a corresponding time online reaction over a corresponding monometallic component. Fig. 4.6 (A) and (B) shows how the rate is influenced upon addition of Pd/TiO_2 after running a standard HMF oxidation over Au/TiO_2 for 15 min, rates are exhibited in Table 4.2, where the monometallic Au/TiO_2 shows a rate of 0.056 $M.h^{-1}$ during 0-15 min of HMF oxidation however the physical mixture of Au/TiO_2 and Pd/TiO_2 has a rate of 0.075 $M.h^{-1}$ during 15-30 min, which is 1.4 times higher with the presence of Pd/TiO_2. After a 60 min reaction, about 65% HMF was consumed over the monometallic Au/TiO_2, find in Fig. 4.6 (A). However, 75% of HMF was consumed after the Pd/TiO_2 was added to the Au/TiO_2. In assumption, this 10% enhancement is due to the additional electron transfer from Au to Pd *via* the semi conductiveTiO_2, which avails the Au more active sites for the consecutive reactions.

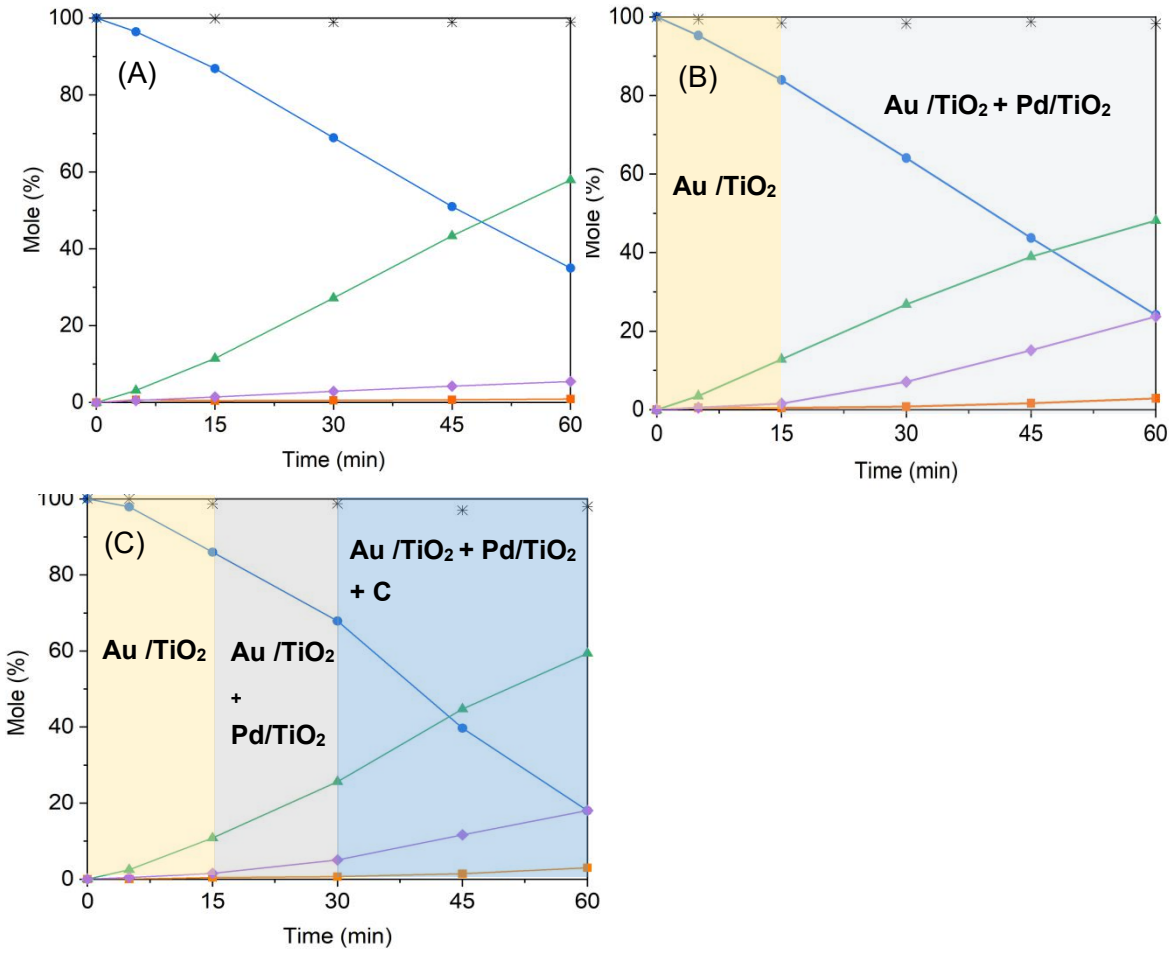

Figure 4.6. Catalytic performance for aqueous HMF oxidation (**A**) over monometallic Au/TiO_2; (**B**) using Au/TiO_2 followed by the addition of Pd/TiO_2 after 15 min; (**C**) using Au/TiO_2 followed by the addition of Pd/TiO_2 after 15 min and addition of C after 30 min. *Key*: FDCA yield (■), FFCA yield (♦), HMFCA yield (▲), HMF conversion (●), mass balance (*). *Reaction conditions*: HMF (0.1 M); $NaHCO_3$ (0.4 M); H_2O (16 mL); 80 °C; pO_2 = 3 bar; catalyst amounts for Au/TiO_2: 72.1 mg; Pd/TiO_2: 71 mg; C: 71 mg.

Table 4.2. Rate calculation based on Fig. 4.6, showing the effect from addition of extra Pd/TiO_2 and C.

Entry	Catalyst	Reaction time (min)	Rate ($M.h^{-1}$)
1	Au/TiO_2	0—15	0.056
2	Au/TiO_2 + Pd/TiO_2	15—30	0.075
3	Au/TiO_2 + Pd/TiO_2 + C	30—45	0.115

In parallel, another experiment involving three distinct steps was performed. In Fig. 4.6 (C), HMF oxidation over Au/TiO_2 was firstly conducted for 15 min (light yellow area on the left) ahead of adding Pd/TiO_2 (light green area in the middle), which is same to the reaction from Fig. 4.6 (B). After a 30 min reaction over the physical mixture of Au/TiO_2 and Pd/TiO_2 (light blue area on the right), extra C material was added to the same reaction. The corresponding changes in reaction rate were exhibited in Table 4.2, based on each of the three reaction sections. Upon the addition of Pd/TiO_2, the reaction rate increased from 0.056 to 0.075 $M.h^{-1}$ as was discussed. Following this, upon the addition of the C to the physical mixture of Au/TiO_2 and Pd/TiO_2, the reaction rate further increased to 0.115 $M.h^{-1}$, which is a big enhancement as twice higher is the rate compare to the addition of Pd. By the other side, over 80% HMF was consumed after reaction for 60 min. C itself was previously found to have no influence on HMF oxidation (see *Chapter 3, Section 3.3*). As such, this “staircase” experiment has provided further evidence that the role of C in the proposed hypothesis is correct; C facilitates electron transfer from one metal component to the other in reactions over physical mixtures of Au/C and Pd/C catalysts.

Subsequently, analogous experiments were conducted where quantities of C, TiO_2 and BN were added to reactions containing physical mixtures of monometallic Au and Pd supported catalysts (Fig. 4.7). The addition of C to a physical mixture of Au/TiO_2

and Pd/TiO_2 resulted in a notable increase in catalytic reactivity based on the mass of C added. On the contrary, the addition of less conductive TiO_2, or non-conductive BN, to a physical mixture of Au/C and Pd/C led to a decrease in the rate of reaction; the suppression was greatest in the reactions where BN was added. These experiments suggest that substrate conversion over physical mixtures of Au and Pd monometallic catalysts can be enhanced, or suppressed, through the incorporation of additives which are electronically conductive, but are not by themselves catalytically active.

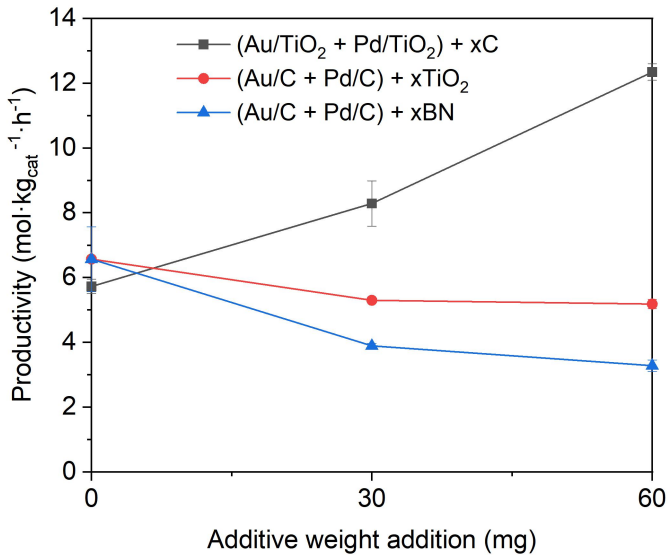

Figure 4.7. The addition of increasing amounts of either carbon, TiO_2 or BN to various physical mixtures and its effect on productivity. Supported Au catalyst: 15 mg; supported Pd catalyst: 15 mg, reaction time of 30 min.

Based on the reactions discussed in this section of work, it is clear that the catalyst support dramatically influences the rates of reaction over physical mixtures of monometallic catalysts. In the next section, further evidence for the proposed electron transfer is acquired through use of various electrochemical experiments.

4.3 Evidences of electron transfer by short circuit current experiment

To support the idea that electrons are transferred from gold sites to palladium sites during the aerobic oxidation of HMF, a series of electrochemical experiments were conducted. The first experiment, involving a short-circuit current (SCC) measurement, was performed to establish the charge transfer. This technique is typically used to evaluate the performance of batteries, fuel- or photovoltaic cells[21] and consists of measuring the maximum current generated over the time in an electrical/electrochemical system, when the associated resistance is minimal (close to zero).

For these experiments, the set-up involves connecting two electrodes, which are loaded with the components of the electrical/electrochemical system under investigation, to the positive and negative poles of an amperemeter. Here, two glassy-carbon electrodes were used to prepare the Au/C and Pd/C electrodes (see experimental part *Chapter 2, Section 2.4.6*). The two electrodes were subsequently placed in a basic aqueous solution of HMF (see Fig. 4.8). Before this however, oxygen was bubbled to the solution for at least 20 minutes at a flow rate of 150 $mL.min^{-1}$ under stirring to ensure the reaction solution was saturated with oxygen. After the electrodes are added, the flow is reduced to 50 $mL.min^{-1}$ for the duration of the experiment to minimize any noise observed in the measured current and to avoid any undesirable loss of catalyst from electrodes.

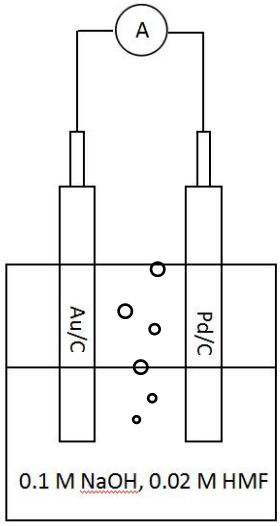

Figure 4.8. Short circuit current (SCC) measurement set-up.

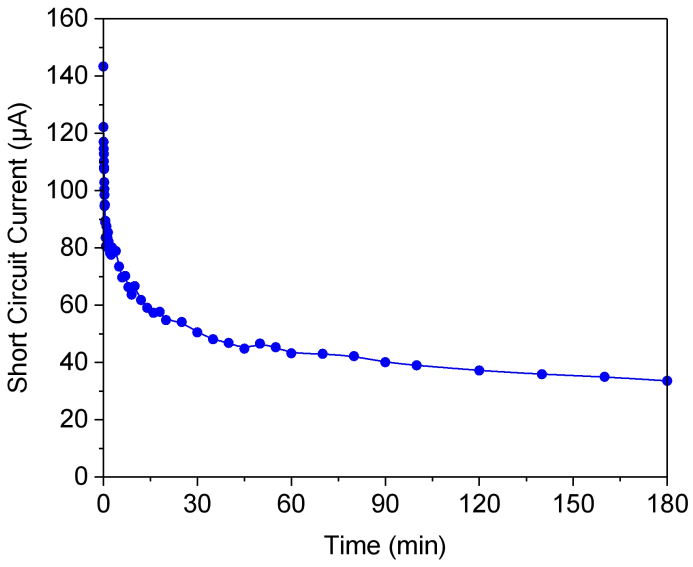

Figure 4.9. Experimental data for measuring short circuit current between Au/C and Pd/C electrodes. *Reaction conditions*: HMF (0.02 M), NaOH (0.1 M), H_2O (50 mL), room temperature, O_2 flow: 50 mL/min, 3 h.

Fig. 4.9 shows the current generated over a 3 hour reaction under constant oxygen flow in the presence of the Au/C and Pd/C electrodes. The current at the initial stage is

very high, approximately 140 μA, before it decreases and reaches a steady state value of approximately 40 μA. The decreased current, observed over time, may be attributed to the deactivation of catalyst due to likely that the Pd/C catalyst (as a whole) is dropping off the electrode. The HMF conversion observed after 3 hours was analyzed by HPLC and determined to be below 1.0 % ($9.3x10^{-8}$ $M.s^{-1}$), which is significantly lower than the rate observed in the thermocatalytic experiments (physical mixture rate at 15 min: $4.7x10^{-5}$ $M.s^{-1}$), the lower rate obtained is due to the different reaction conditions applied, where in thermal catalysis, the reaction temperature (80°C) and pressure (3 bar O_2) are much higher. Furthermore, the catalyst amount used (143 mg) is much higher than that used in the SCC experiment (0.14 mg), which is conducted at room temperature and under atmospheric pressure. It is interesting however, that no induction time is observed. Indeed, the highest observed current is generated immediately, as the two electrodes are connected. This experiment confirms that electrons are indeed transferred from Au- to Pd sites in the oxidation of HMF. To gain understanding into the role of oxygen on the electron transfer process, an additional experiment was conducted which involved monitoring the current during 30 min periodic cycles in the presence of O_2 and N_2. The results from these experiments are displayed in Fig. 4.10.

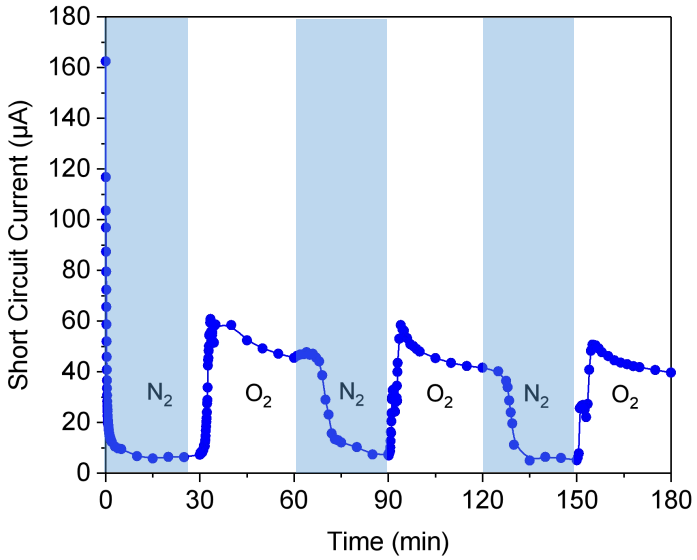

Figure 4.10. Experimental data for measuring short circuit current between Au and Pd electrodes. *Reaction conditions*: HMF (0.02 M), NaOH (0.1 M), H_2O (50 mL), room temperature, O_2/N_2 flow: 50 mL/min, 3 h.

It is evident from this data that under inert conditions (N_2), the current drops drastically (current number close to 5 μA). As oxygen is re-introduced, the current increases. This observation indicates that oxygen is involved in the generation of an electric current between gold and palladium. In the proposed hypothesis, oxygen is required to oxidize the Pd to Pd^0, which is subsequently reduced to OH^- in the reaction solution; a process which consumes electrons. The roles of Au/C and Pd/C in the aerobic oxidation of HMF are therefore similar to an electrochemical cell, such as a fuel cell or a battery, where the role of Au is to oxidize HMF; generating electrons, which are rapidly transferred to and consumed on Pd sites. The role of the oxygen is therefore to drive electron transfer from one electrode to the other electrode. The results presented herein therefore support the proposed mechanism.

4.4 Influence of Au/Pd mole ratios on rate enhancements

To this point, all the work discussed is based on systems which possess a Au/Pd molar ratio of 4/1. However in most cases, the largest synergistic enhancements observed in alloy catalysts with equimolar quantities of Au and Pd[12,22], see *Chapter 1, Section 1.4.3*. It is therefore important to investigate whether the enhancement from this electron transfer could be further increased by optimizing the Au:Pd ratio. The results from this work could provide an enhanced understanding on the nature of the interaction between Au and Pd. As listed in Table 4.3, seven different molar ratios of Au and Pd were screened for HMF oxidation, as alloyed supported catalysts and as physical mixtures. For each of these experiments, the total metal loading and quantity of carbon support used were always kept the same. Further details relating to the preparation method is presented in *Chapter 2, Section 2.2.5*.

Table 4.3. Prepared different molar ratios for series of catalysts in HMF oxidation.

Molar ratio (mol/mol)	Metal loading of Au/C + Pd/C physical mixture and its counterpart (wt.%)			Metal loading of Au-Pd/C alloy (wt.%)
Au-Pd	Au/C	Pd/C	Au/C + Pd/C	Au-Pd/C
9-1	1.85	0.11	1	1
4-1	1.75	0.24	1	1
2-1	1.55	0.42	1	1
1-1	1.28	0.70	1	1
1-2	0.95	1.03	1	1
1-4	0.63	1.35	1	1
1-9	0.34	1.63	1	1

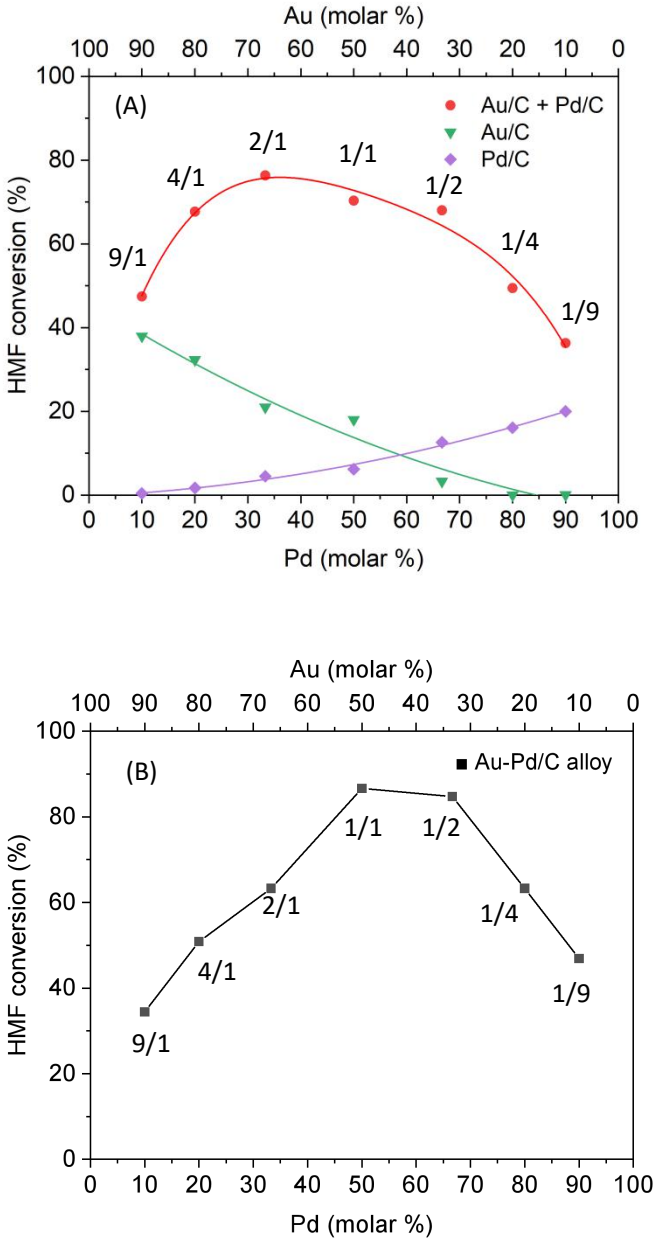

Figure 4.11. Catalytic behavior of supported Au and Pd catalyst with different molar ratios in aqueous HMF oxidation in a presence of (**A**) physical mixture Au/C + Pd/C and its monometallics; (**B**) Au-Pd/C alloy. Mole ratio between Au and Pd are marked on the curves. *Reaction conditions*: HMF (0.1 M), $NaHCO_3$ (0.4 M), H_2O (16 mL); 80 °C; pO_2 = 3 bar; 30 min; catalyst amounts for Au/C + Pd/C and Au-Pd/C: 143.1 mg; Au/C: 72.1 mg; Pd/C: 71 mg.

As is shown in Fig.4.11 (A), the green curve is representative of the monometallic Au/C catalyst, in the absence of any Pd/C. The activity of this catalyst decreases as the quantity of Au in the reaction is decreased. This is anticipated, as the catalyst testing is conducted under kinetic conditions and no mass transfer is observed (see Fig. S4 in the *Appendix*). A maximum HMF conversion of 40 % is obtained when 1.85 mg Au metal quantity is used; this is the amount of the Au/C catalyst which would be used in a typical experiment with a physical mixture, where the Au/Pd ratio is 9/1. Interestingly, close to no activity is observed when 0.63 mg and 0.34 mg of Au are used, see *Chapter 2, Table 2.1*. This suggests that the monometallic Au/C catalyst is unlikely to be responsible for converting HMF in reactions over the physical mixtures at ratios of 1/4 and 1/9 Au/Pd mol/mol, respectively. The corresponding reactions over the monometallic Pd/C (curve with purple color in Fig. 1.11 (A)) exhibit a similar trend however lower maximum activity is observed, than that exhibited Au/C catalyst, which agrees with previous literature[23–25]. The activity trends of Au and Pd catalysts appear to cross at a molar ratio of approximately 60/40 (Pd/Au), where a similar quantity of HMF conversion is likely to be obtained.

In the activity profile for the physical mixture of Au/C and Pd/C (red line in Fig.4.11(A)), a ‘volcano-type’ relationship is observed. The highest HMF conversion was obtained at Au/Pd mole ratio of 2/1 (*ca.* 75% conversion). It’s noteworthy that at Au/Pd mole ratios of 2/1, 1/1 and 1/2, the gaps of HMF conversion between the physical mixture and the corresponding monometallic catalysts were the greatest. This suggests that the enhancement effect is greatest at those molar ratios.

In addition to reactions over monometallic and physical mixtures, additional experiments were conducted using alloyed catalyst with different Au to Pd mole ratios were tested, see Fig. 4.11(B). The most active alloy catalysts were those which possessed molar ratios of 1/1 and 1/2; *ca.* 90% HMF conversion is obtained. In Au rich catalysts, the physical mixture displayed a higher activity than the alloy. This suggests that the highest enhancement, promoted by electron transfer, is observed

under Au rich catalysts, *e.g.*, Au/Pd mole ratios of 2/1, 4/1 and 9/1.

In contrast, in Pd rich systems the opposite it observed. The alloyed Pd rich catalysts are more active than the corresponding physical mixtures. Previously, it was reported that Pd could be easily over oxidized in solution, any aldehyde molecules will adsorb on the surface of PdO and get hardly desorbed, leading to the poison of Pd[26–29], Due to this poison, Pd is decreasing its activity during reaction, which explains the deactivation of physical mixture at mole ratios of 1/4 and 1/9. This is not observed with the Au-Pd alloy, due 'ligand and dilution effect', which leads to a more filled Pd d-band structure[30], which suppressed Pd poisoning. This is a possible explanation as to why the Au-Pd alloy is more active than the corresponding physical mixture with Pd rich catalysts.

Another interesting observation is that in general within the physical mixtures, the Au rich catalysts are more active than the Pd rich Au catalysts. However interestingly, regardless of the molar ratio used, the enhancement effect is observed throughout; the activity observed over the physical mixture is always greater than that observed over the combined sum of the monometallic catalysts. It is therefore possible, that the roles of Pd and Au exchange; an effect which appears to be dependent on the metal loading. Both metals have be shown previously to be effective monometallic catalysts for ORRs and alcohol oxidation[31]. Experimentally, it is observed that for Au rich physical mixtures, *i.e.* 4/1 (Au/Pd) mol/mol, the enhancement is attributable to alcohol oxidation over Au and oxygen reduction over Pd. However, as the mole proportion of Au decreases while the Pd mole proportion increases in the physical mixture, it's likely that dominant sites responsible for alcohol oxidation switch from Au to Pd. This swapping of roles may be attributed to a particle size effect, which has been shown previously to influence ORR and dehydrogenation rate[32–36]. It is well known from literature that as nanoparticles size of Au and Pd change, the rate of the ORR over Au or Pd changes too[34,36–39]. This can be attributed to several effects; the ORR activities of different low index planes, types of surface sites and electronic effects in catalysis[40].

Though the sol-immobilization method for catalyst preparation was used to control these variables, previous studies have shown that the weight loading of the supported metal can have a significant impact on the particle size using this method[41].

To confirm this, freshly prepared colloidal catalysts containing Au and Pd, with varied Au/Pd mole ratios, were characterized by TEM. The corresponding images are shown in Fig. 4.12 From the particle size distribution in Fig. 4.13, the 0.34 wt.% Au displayed a mean particle size of 3.0 nm while the 1.85 wt.% Au shows a mean particle size of 4.82 nm. For Pd colloids, the same phenomenon was obtained where the 0.11 wt.% Pd displayed a mean particle size of 1.55 nm, whilst the 0.7 wt.% Pd has a mean particle size of 3.88 nm. It proves that higher is the catalyst metal loading, the bigger the mean particle size. To further support the hypothesis that ORR predominantly occurs on the Au nanoparticles when its particle size is small, additional experiments were conducted for HMF oxidation using a physical mixture of Au-Pd/C alloy catalyst (mole ratio of 1/9) and monometallic Au/C catalyst (mole proportion of 10 %), see Fig. 4.14.

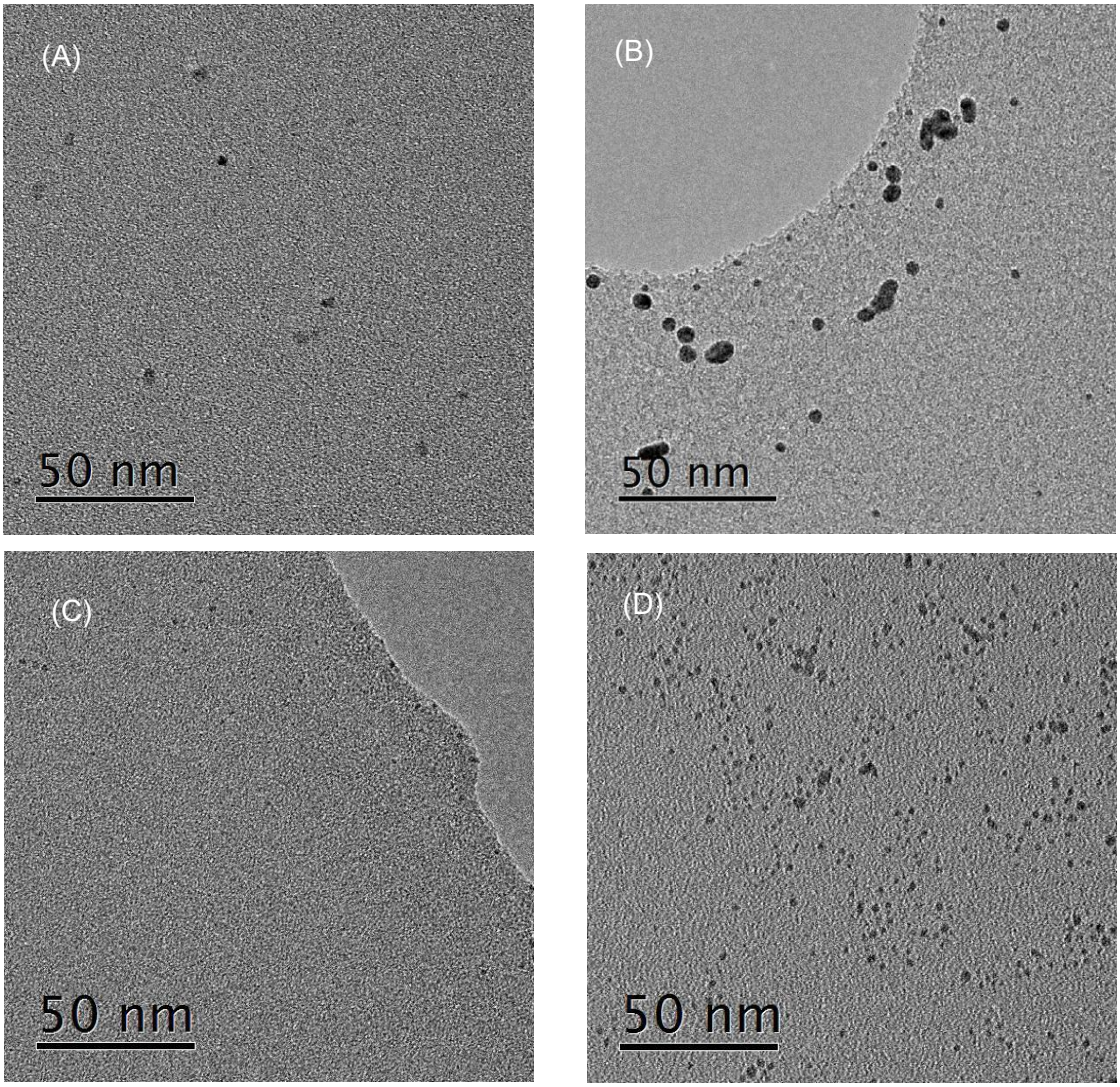

Figure 4.12. Microscopic characterization of Au colloids with (**A**) weight loading of 0.34 wt.%; (**B**) weight loading of 1.85 wt.%. Pd colloids with (**C**) weight loading of 0.11 wt.%; (**D**) weight loading of 0.70 wt.%. TEM characterization of these samples was conducted by Dr. Thomas Davis from Cardiff University.

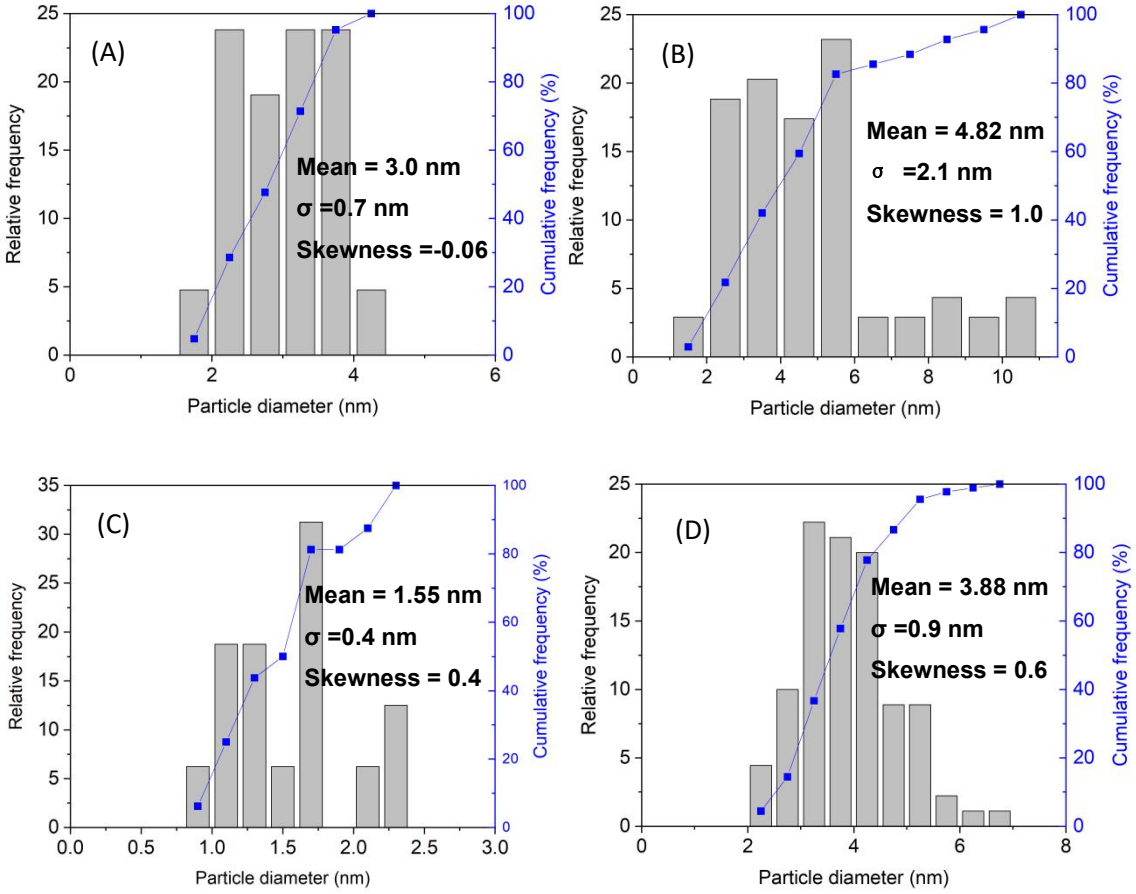

Figure 4.13. Measured particle size distributions for Au colloids with (**A**) weight loading of 0.34 wt.%; (**B**) weight loading of 1.85 wt.%. Pd colloids with (**C**) weight loading of 0.11 wt.%; (**D**) weight loading of 0.70 wt.%. σ refers the deviation of mean particle size(calculation methodology see appendix eq. (1)), skewness is a measure of the asymmetry of the probability distribution of a real-valued random variable about its mean.

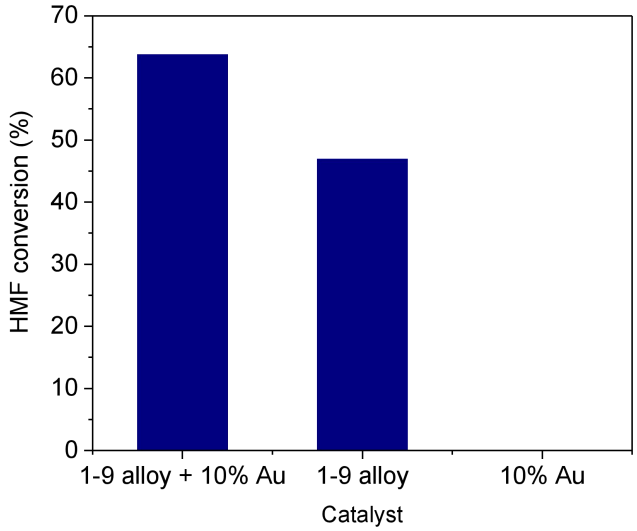

Figure 4.14. Aqueous HMF oxidation over Au (molar 10%); Au-Pd/C alloy (Au/Pd of 1/9, mole/mole) and their physical mixture. *Reaction conditions*: HMF (0.1 M), $NaHCO_3$ (0.4 M), H_2O (16 mL); 80 °C; pO_2 = 3 bar; 30 min; catalyst amounts for Au-Pd/C: 143.1 mg; Au/C: 72.1 mg.

Fig. 4.14 clearly shows that the 0.34 wt.% Au catalyst does not catalyse HMF oxidation on its own. However when it is combined with the Au-Pd/C alloy catalyst, the synergistic effect is observed once again. In this case, it is hypothesized that Au/C (molar 10%) is predominantly catalyzing the ORR, part of the electrons generated from alcohol oxidation over the alloyed catalyst are transferred to Au *via* the C support. This provides evidence that the particle size has a big impact on whether a supported metal particle catalyzes the ORR or HMF dehydrogenation.

The study of aqueous HMF oxidation over series of Au and Pd catalysts with varied metal mole ratios has provided a more comprehensive understanding on the cooperative behavior between Au and Pd in alcohol oxidation under basic conditions. By controlling the particle size, the preference for alcohol oxidation or oxygen reduction can be controlled for metal nanoparticles.

4.5 Summary

Based on all the experiments performed in *Chapter 3*, it has been possible to propose a mechanism for HMF oxidation over a mixture catalyst of Au/C and Pd/C, which was confirmed by further electrochemical and thermochemical experiments. Under the standard ratio (Au/Pd = 4/1, mol/mol), it is proposed that Au/C is predominantly catalyzing the dehydrogenation of HMF; a process which produces electrons which are consumed on Pd sites through oxygen reduction. The C support serves as a medium for transferring the electrons from one metal to the other, facilitated by its high conductivity. When the support is replaced by TiO_2 or BN, lower activity was observed. This process has been demonstrated by electrocatalytic short circuit current measurements; current between Au and Pd was observed, showing that electrons flow from Au to Pd. This confirms that under a molar ratio of 4/1 (Au/Pd mol/mol), Pd is working on electron consumption rather production. Different mole ratios between Au/Pd were subsequently investigated showing the mechanism is still working when there is excess amount Au in the mixture catalyst. However, when Pd is in excess, the mechanism works in an opposite way; Pd is producing electrons through dehydrogenation and oxygen reduction occurs at Au sites.

4.6 References

1 R. A. P. Smith, *Platin. Met. Rev.*, 2009, **53**, 55–56.

2 R. A. P. Smith, *Platin. Met. Rev.*, 2009, **53**, 109–110.

3 P. der Heide, *X-ray photoelectron spectroscopy : an introduction to principles and practices*, 2012.

4 J. Cai, H. Ma, J. Zhang, Q. Song, Z. Du, Y. Huang and J. Xu, *Chem. - A Eur. J.*, 2013, **19**, 14215–14223.

5 Y. Wang, K. Yu, D. Lei, W. Si, Y. Feng, L. L. Lou and S. Liu, *ACS Sustain. Chem. Eng.*, 2016, **4**, 4752–4761.

6 L. P. Zhang, M. Li and U. Diebold, *Surf. Sci.*, 1998, **412**–**413**, 242–251.

7 A. Wu and W. Ren, *TiO2 Nanoparticles: Applications in Nanobiotechnology and Nanomedicine*, John Wiley & Sons, 2020.

8 G. Neri, M. G. Musolino, C. Milone, D. Pietropaolo and S. Galvagno, *Appl. Catal. A, Gen.*, 2001, **208**, 307–316.

9 H. Zhu, Z. Qin, W. Shan, W. Shen and J. Wang, *J. Catal.*, 2004, **225**, 267–277.

10 M. Luo, W. Shan, P. Ying, J. Lu and C. Li, in *Studies in Surface Science and Catalysis*, Elsevier Science & Technology, 2001, vol. 138, pp. 61–68.

11 S.-Y. Wang, N. Li, R.-M. Zhou, L.-Y. Jin, G.-S. Hu, J.-Q. Lu and M.-F. Luo, *J. Mol. Catal. A. Chem.*, 2013, **374**–**375**, 53–58.

12 X. Wan, C. Zhou, J. Chen, W. Deng, Q. Zhang, Y. Yang and Y. Wang, *ACS Catal.*, 2014, **4**, 2175–2185.

13 S. E. Davis, B. N. Zope and R. J. Davis, *Green Chem.*, 2012, **14**, 143–147.

14 T. Schalow, B. Brandt, D. E. Starr, M. Laurin, S. K. Shaikhutdinov, S. Schauermann, J. Libuda and H. J. Freund, *Angew. Chemie - Int. Ed.*, 2006, **45**, 3693–3697.

15 A. Baylet, P. Marécot, D. Duprez, P. Castellazzi, G. Groppi and P. Forzatti, *Phys. Chem. Chem. Phys.*, 2011, **13**, 4607–4613.

16 S. P. Mahapatra and D. K. Tripathy, *Cell. Polym.*, 2004, **23**, 127–144.

17 D. J. Chadderdon, L. Xin, J. Qi, Y. Qiu, P. Krishna, K. L. More and W. Li, *Green Chem.*, 2014, **16**, 3778–3786.

18 B. Rajesh, K. Ravindranathan Thampi, J. M. Bonard, H. J. Mathieu, N. Xanthopoulos and B. Viswanathan, *J. Power Sources*, 2005, **141**, 35–38.

19 M. Pelaez, N. T. Nolan, S. C. Pillai, M. K. Seery, P. Falaras, A. G. Kontos, P. S. M. Dunlop, J. W. J. Hamilton, J. A. Byrne, K. O'Shea, M. H. Entezari and D. D.

Dionysiou, *Appl. Catal. B Environ.*, 2012, **125**, 331–349.

20 D. Golberg, Y. Bando, Y. Huang, T. Terao, M. Mitome, C. Tang and C. Zhi, *ACS Nano*, 2010, **4**, 2979–2993.

21 T. H. Nguyen, A. Fraiwan and S. Choi, *Biosens. Bioelectron.*, 2014, **54**, 640–649.

22 Z. Gui, W. Cao, S. Saravanamurugan, A. Riisager, L. Chen and Z. Qi, *ChemCatChem*, 2016, **8**, 3636–3643.

23 D. Bonincontro, A. Lolli, A. Villa, L. Prati, N. Dimitratos, G. M. Veith, L. E. Chinchilla, G. A. Botton, F. Cavani and S. Albonetti, *Green Chem.*, 2019, **21**, 4090–4099.

24 S. E. Davis, M. S. Ide and R. J. Davis, *Green Chem.*, 2013, 15, 17–45.

25 A. Villa, M. Schiavoni, S. Campisi, G. M. Veith and L. Prati, *ChemSusChem*, 2013, **6**, 609–612.

26 J. Naughton, A. F. Lee, S. Thompson, C. P. Vinod and K. Wilson, *Phys. Chem. Chem. Phys.*, 2010, **12**, 2670–2678.

27 M. Bowker, L. Cookson, J. Bhantoo, A. Carley, E. Hayden, L. Gilbert, C. Morgan, J. Counsell and P. Yaseneva, *Appl. Catal. A Gen.*, 2011, **391**, 394–399.

28 A. F. Lee, J. N. Naughton, Z. Liu and K. Wilson, *ACS Catal.*, 2012, **2**, 2235–2241.

29 C. M. A. Parlett, L. J. Durndell, A. Machado, G. Cibin, D. W. Bruce, N. S. Hondow, K. Wilson and A. F. Lee, *Catal. Today*, 2014, **229**, 46–55.

30 F. Gao and D. W. Goodman, *Chem. Soc. Rev.*, 2012, **41**, 8009–8020.

31 J. B. Xu, T. S. Zhao, Y. S. Li and W. W. Yang, *Int. J. Hydrogen Energy*, 2010, **35**, 9693–9700.

32 S. C. Cook, J. D. Padmos and P. Zhang, *J. Chem. Phys.*, , DOI:10.1063/1.2901034.

33 F. Liu and P. Zhang, *Appl. Phys. Lett.*, 2010, **96**, 3–6.

34 L. Wang, Z. Tang, W. Yan, H. Yang, Q. Wang and S. Chen, *ACS Appl. Mater. Interfaces*, 2016, **8**, 20635–20641.

35 T. Fujigaya, C. Kim, Y. Hamasaki and N. Nakashima, *Sci. Rep.*, 2016, **6**, 2–11.

36 W. Xiao, M. A. Liutheviciene Cordeiro, M. Gong, L. Han, J. Wang, C. Bian, J. Zhu, H. L. Xin and D. Wang, *J. Mater. Chem. A*, 2017, **5**, 9867–9872.

37 T. Inasaki and S. Kobayashi, *Electrochim. Acta*, 2009, **54**, 4893–4897.

38 W. Zhou, M. Li, O. L. Ding, S. H. Chan, L. Zhang and Y. Xue, *Int. J. Hydrogen Energy*, 2014, **39**, 6433–6442.

39 H. Erikson, M. Lüsi, A. Sarapuu, K. Tammeveski, J. Solla-Gullón and J. M. Feliu, *Electrochim. Acta*, 2016, **188**, 301–308.

40 W. Zhou, M. Li, O. Ding, S. Chan, L. Zhang and Y. Xue, *Int. J. Hydrogen Energy*, 2014, **39**, 6433–6442.

41 J. Pritchard, L. Kesavan, M. Piccinini, Q. He, R. Tiruvalam, N. Dimitratos, J. A. Lopez-Sanchez, A. F. Carley, J. K. Edwards, C. J. Kiely and G. J. Hutchings, *Langmuir*, 2010, **26**, 16568–16577.

Catalysis promotion and its application

5

Introduction

This chapter further investigates the enhanced catalytic activity observed in *Chapter 4* through spatial separation of Au and Pd for the oxidation of HMF. Within this chapter a 'binary mixture' catalyst (Au+Pd/C) (a spatially separated catalyst with no alloyed nanoparticles present) was prepared and was observed to offer an even higher catalytic activity than the physical mixture system in several alcohol oxidation reactions. The catalyst was characterized by a number of techniques including HAADF-STEM and TPR, to elucidate the nature of the supported nanoparticles, including the extent of alloy formation during catalyst preparation and use in alcohol oxidation. From these detailed investigations no evidence for the formation of alloyed Au-Pd nanoparticles was observed in the as-prepared catalyst. Meanwhile, to show how widely applicable the method for catalyst design is, catalysts prepared using a polyvinyl pyrrolidone (PVP) ligand were found to offer similar activity to the one prepared by polyvinyl alcohol (PVA), and substrates of glycerol and ethanol were selected as new probe molecules to determine if catalytic trends observed in *Chapter 4* for aqueous 5-hydoxymethylfurfural oxidation were the same for other substrates. Finally, an electrochemical system was developed in order to expand the understanding of the role of bi-metallic AuPd catalysts in selective oxidation reactions and to further clarify benefit of spatially separating Au and Pd.

5.1 Binary mixture (Au + Pd)/C

Based on the enhanced activity of the physical mixture of Au and Pd monometallic catalysts compared to the AuPd alloy, a new catalyst has been prepared consisting of discrete Au and Pd nanoparticles deposited on common carbon support grains (denoted (Au + Pd)/C, preparation method see *Chapter 2*). It is hypothesized that this catalyst would exhibit an even higher activity than the physical mixture of Au/C and Pd/C, due to the enhanced electron transfer afforded by virtue of the Au and Pd particles being spatially much closer to each other, yet still separate, and the high conductivity of the carbon support. This would also provide crucial evidence to support the proposed mechanism, outlined in *Chapter 4*.

Indeed, as predicted, the (Au + Pd)/C catalyst did exhibit a higher activity than the other catalysts as it is shown in Fig. 5.1-5.3 and Table 5.1. The (Au + Pd)/C catalyst showed a HMF conversion with the highest efficiency (full conversion was achieved at approximately 45 min), the highest yield of the intermediate product HMFCA during the first 30 min (yield > 45 %) and the highest product yield of FDCA at the end of reaction(FDCA productivity: 80 $mol_{FDCA}.mol_{metal}.h^{-1}$, in literature so far the best one is 99 $mol_{FDCA}.mol_{metal}.h^{-1}$, see Table S1 in *Appendix*). Based on the proposed mechanism it is proposed that by using the catalyst of (Au + Pd)/C, Au nanoparticles could efficiently convert the HMF into the intermediate products of HMFCA and FFCA under the attack of hydroxyl ^{-}OH in base. After the HMF molecules were totally converted, the yield towards final product FDCA starts to raise up quickly because of the consecutive conversion from the intermediate molecules, as shown in Fig. 5.3, yield of FDCA was less than 5 % during the first 30 min, however, it increased dramatically from 30 min on, where more than 25 % yield were achieved at 60 min, From the reaction route exhibited in Scheme 5.1, the reaction step from HMFCA to FFCA is considered to be the rate limiting step according to literature[1–3]. On the other side, the observed yield from FFCA is always negligible because its oxidation to FDCA takes place rapidly[2] which is similar to the first step from HMF to HMFCA

because these two reactions are mainly the oxidation of aldehyde functional group. Electrons liberated from the substrate on Au are consumed *via* an oxygen reduction reaction (ORR) on Pd, when the presence of Au and Pd on the same C grain in the (Au + Pd)/C catalyst, the facile electron transfer from Au to Pd in propose is attributed to be the reason for its enhanced activity over a physical mixture of the monometallic catalysts, which would rely on electron transfer to occur either through collision between support grains or *via* the reaction solution. Overall, the catalyst activity follows the order of: (Au + Pd)/C > Au/C + Pd/C > Au-Pd/C > Au/C >> Pd/C, data of productivity towards to FDCA are presented in Table 5.1.

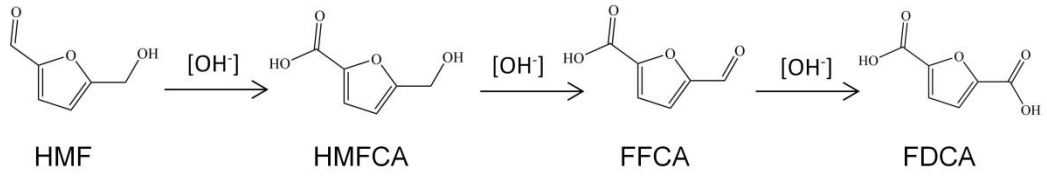

Scheme 5.1. Reaction route of aqueous HMF oxidation to terminal product FDCA.

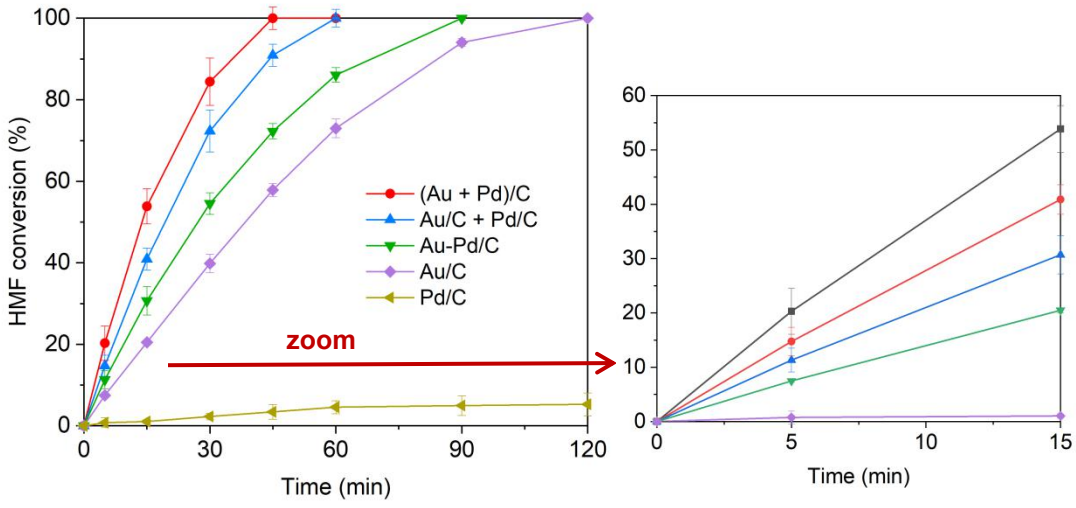

Figure 5.1. Catalytic performance of series catalysts in regard of HMF conversion. *Reaction conditions*: HMF (0.1 M); $NaHCO_3$ (0.4 M); H_2O (16 mL); 80 °C; pO_2 = 3 bar; catalyst amounts for (Au + Pd)/C, Au/C + Pd/C and Au-Pd/C: 143.1 mg; Au/C: 72.1 mg; Pd/C: 71 mg. Error bars were provided by Kai Wang at Cardiff University.

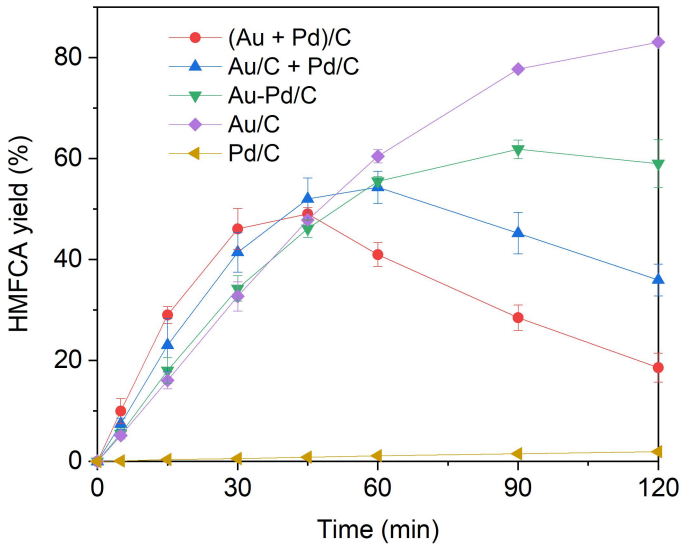

Figure 5.2. Catalytic performance of series catalysts in regard of intermediate product HMFCA yield. *Reaction conditions*: HMF (0.1 M); $NaHCO_3$ (0.4 M); H_2O (16 mL); 80 °C; pO_2 = 3 bar; catalyst amounts for (Au + Pd)/C, Au/C + Pd/C and Au-Pd/C: 143.1 mg; Au/C: 72.1 mg; Pd/C: 71 mg. Error bars were provided by Kai Wang at Cardiff University.

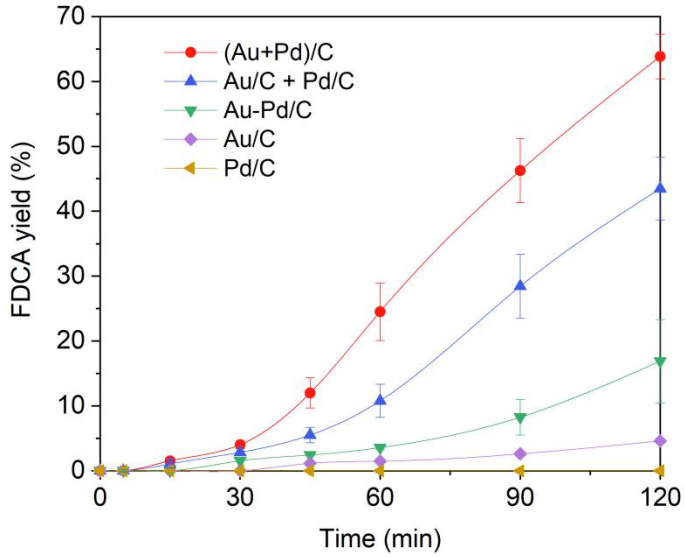

Figure 5.3. Catalytic performance of series catalysts in regard of FDCA product yield. *Reaction conditions*: HMF (0.1 M); $NaHCO_3$ (0.4 M); H_2O (16 mL); 80 °C; pO_2 = 3 bar; catalyst amounts for (Au + Pd)/C, Au/C + Pd/C and Au-Pd/C: 143.1 mg; Au/C: 72.1 mg; Pd/C: 71 mg. Error bars were provided by Kai Wang at Cardiff University.

Table 5.1. The performance of supported metal catalysts in the aqueous phase aerobic oxidation of 5-hydroxymethylfurfural (HMF) to furandicarboxylic acid (FDCA).

Entry	Catalyst	T (°C) / t (h)	*P* O_2, bar	Productivity, mol_{FDCA} . mol_{metal} .h^{-1}
1	(Au + Pd)/C	80 / 2	3	64.0
2	Au/C + Pd/C	80 / 2	3	43.5
3	Au-Pd/C	80 / 2	3	17.0
4	Au/C	80 / 2	3	6.3
5	Pd/C	80 / 2	3	0
6	*(Au + Pd)/C	80 / 2	3	80.0
7	*Au/C + Pd/C	80 / 2	3	54.4
8	*Au-Pd/C	80 / 2	3	21.3

* Productivity calculated based on moles of Au only

5.2 Characterizations for (Au + Pd)/C by STEM

To know the structure of (Au + Pd)/C, including the extent of nanoparticle dispersion, nanoparticle size distribution (PSD) and the extent of Au-Pd alloy formation, if any, the fresh (Au + Pd)/C catalyst was characterized by HAADF-STEM, seen in Fig. 5.4. It is showing clearly a high dispersion of Au and Pd nanoparticles on the carbon support, with a mean particle size of 3.87 nm determined *via* nanoparticle tracking, where its average particle size becomes larger (4.5 nm) after use as a catalyst, see Fig. 5.5. The size of fresh binary mixture catalyst is comparable to that previously reported for the monometallic and alloyed catalysts (Au/C: 3.1 nm; Pd/C: 3.4 nm; Au-Pd/C: 2.8 nm). At the meantime, no alloyed nanoparticles were observed *via* HAADF-STEM

analysis for the fresh (Au+Pd)/C catalyst, indicating Au and Pd are elementally separated on the carbon support.

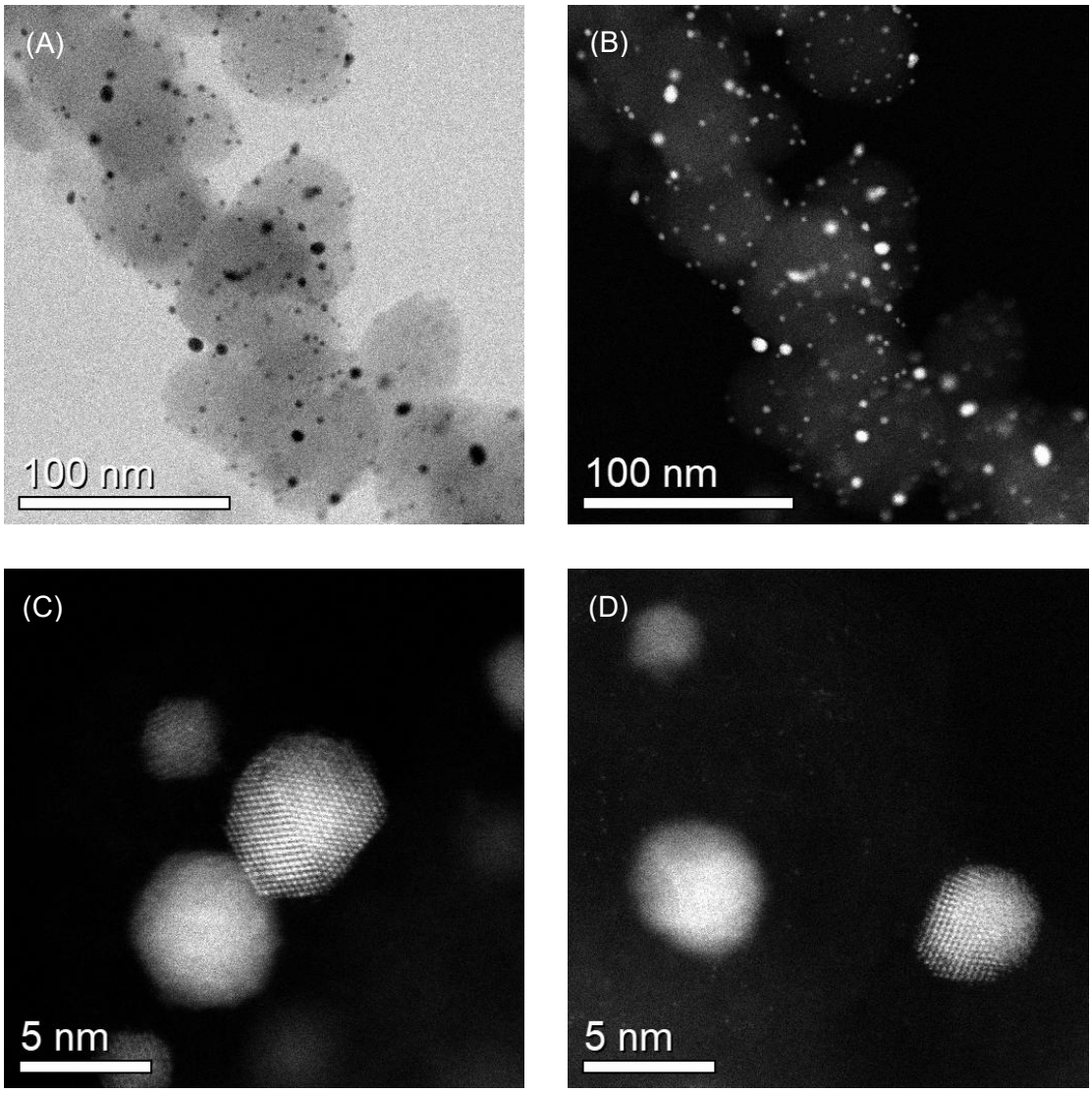

Figure 5.4. Electron microscopy analysis of (Au + Pd)/C (binary mixture) sample before use as a catalyst: (**A**) and (**B**) Complementary pair of BF- and HAADF - STEM images showing particle size and spatial distribution; (**C**) and (**D**) Atomic resolution HAADF STEM images showing the co-existence of Au and Pd nanoparticle as well as some sub-nm clusters and dispersed atoms. All the images were obtained by Dr. Sultan M. Althahban from Lehigh University.

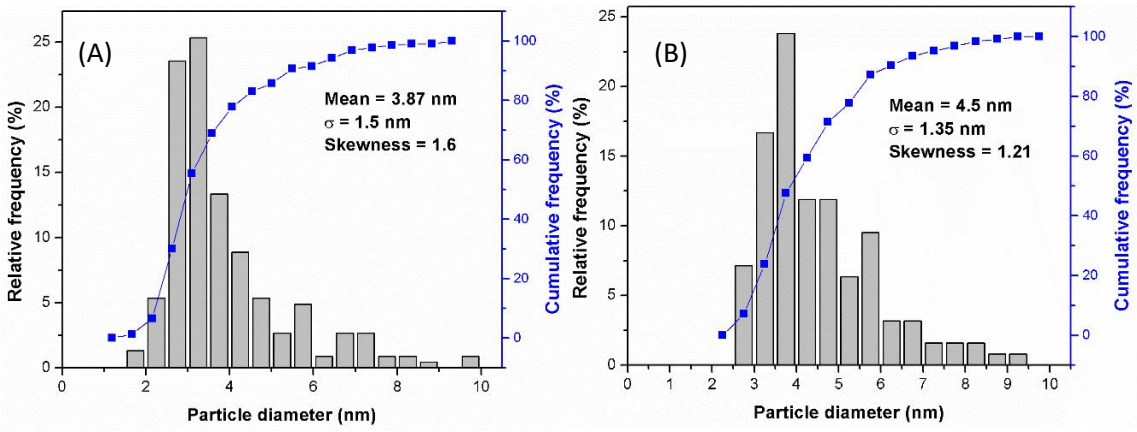

Figure 5.5. Measured particles size distributions for (**A**) fresh (Au + Pd)/C (binary mixture) catalyst, (**B**) binary mixture after use as a catalyst. σ refers the deviation of mean particle size(calculation methodology see appendix eq. (1)), skewness is a measure of the asymmetry of the probability distribution of a real-valued random variable about its mean. These bar charts were provided by Dr. Sultan M. Althahban from Lehigh University.

5.3 Re-usability of (Au + Pd)/C

In order to determine the stability of the (Au + Pd)/C catalyst in the oxidation of HMF the activity of the catalyst was studied over three uses, after each cycle it was washed with 500 mL distilled water followed by 250 mL acetone, and then dried at 110 °C for 16 hours[4]. As is shown in Fig. 5.6, catalyst activity is seen to decrease marginally upon second and third use. This decrease becomes more apparent in the third cycle as only small amounts of FDCA yield were obtained, *ca*. 8 % (there is 25% in the first cycle) where the recycle was investigated to be durable with a 10 % FDCA yield for all the cycles over the physical mixture in *Chapter 3, Section 3.5*. Based on this observation, it is assumed there might have some migration of nanoparticles during the reaction, resulting in the formation of alloyed structures, and an inhibition of

catalyst activity. Therefore microscopic characterization for this used catalyst was carried out, see Fig. 5.7, which confirmed the formation of some Au-Pd alloyed particles, it may be the reason why the mean particle size was found larger than the catalyst before use, as was discussed in the last section. All these have contributed to the decrease in catalytic activity observed upon re-use, as shown of time online data in Fig. 5.8. A clear loss in HMF conversion and product yield is observed with re-use. The extent of possible leaching was evaluated *via* microwave plasma atomic emission spectroscopy (MP-AES) analysis of post-reaction samples whereby no metal was observed in solution, suggesting Au and Pd nanoparticles are stable on C support.

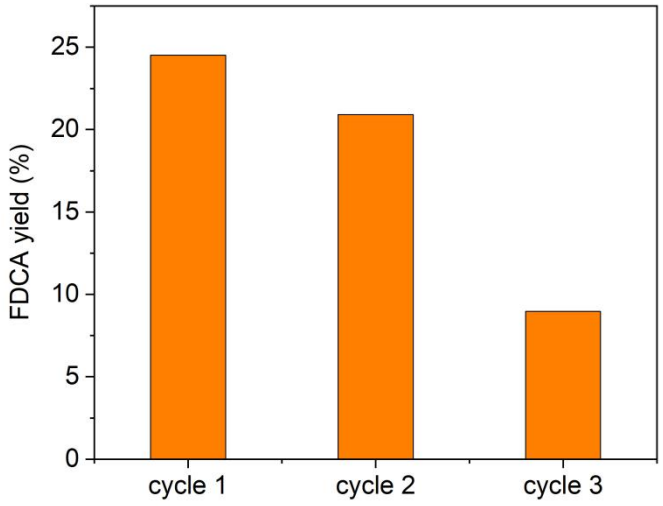

Figure 5.6. Catalyst re-usability data for the binary mixture (Au + Pd)/C in terms of FDCA yield. *Reaction conditions*: HMF (0.1 M); $NaHCO_3$ (0.4 M); H_2O (16 mL); 80 °C; pO_2 = 3 bar; 60 min; catalyst amount: 143.1 mg, carbon balance all around 98%.

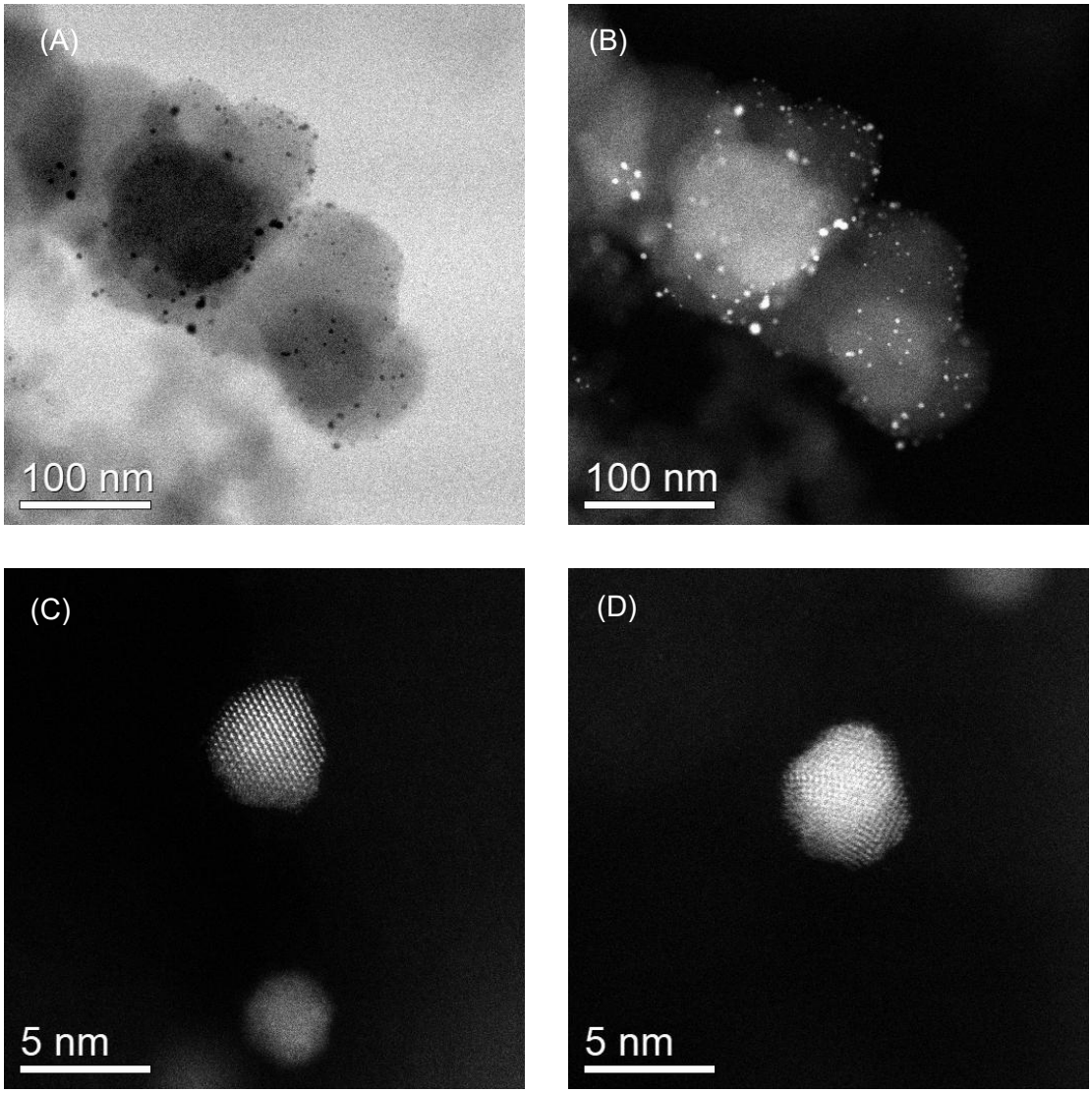

Figure 5.7. Electron microscopy analysis of (Au + Pd)/C (binary mixture) sample after use as a catalyst: (**A**) and (**B**) Complementary pair of BF- and HAAD-STEM images showing metal nanoparticle size and spatial distribution; (**C**) and (**D**) Atomic resolution HAADF-STEM images showing that during use there is a tendency for some Au-Pd alloyed particles to form. All the images were obtained by Dr. Sultan M. Althahban from Lehigh University.

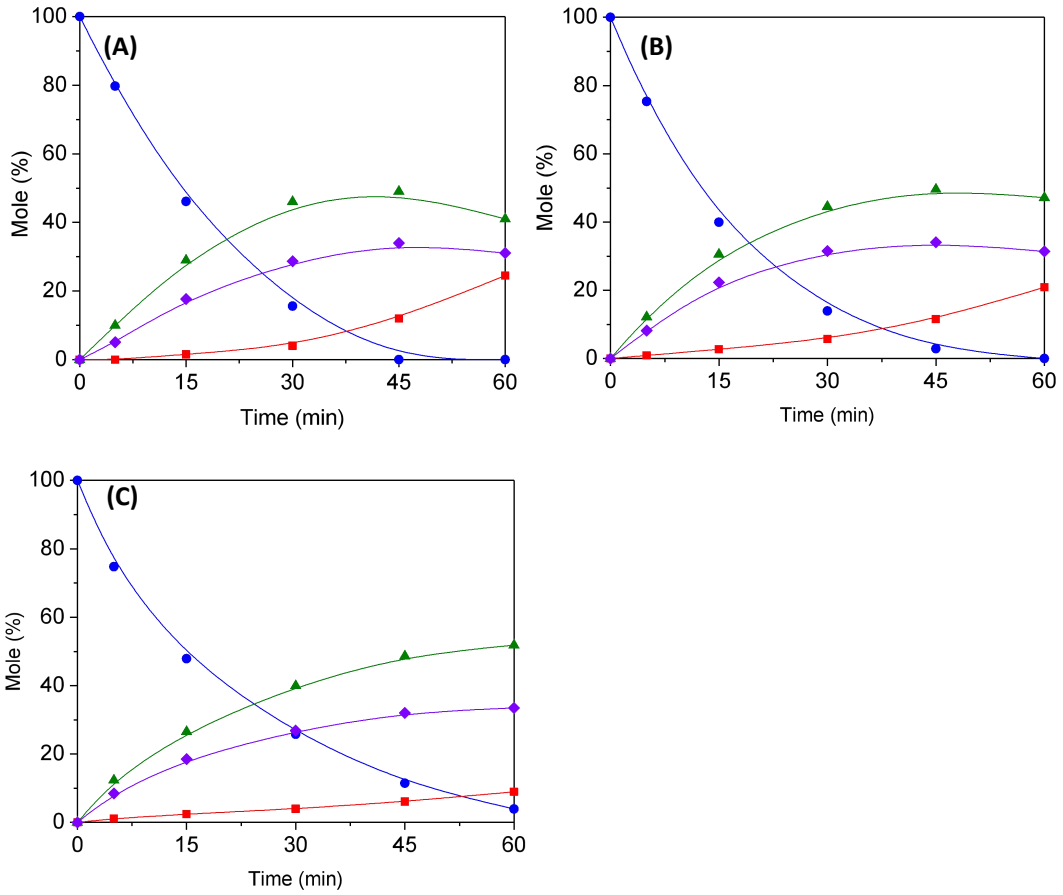

Figure 5.8. Time-on-line data of catalyst re-usability in aqueous HMF oxidation using (Au + Pd)/C for (**A**) first cycle; (**B**) second cycle; (**C**) third cycle. *Reaction conditions*: HMF (0.1 M), $NaHCO_3$ (0.4 M), H_2O (16 mL), catalyst amount: 143.1 mg, 80 °C, pO_2 = 3 bar, 60 min. HMF conversion (●); HMFCA yield (▲); FFCA yield (♦); FDCA yield (■).

With Pd well known to be readily oxidized in water, especially under an oxidative atmosphere.[5,6] Further study by temperature programmed reduction (TPR) (Fig 5.9) was carried out to characterize the state of Pd in the fresh and used (Au + Pd)/C catalyst with comparison made to the physical mixture system.

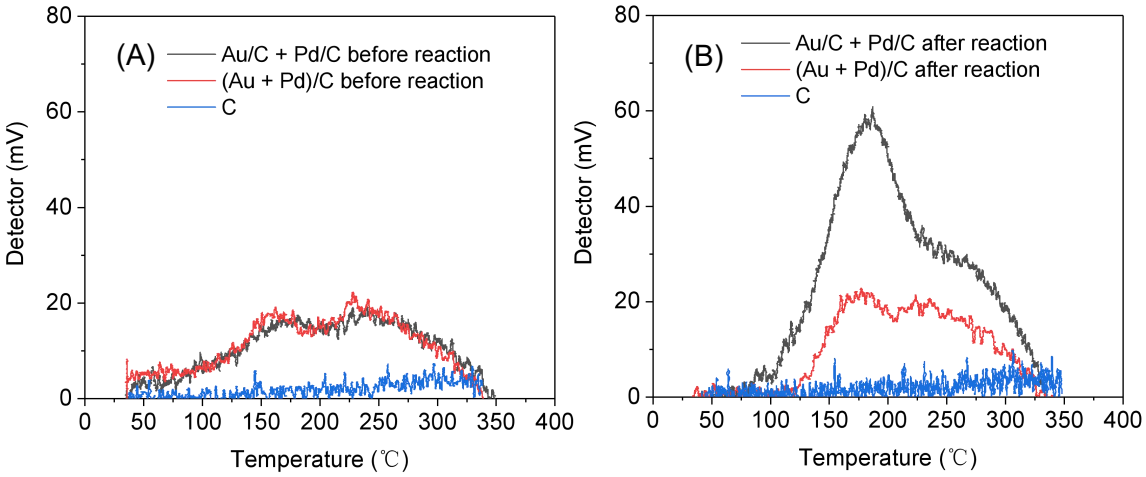

Figure 5.9. Compared temperature programmed reduction data for physically mixed Au/C + Pd/C catalyst and the binary mixture (Au + Pd)/C catalyst (**A**) before and (**B**) after reaction.

TPR analysis of the as-prepared Au/C + Pd/C and (Au + Pd)/C catalysts show no discernible differences at peak position *ca.* 175 °C[7], see Fig. 5.9 A. However, after reaction, the physical mixture Au/C + Pd/C displays a larger/more intense peak at *ca.* 175 °C compared to the binary mixture (Au + Pd)/C catalyst (Fig. 5.9 B), which suggests the change of Pd oxidation state from Pd^0 to Pd^{2+} in the physical mixture, whereas Pd2+ formation is inhibited in the binary mixture. This difference of oxidation state of Pd in the two catalysts after reaction is attributed to the different rate efficiency of electron transfer during reaction. The electron transfer is facile in (Au + Pd)/C which leads to a faster reduction of PdO and therefore less Pd^{2+} is observed in the post-reaction sample as a smaller reduction peak appeared. By comparison in the physical mixture system, where Au and Pd nanoparticles are supported on different C grains, electron transfer is likely less efficient, resulting in a reduced rate of electron transfer from Au to Pd, as such a greater concentration of PdO is observed. Bare C support was measured in TPR as a background before and after reaction shows

negligible H_2 consumption for both, indicating the peaks observed in supported catalyst originate not from the catalyst carrier.

It has previously been shown that the alloyed Au-Pd/C catalyst offers significantly lower activity towards HMF oxidation (FDCA productivity of 21.3 mol_{FDCA} . mol_{metal} .h^{-1}), see Table 5.1. With the inhibition of the Pd-redox cycle, resulting from alloying with Au[8,9]. In turn a reduction in the ability of Pd to accept substrate liberated electrons is likely with this effect believed to be responsible for this loss of catalyst activity upon alloying[10]. By comparison the donation of electron density from Au to Pd in the fresh (Au+Pd)/C catalyst is unlimited due to elemental separation and a loss in activity is only observed with the agglomeration of metal nanoparticles over several uses. This can be related to the weak interaction between the metal nanoparticles and the carbon support[11,12]

5.4 (Au + Pd)/C with different aging time for colloid.

The observed migration of Au and Pd, and resulting formation of Au-Pd alloyed nanoparticles in the used catalyst (Au + Pd)/C catalyst, as seen in *Section 5.3* above, next prompted the investigation of the effect of aging time for the binary colloid before immobilization onto the C support. The goal of this study was to establish the relationship between catalyst activity and the extent of Au-Pd alloy formation and to provide new insight into this method of catalyst preparation. With previous studies revealing the relationship between nanoparticle stability and catalytic performance[13,14].

Several aging times, *i.e*. 2 h, 4 h and 6 h were selected for preparation of the PVA stabilized Au and Pd colloid (method details see *Chapter 2, Section 2.2.4*). By extending the aging time it was hypothesized that the prepared Au and Pd colloids would agglomerate forming a bimetallic Au-Pd colloid. This hypothesis was then

examined by electron microscopy. Fig. 5.10 shows that Au and Pd colloids after mixing for 2 hours, some AuPd alloy and core-shell structure were formed. The decreased activity of the resulting C supported catalyst was determined, as a corresponding lower HMF conversion is obtained, see Fig.5.11. It is observed that when the colloid is aged for 6 h, the extent of HMF conversion is similar to that observed for the alloyed catalyst. This loss in activity, compared to the conventional (Au + Pd)/C catalyst may attribute to the formation of alloyed nanoparticles.

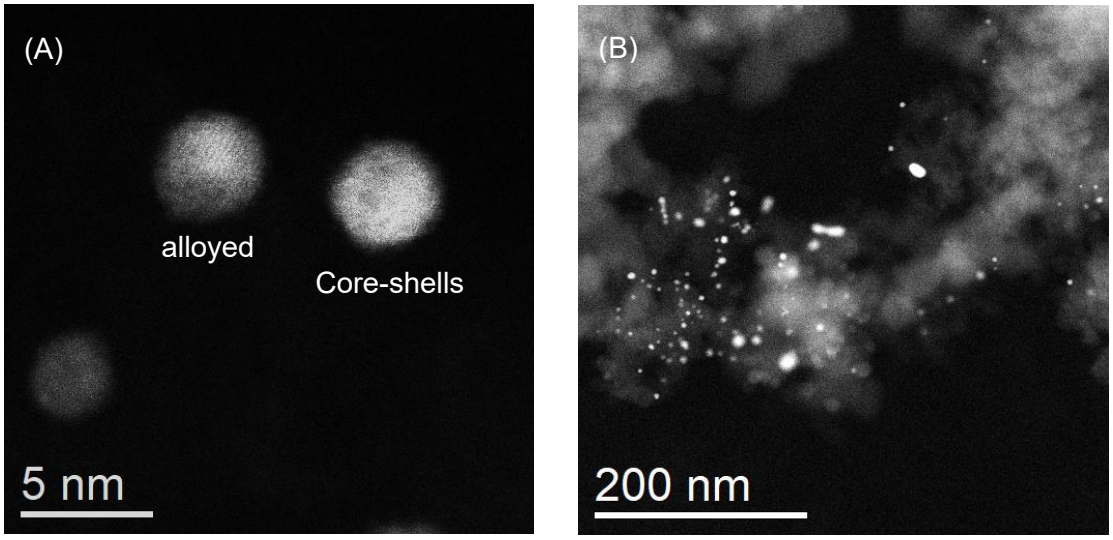

Figure 5.10. Electron microscopy analysis of mixed Au and Pd colloids sample after 2 hours. (**A**) Atomic resolution HAADF-STEM images showing that during use there is some Au-Pd alloyed particles to form; (**B**) HAAD-STEM images showing metal nanoparticle size and spatial distribution. All the images were obtained by Dr. Sultan M. Althahban from Lehigh University.

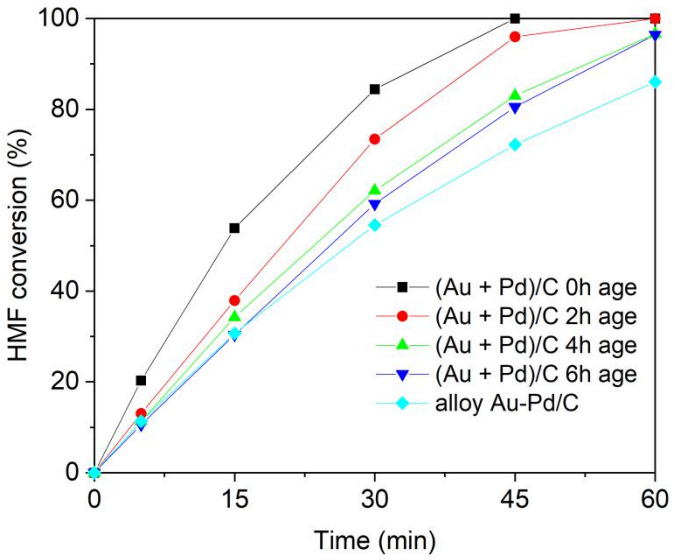

Figure 5.11. Catalytic performance of (Au + Pd)/C with different aging time of Au and Pd colloid stabilized by PVA. *Reaction conditions*: HMF (0.1 M); $NaHCO_3$ (0.4 M); H_2O (16 mL); 80 °C; pO_2 = 3 bar; 1 h; catalyst amount for (Au + Pd)/C: 143.1 mg, carbon balance all around 98%.

To further conform that decrease of catalyst activity does not result from an increase in particle size during the time aging process, the monometallic Au and Pd colloids were aged for 2 h separately (protocols in *Chapter 2*) before their immobilization. With catalyst activity compared to the unaged (Au + Pd)/C catalyst and (Au + Pd)/C with Au and Pd colloid aged for 2 h in a common container. As shown in Fig. 5.12, the (Au + Pd)/C catalyst prepared from the colloid aged for 2 h separately by two beakers has the same activity to the analogues unaged catalyst, suggesting either there is no growth in nanoparticle size during the aging procedure or the effect coming from nanoparticle size is negligible. However, in terms of (Au + Pd)/C where the Au and Pd colloid were aged for 2 h in a common container, the observed activity decreases due to the interaction between the colloid of Au and Pd and formation of alloyed nanoparticles.

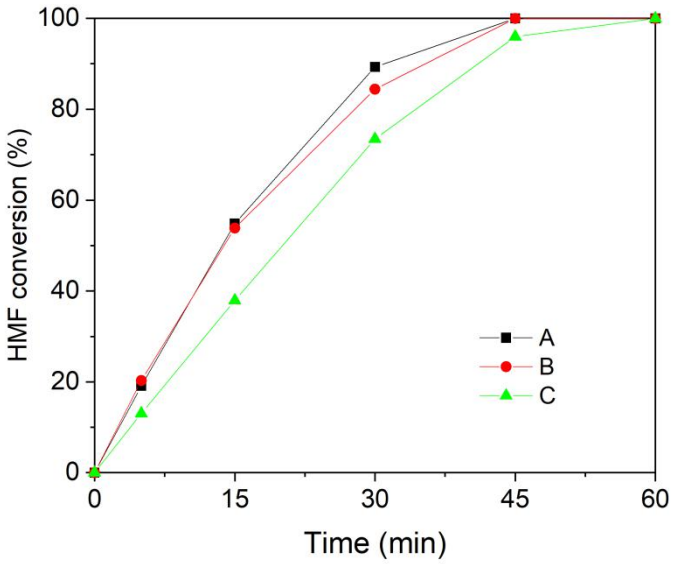

Figure 5.12. Catalytic performance of (Au + Pd)/C with A: Au and Pd colloid aged for 2 h in two separate beakers; B: Au and Pd colloid without age; C: Au and Pd colloid aged for 2 h in a common beaker before immobilization. *Reaction conditions*: HMF (0.1 M); $NaHCO_3$ (0.4 M); H_2O (16 mL); 80 °C; pO_2 = 3 bar; 1 h; catalyst amounts for (Au + Pd)/C: 143.1 mg, carbon balance all around 98%.

5.5 Effect of stabilizing ligand on catalytic activity.

At present, catalyst synthesis is with PVA stabilizer to control the initial size of colloid. However, it was reported that PVA can dissolve and degrade in water, especially under conditions similar to that used for the oxidation of HMF.[15] This could result in the loss of stabilizing ligands from the Au and Pd nanoparticles and potentially lead to particle agglomeration during the reaction and catalyst deactivation[16]. To prove this hypothesis, a different stabilizer Polyvinylpyrrolidone(PVP) were used in the preparation of the metal colloid as PVP is reported to offer greater stability than PVA in water[17], and the catalysts were examined in a same way as the PVA-catalyst, see Fig. 5.13.

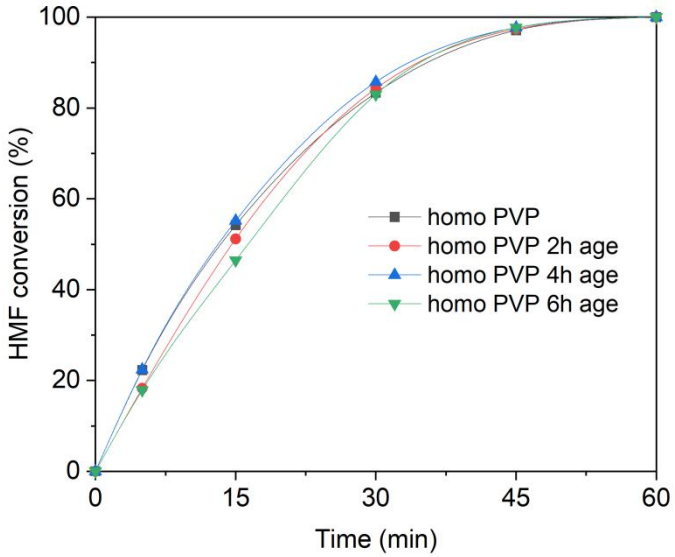

Figure 5.13. Catalytic performance of (Au + Pd)/C with different aging time of Au and Pd colloid stabilized by PVP. *Reaction conditions*: HMF (0.1 M); $NaHCO_3$ (0.4 M); H_2O (16 mL); 80 °C; pO_2 = 3 bar; 1 h; catalyst amount for (Au + Pd)/C: 143.1 mg, carbon balance all around 98%.

Through comparison of Fig. 5.11 and 5.13, catalytic performance are comparable when there is no aging time for both catalysts prepared *via* PVA and PVP, however it is explicit to observe that catalytic performance is maintained, regardless of ageing time when replacing the PVA ligand with PVP, with this attributed to the inhibition of alloyed Au-Pd nanoparticle formation. Therefore, by applying a different stabilizer in the preparation of the metallic colloid an enhanced catalytic performance is observed. It is possible that the use of the PVP ligand can inhibit the formation of agglomerates to a greater extent than PVA[18–20].

These results indicate the versatility of this approach to catalyst design and highlights that there is further optimization possible. Compared to conventional methods of catalyst preparation[21–26], where the metallic nanoparticles are usually co-immobilized on to the support this methodology has shown that significant improvements in

catalytic performance can be achieved through elemental spatial separation. Though this method depends on the choice of stabilizer, ***e.g.***, when PVP was used catalyst stability and activity was greater than when PVA was utilized. In the following sections, HMF oxidation using the series of catalysts prepared by PVP are tested to expand the proposed mechanism to another stabilizer, furthermore the oxidation of several other alcohols were investigated, to determine if the proposed mechanism is applicable to different substrates.

5.6 Application of the newly found catalysis system

5.6.1 AuPd/C catalysts prepared with PVP for HMF oxidation

Using different capping ligands on supported nanoparticles have previously shown to have a dramatic effect on catalytic performance in selective oxidation reactions due to surface blocking, electronic and site-isolating effects[27]. Given the fact that the choice of stabilizer is known to have a significant influence on many catalytic properties further study into the effect of ligand on the oxidation of HMF over carbon supported AuPd catalysts has been conducted. A series of Au and Pd catalysts, previously developed in *Chapter 3 and 4*, were prepared replacing PVA with PVP as the stabilizing ligand. These catalysts were subsequently tested for HMF oxidation under the same reaction conditions. As shown in Fig. 5.14 (A), the same activity trend from series of Au and Pd catalytic performance was observed with PVA and PVP as the capping ligand; namely (Au + Pd)/C > Au/C + Pd/C > Au-Pd/C > Au/C >> Pd/C in terms of HMF conversion. Also, the activities of all these PVP-catalysts are comparable to the PVA-catalysts, compared with Fig. 5.14 (B). It is therefore conclusive that the catalytic trend observed is not dependent on the choice of stabilizer. The proposed mechanism has a wide application to different ligands.

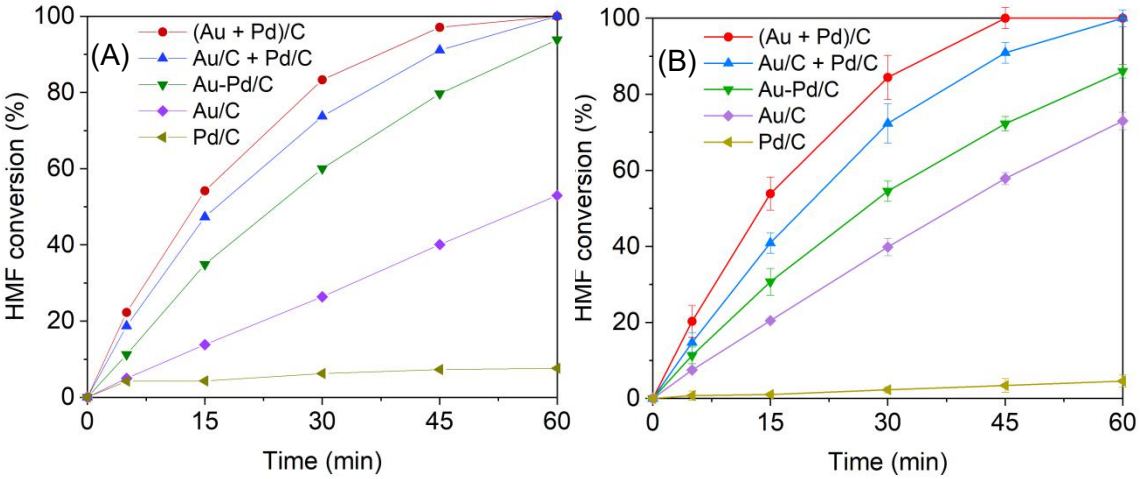

Figure 5.14. Time-on-line data for aqueous HMF conversion over a systematic series of catalysts stabilized by (**A**) PVP ligands; (**B**) PVA ligands. *Reaction conditions*: HMF (0.1 M), $NaHCO_3$ (0.4 M), H_2O (16 mL), catalyst amount: 143.1 mg, 80 °C, pO_2 = 3 bar, 60 min.

5.6.2 Glycerol and ethanol oxidation.

The enhancement in catalytic activity observed through spatial separation is extremely promising. To determine if the efficacy of spatially separated catalysts is widely applicable it was decided to investigate the AuPd catalyst series for the selective oxidation of glycerol and ethanol. In particular glycerol and ethanol were chosen, as it is known that glycerol is a highly functionalized molecule, its oxidation reaction can produce a large number of value added products[28], *e.g.*, glyceric acid, oxalic acid, tartronic acid, with its main reaction route presented in Scheme 5.2. Apart from glycerol, ethanol is also a widely use molecule as a platform molecule to study alcohol oxidation[29,30].

In this study, the oxidation of glycerol and ethanol were performed under similar reaction conditions to those used for HMF oxidation, as described in *Chapter 2*. Fig. 5.15 and Table 5.2 compare the activity of the previously studied AuPd catalysts series towards glycerol oxidation. It is clear that a similar trend in catalytic activity is observed to that previously reported for HMF oxidation, namely: (Au + Pd)/C > Au/C +

Pd/C > Au-Pd/C > Au/C > Pd/C. Fig. 5.16, displays the product distribution of glycerol oxidation after 2 h for each catalyst, in which glyceric acid is the dominant product followed by the tartronic acid.

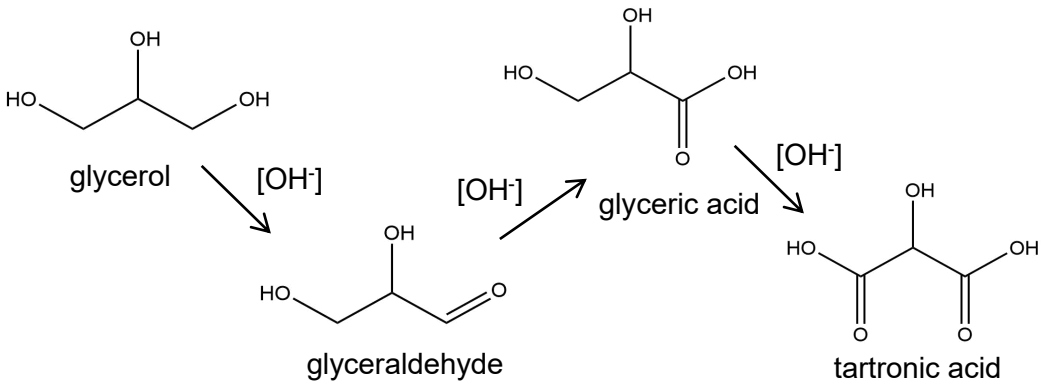

Scheme 5.2. Reaction route of aqueous glycerol oxidation to tartronic acid.

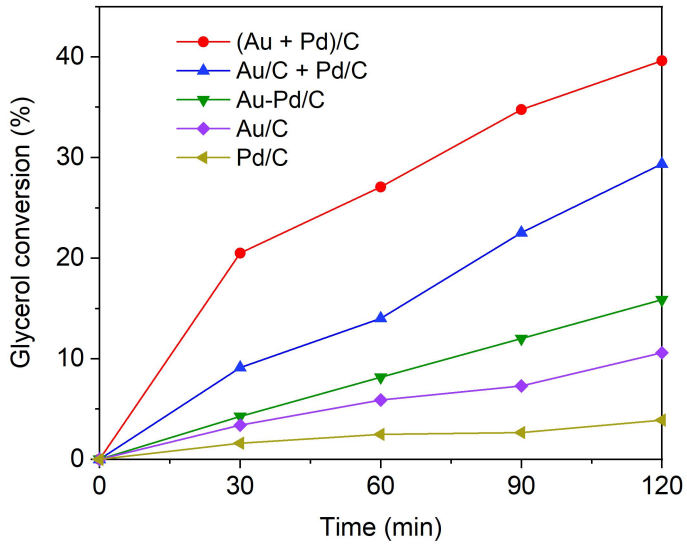

Figure 5.15. Comparison of catalyst formulations in glycerol oxidation. *Reaction conditions*: glycerol (0.6 M), Na_2CO_3 (1.2 M), H_2O (16 mL); 60 °C; pO_2 = 3 bar; catalyst amount: (Au + Pd)/C, Au/C + Pd/C and Au-Pd/C: 143.1 mg; Au/C: 72.1 mg; Pd/C: 71 mg, glycerol/metal = 1200/1, mol/mol, carbon balance are all around 98%.

Table 5.2. The performance of supported metal catalysts in the aqueous phase aerobic oxidation of glycerol.

Entry	Catalyst	T (°C) / t (h)	*P* O_2, bar	Reaction rate, mmol . L .h^{-1}
1	(Au + Pd)/C	80 / 0.5	3	246
2	Au/C + Pd/C	80 / 0.5	3	109
3	Au-Pd/C	80 / 0.5	3	50
4	Au/C	80 / 0.5	3	40
5	Pd/C	80 / 0.5	3	19

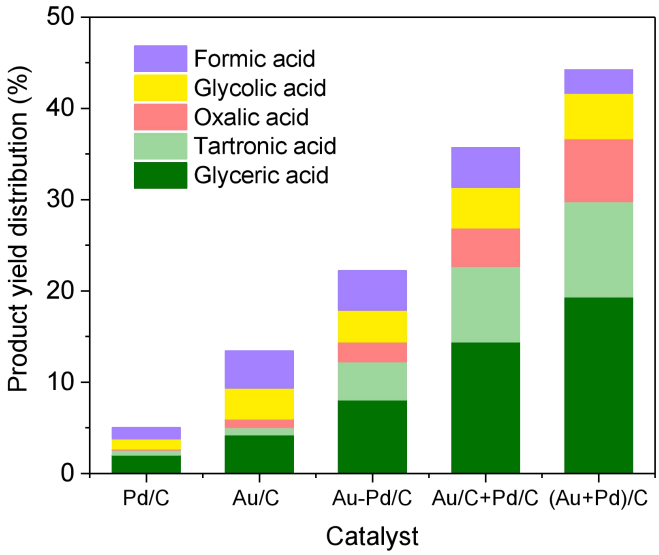

Figure 5.16. Product distribution in glycerol oxidation after 2 h. *Reaction conditions*: glycerol (0.6 M), Na_2CO_3 (1.2 M), H_2O (16 mL); 60 °C; pO_2 = 3 bar; catalyst amount: (Au + Pd)/C, Au-Pd/C: 143.1 mg; Au/C: 72.1 mg; Pd/C: 71 mg, glycerol/metal = 1200/1, mol/mol, carbon balance are all around 98%.

Further comparison of catalytic activity towards ethanol oxidation is seen in Fig. 5.17. The same activity trend is observed as previously reported for both HMF and glycerol oxidation, namely: (Au + Pd)/C > Au/C + Pd/C > Au-Pd/C > Au/C > Pd/C. It is therefore possible to conclude that the enhanced activity achieved through spatial separation is widely applicable to a range of selective oxidation reactions. Similar to the mechanism proposed for HMF oxidation in the presence of a physical mixture of Au/C and Pd/C, ethanol transforms to acetaldehyde *via* a dehydrogenation process on the surface of Au where two protons are generated and immediately neutralised in solution, meanwhile two electrons are produced and transferred to Pd through the carbon support, where they can be consumed *via* an ORR process leading to the liberation of the Au active sites, see equations (1) - (5) below. The oxidation of the intermediate product acetaldehyde to acetic acid follows the same mechanism as ethanol oxidation[31], with the oxidation of acetalaldehyde known to occur more efficiently over Au-based catalysts[32], in the presence of base, which means once there is yield of acetaldehyde it will quickly be converted to acetic acid. The generated electrons are consumed by ORR as well to accelerate the generation of the final product acetic acid.

(1) CH_3CH_2OH (ethanol) + 2 OH^- → CH_3CHO (acetaldehyde) + 2 H_2O + 2 e^-

(2) CH_3CHO (acetaldehyde) + H_2O → $CH_3CH_3O_2$ (geminal diol)

(3) $CH_3CH_3O_2$ (geminal diol) + 2 OH^- → CH_3COOH (acetic acid) + 2 H_2O + 2e^-

(4) O_2 + 2 H_2O + 4 e^- → 4 OH^-

(5) O_2 + H_2O + 2 e^- → HO_2^- + OH^-

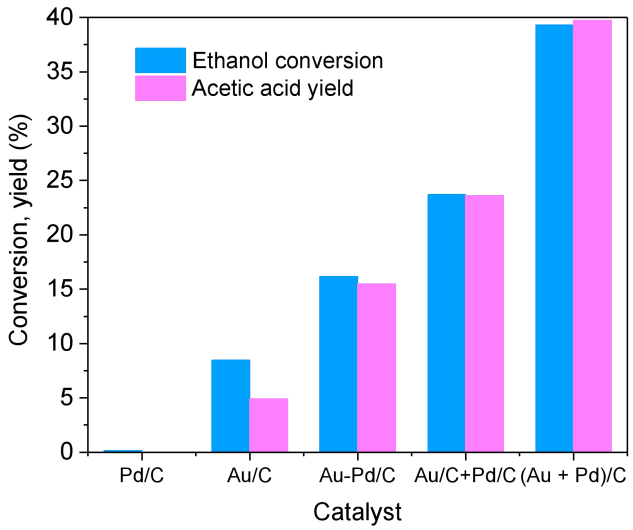

Figure 5.17. Comparison of catalyst mixtures in ethanol oxidation. *Reaction conditions*: ethanol (0.8 M), Na_2CO_3 (1.6 M), H_2O (16 mL); 60 °C; pO_2 = 3 bar; 2 h; catalyst amount: (Au + Pd)/C, Au/C + Pd/C and Au-Pd/C: 143.1 mg; Au/C: 72.1 mg; Pd/C: 71 mg.

In conclusion, it has been demonstrated that the catalytic trends previously outlined in *Chapter 4* are not dependent on either the stabilizing ligand utilized in the catalyst preparation or the chosen substrate. A synergistic effect was observed between Au and Pd nanoparticles when present as a physical mixture or spatially separated on the same grain of support.

5.6.3 Electrocatalytic oxidation

As was reviewed in *Chapter 1*, instead of thermal catalysis, David *et al*. have previously reported the electro catalytic oxidation of HMF using Au and Pd catalyst to demonstrate the synergy between Au and Pd[9]. From their work, the C supported bimetallic AuPd catalyst showed a higher peak intensity than the corresponding monometallic Au or Pd in the experiment of cyclic voltammetry (CV), which is consistent to the thermal catalysis results in this study. Especially at 0.9 V *vs*. RHE, the bimetallic catalyst is reported by Davies *et al*. to present a net current density of approximate 7 mA/cm^2, whereas the net current density of the Au- or Pd-only catalysts are much lower, 3 mA/cm^2 (Fig. 1.12 in *Chapter 1*). Additional CV works were performed in same condition but with absence of HMF showing that Pd is easily oxidized in the forward loop (oxidation scan), with a a higher PdO reduction peak observed in the backward loop (reduction scan). While for, in the case of the Au-only catalyst the oxidation state of Au remained stable (Au^0). These results suggest that there is a continual Pd redox cycle (Pd^0/Pd^{2+}) whilst the Au is mainly focusing on HMF oxidation within its metallic statues. This is consistent with the XPS (*Chapter 4*, Fig. 4.1) and TPR results in this study, Fig. 5.9, where Pd was found to exist in the oxidized form, while Au remains in the metallic state after use in the HMF oxidation reaction. Beside, Latsuzbaia *et al.* have also reported a similar phenomenon from HMF electro catalytic oxidation over AuPd bimetallic systems showing a higher CV signal than the monometallic Au[33], as reviewed in *Chapter 1.* At present in this study, the enhanced activity of the physical mixture (Au/C + Pd/C) and binary mixture (Au + Pd)/C have been heavily studied for thermal oxidation of a range of alcohols in the liquid phase.To expand on these studies the current catalysis system was investigated for the electrochemical oxidation of HMF in order to compare the trends between thermo- and electro-catalysis and to gain insight into the benefits of spatially separating the component metals, using similar conditions to those previously used by Davis *et al.*[10]

Building on these previous studies, CV was performed over the series of AuPd catalysts discussed above using a half cell reactor, identical amounts of catalyst were placed onto the surface of a glassy carbon electrode with a Nafion solution (procedure outlined in *Chapter 2, Section 2.3.4*). The electrochemical system was under an inert atmosphere of N_2 gas with vigorous stirring, electron removal from the surface of Au, typically facilitated by O_2[34,35], was replaced with an applied potential. Meanwhile, a Pt wire was applied as the counter electrode with Saturated Calomel Electrode (SCE) as reference electrode, more details are described in *Chapter 2*. Experimental results are shown in Fig. 5.18.

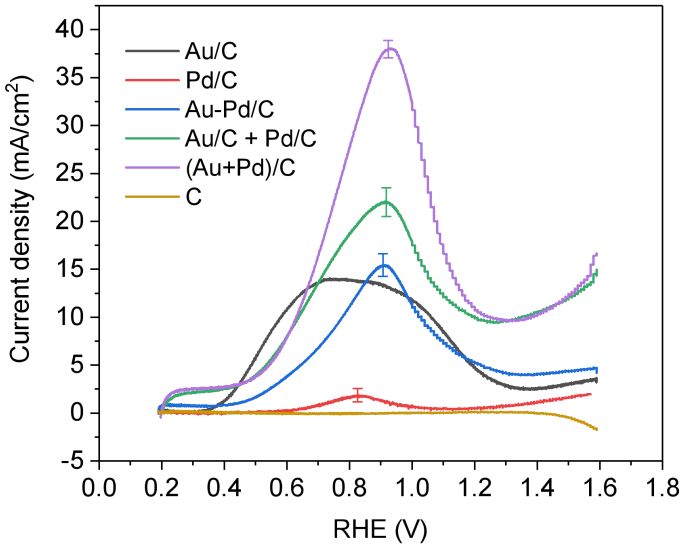

Figure 5.18. Cyclic voltammetry, forward scan of HMF solution over each catalyst on glassy carbon electrode (blank current density subtracted). Reaction conditions: room temperature; scan rate 50 $mV.s^{-1}$; 4 loops; ambient temperature under N_2 flow and vigorous stirring, NaOH (0.1 M), HMF (0.02 M), 50 mL H_2O.

As shown in Fig.5.18, HMF oxidation peak is obtained at *ca* 0.9 V *vs*. RHE, which is at a same potential range to literature (SCE has been normalized to Reversible

Hydrogen Electrode, E(RHE) = E(SCE) + 0.0591pH + 0.24). The trend observed in peak current density for the Au/C, Pd/C and Au-Pd/C catalysts align well with recent literature[9]. The physical mixture of Au/C and Pd/C catalysts and the (Au+Pd)/C catalyst both provide increased peak current density at the same potential; the trend in electrocatalytic activity across the catalysts studied is in good agreement with that of their thermal catalytic performance, showing a good linear free energy relationship (LFER) correlation, see Fig. 5.19.

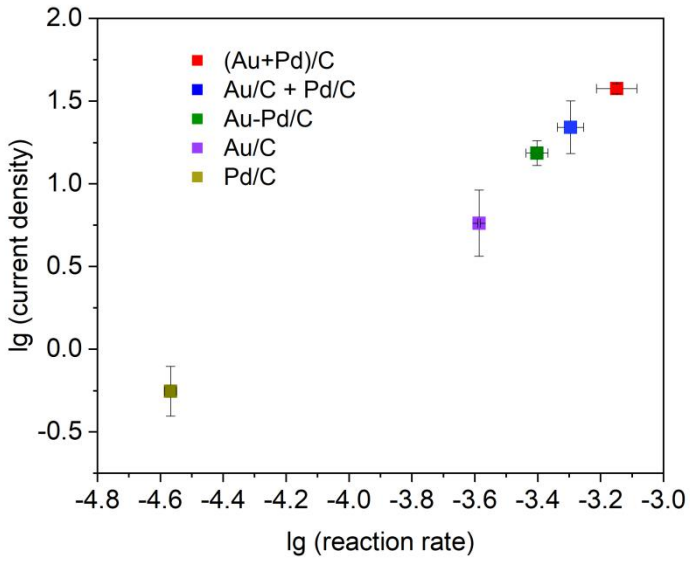

Figure 5.19. Linear free energy relationship plot to demonstrate correlation between the thermo and electro catalytic HMF oxidation experiments, over the series of catalysts. For the thermocatalytic experiments, the initial rate measurements were taken after 5 minutes of reaction. The current density measurements were taken from the maxima observed in the corresponding CV experiments (Fig. 5.18).

The thermal catalytic experiments demonstrate that, for the oxidation studied here, the Au and Pd work through redox cooperation, requiring a conductive support; initial electrochemical experiments are consistent with this view, thereby the thermal catalytic system is applicable to electrocatalytic system. It is considered that the

discovery of enhancement effect by spatially separating Au and Pd nanoparticles will provide deep insight into the future design of bimetallic catalysts. Further works will focus on identifying other electrochemical reactions where such mechanisms might give rise to analogous separation effects, *e.g.*, ketone oxidation to lactone[36].

5.7 Summary

The (Au + Pd)/C catalyst, where metal nanoparticles are spatially separated yet immobilized on the same grain of support, has been observed to offer greater activity in the oxidation of a range of alcohols, compared to an analogous physical mixture of monometallic catalysts. The close proximity, but elemental separation, of nanoparticles is found to be crucial in enhancing catalytic activity for a number of selective oxidation reactions. Detailed catalyst characterization by microscopy shows no evidence for the formation of Au-Pd alloy in the fresh catalyst of (Au + Pd)/C. However, after reaction nanoparticle morphology is seen to alter, with the formation of Au-core-Pd-shell alloys observed and a subsequent loss in activity, giving further support for the need for elemental separation. Identical trends in catalytic activity to that seen for HMF oxidation are observed for the oxidation of both glycerol and ethanol, indicating the versatile nature of these materials. In keeping with results from thermal catalytic batch reactions, cyclic voltammetry (CV) analysis, using a half cell reactor, displayed the same catalytic trend, with the (Au + Pd)/C catalyst observed to offer greatest peak intensity of the catalysts studied. On the basis of these observations, the new explanation for synergistic interactions in Au and Pd bimetallic nanoparticles in liquid phase aerobic oxidation reactions proposed in *Chapter 4* is further supported. The Au and Pd system can work in tandem through redox cooperation on a conductive support. It is strongly considered that this discovery will play a crucial role in the design and synthesis of heterogeneous catalysts moving forward.

5.8 References

1 O. Casanova, S. Iborra and A. Corma, *ChemSusChem*, 2009, **2**, 1138–1144.

2 N. K. Gupta, S. Nishimura, A. Takagaki and K. Ebitani, *Green Chem.*, 2011, **13**, 824–827.

3 Y. Y. Gorbanev, S. K. Klitgaard, J. M. Woodley, C. H. Christensen and A. Riisager, *ChemSusChem*, 2009, **2**, 672–675.

4 M. Douthwaite, X. Huang, S. Iqbal, P. J. Miedziak, G. L. Brett, S. A. Kondrat, J. K. Edwards, M. Sankar, D. W. Knight, D. Bethell and G. J. Hutchings, *Catal. Sci. Technol.*, 2017, **7**, 5284–5293.

5 B. Brandt, T. Schalow, M. Laurin, S. Schauermann, J. Libuda and H. J. Freund, *J. Phys. Chem. C*, 2007, **111**, 938–949.

6 G. Zheng and E. I. Altman, 2000, **462**, 151–168.

7 H. Zhu, Z. Qin, W. Shan, W. Shen and J. Wang, *J. Catal.*, 2004, **225**, 267–277.

8 J. B. Xu, T. S. Zhao, Y. S. Li and W. W. Yang, *Int. J. Hydrogen Energy*, 2010, **35**, 9693–9700.

9 D. J. Chadderdon, L. Xin, J. Qi, Y. Qiu, P. Krishna, K. L. More and W. Li, *Green Chem.*, 2014, **16**, 3778–3786.

10 D. J. Chadderdon, L. Xin, J. Qi, Y. Qiu, P. Krishna, K. L. More and W. Li, *Green Chem.*, 2014, **16**, 3778–3786.

11 X. Ning, Y. Li, B. Dong, H. Wang, H. Yu, F. Peng and Y. Yang, *J. Catal.*, 2017, **348**, 100–109.

12 B. Zhang and D. S. Su, *ChemCatChem*, 2015, **7**, 3639–3645.

13 P. Sahu and B. L. V. Prasad, *Chem. Phys. Lett.*, 2012, **525**–**526**, 101–104.

14 D. Jose and B. R. Jagirdar, 2008, 10089–10094.

15 Y. Chen, Z. Sun, Y. Yang and Q. Ke, *J. Photochem. Photobiol. A Chem.*, 2001, **142**, 85–89.

16 A. Villa, D. Wang, D. S. Su and L. Prati, *ChemCatChem*, 2009, **1**, 510–514.

17 K. M. Koczkur, S. Mourdikoudis, L. Polavarapu and S. E. Skrabalak, *Dalt. Trans.*, 2015, **44**, 17883–17905.

18 S. Gil, C. Jiménez-Borja, J. Martin-Campo, A. Romero, J. L. Valverde and L. Sánchez-Silva, *J. Colloid Interface Sci.*, 2014, **431**, 105–111.

19 Y. Xiong, I. Washio, J. Chen, H. Cai, Z. Y. Li and Y. Xia, *Langmuir*, 2006, **22**, 8563–8570.

20 L. Kemal, X. C. Jiang, K. Wong and A. B. Yu, *J. Phys. Chem. C*, 2008, **112**, 15656–15664.

21 M. M. Forde, L. Kesavan, M. I. Bin Saiman, Q. He, N. Dimitratos, J. A. Lopez-Sanchez, R. L. Jenkins, S. H. Taylor, C. J. Kiely and G. J. Hutchings, *ACS Nano*, 2014, **8**, 957–969.

22 W. C. Li, M. Comotti and F. Schüth, *J. Catal.*, 2006, **237**, 190–196.

23 M. Peroni, I. Lee, X. Huang, E. Baráth, O. Y. Gutiérrez and J. A. Lercher, *ACS Catal.*, 2017, **7**, 6331–6341.

24 A. Villa, D. Wang, G. M. Veith, F. Vindigni and L. Prati, *Catal. Sci. Technol.*, 2013, **3**, 3036–3041.

25 Y. Shang, C. Min, J. Hu, T. Wang, H. Liu and Y. Hu, *Solid State Sci.*, 2013, **15**, 17–23.

26 T. Loewenstein, A. Hastall, M. Mingebach, Y. Zimmermann, A. Neudeck and D. Schlettwein, *Phys. Chem. Chem. Phys.*, 2008, **10**, 1844–1847.

27 K. Chen, H. Wu, Q. Hua, S. Chang and W. Huang, *Phys. Chem. Chem. Phys.*, 2013, **15**, 2273–2277.

28 M. Pagliaro, R. Ciriminna, H. Kimura, M. Rossi and C. Della Pina, *Angew. Chemie - Int. Ed.*, 2007, **46**, 4434–4440.

29 B. N. Zope, D. D. Hibbitts, M. Neurock and R. J. Davis, *Science*, 2010, **330**, 74.

30 A. Ehsani, A. A. Heidari and R. Asgari, *Chem. Rec.*, 2019, **19**, 2341–2360.

31 B. N. Zope, D. D. Hibbitts, M. Neurock and R. J. Davis, *Science (80-.).*, 2010, **533**, 74–79.

32 C. Marsden, E. Taarning, D. Hansen, L. Johansen, S. K. Klitgaard, K. Egeblad and C. H. Christensen, *Green Chem.*, 2008, **10**, 168–170.

33 R. Latsuzbaia, R. Bisselink, A. Anastasopol, H. van der Meer, R. van Heck, M. S. Yagüe, M. Zijlstra, M. Roelands, M. Crockatt, E. Goetheer and E. Giling, *J. Appl. Electrochem.*, 2018, **48**, 611–626.

34 Z. Bhushan N., H. David D., N. Matthew and D. Robert J., *Science (80-.)*., 2010, **330**, 74–78.

35 S. E. Davis, B. N. Zope and R. J. Davis, *Green Chem.*, 2012, **14**, 143–147.

36 J. H. Maalouf, K. Jin, D. Yang, A. M. Limaye and K. Manthiram, *ACS Catal.*, 2020, **10**, 5750–5756.

Conclusions and future plans

6

Introduction

In this chapter, key conclusions from the previous results chapters are summarized. Furthermore, the advantages and disadvantages from the investigated catalytic systems are considered. Building on this, future work is proposed which highlights areas which could be further improved in liquid phase aerobic alcohol oxidation.

6.1 Conclusions

As discussed in *Chapter 1*, Hydroxymethylfurfural (HMF) is regarded as one of the most important biomass derived molecules. Reaction route see Scheme 6.1 below.

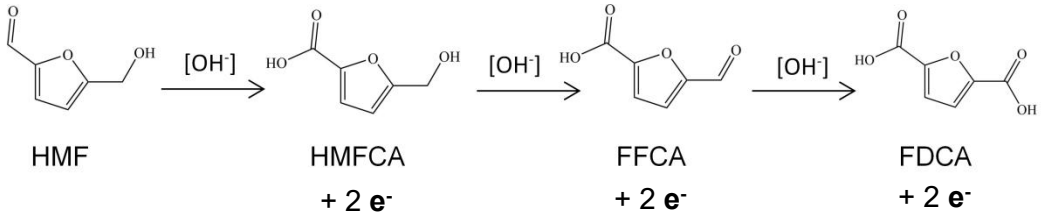

Scheme 6.1. Reaction route of aqueous HMF oxidation to terminal product FDCA.

The terminal oxidation product from this reaction, 5-furandicarboxylic acid (FDCA), is considered to be a cost-effective component for the production of bio-based plastics and offers a green alternative to petroleum-based terephthalate polyesters. For this reason, an abundance of resource has been focused towards developing materials which catalyse this reaction efficiently, as discussed in *Chapter 1*. Bimetallic catalysts possessing both Au and Pd in particular have been assessed extensively for this reaction. This is because high activities are often observed with such catalysts, which is often attributed to synergistic interactions between Au and Pd, and such relationships are applicable to many other reactions too, listed in *Chapter 1*. However, understanding the origin of this synergistic effect is challenging. The work presented in this thesis provides a possible explanation for the enhancements observed through combining Au and Pd in such reactions.

The first results chapter, *Chapter 3*, focused on assessing the reactivity of Au/C + Pd/C physical mixtures for aqueous HMF oxidation. The first interesting observation was that monometallic Au and Pd exhibited less activity when compared to their use as a physical mixture; the sum of HMF converted over the monometallic catalysts

separately was notably less than in a reaction where they were combined. The first thought was that the monometallic catalyst may have been leaching in reaction solution, thus the alloyed AuPd particles are formed. However, ICP-AES analysis indicated no leaching from the post reaction solution. Furthermore, this enhancement from the physical mixture is found to be even greater than the corresponding Au-Pd alloy, which is unexpected. For most cases in Au-Pd alloy, the incorporation of Pd into these materials, to produce supported bimetallic AuPd nanoparticles, leads to an increase in catalytic performance.. Therefore, intermediate products from HMF oxidation, *i.e*. HMFCA, FFCA were also investigated and a similar trend in reactivity was observed again; Au/C + Pd/C > Au-Pd/C > Au/C > Pd/C. STEM-EDS analysis has confirmed that there is no evidence to suggest transfer of Au or Pd from the components of the physical mixture occurred during the reaction. The mechanism over physical mixture catalyst was proposed in *Chapter 4* and meanwhile strengthened in the same chapter using different catalyst supports. it was found that Au is generating electrons from HMF oxidation on its nanoparticle surface with consumption of OH^- where the Pd is working like electron scavenger which consumes the electrons through a cooperative redox cycle (Pd^0/Pd^{2+}). Carbon is serving as the medium for electron mobile from one metal to the other due to its high conductivity. However, when TiO_2 and BN were used as semi-conductive and non-conductive material instead of C in the preparation for the supported Au and Pd catalysts, catalytic activity decreased drastically. Therefore, the charge transfer between Au and Pd with different supports may strongly be affected by the conductivity of the support. However looking forward, the determination of rate limiting step in HMF oxidation remains unclear in this study. It could be the oxidative dehydrogenation (ODH) of alcohol occurs mainly on the surface of Au. Alternatively, the rate limiting step is from the oxygen reduction over Pd which slows down the whole reaction due to the efficiency of electron consumption. In fact, this ORR process is crucial because it avails more Au catalyze the ODH once electrons are transferred away from Au to Pd. Alternatively, the electron transfer process through the C support could be the rate

limiting step due to coupling of two half reactions of oxidation and reduction. More future work need to be done in order to understand what is the rate limiting step in the physical mixture system, ***e.g.***, to run D-HMF (α-hydrogens are deuterated) oxidation; or HMF oxidation with addition of electron trap[1], more details are described in next *Section 6.3.* All these works are significant for future catalyst design in looking for the most reactive catalyst in alcohol oxidation.

In addition to the thermo-catalysis, analogous electro-catalysic experiments were conducted to conclude the existence of electron transfer between Au and Pd are under flow of O_2. In contrast, when the system is under an environment of N_2, the observed current decreased immediately down to nearly zero, this switch between O_2 and N_2 was repeated for 3 cycles with current number increases and decreases periodically. Overall, this part has firmly evidenced the reliability of the proposed mechanism, the interaction between Au and Pd is through the electron transfer on C.

In *Chapter 4,* the molar ratio between Au and Pd was altered, where the nanoparticle size of Au an Pd changed accordingly. Such size effect determines the role of Au and Pd in the alcohol oxidation, where for the Au rich Pd catalysts, the Au is working on electron generation and then consumed on Pd, while for the Pd rich Au catalysts, in opposite, the Pd is working on electron generation and then consumed on Au. Such effect of one metal catalyze ODH of alcohol, the other on oxygen reduction is denoted as 'CORE' (cooperative redox enhancement), implicated and building on this CORE, it would be very important for the future work to look for this CORE effect between any two different metals in alcohol oxidation reactions, for example, Au and Ag, Au and Pt, Au and Ir. Because all those Pt, Au or Ir metals are reported to be very reactive at oxygen reduction[2]. More details are described in next future work *Section 6.3.* This investigation could offer people more ideas in designing and synthesizing multi component heterogeneous catalysts for the future. For the last *Chapter 5*, it is mainly an application of the newly discovered catalysts system. Based on the proposed mechanism another new catalyst where Au and Pd nanoparticles deposited on a

common C grain was prepared. Through spatial separation, the catalyst exhibited an even higher activity than the physical mixture and the alloy. This exceptional performance is attributed to a closer distance between Au and Pd nanoparticles. Electron transfer can happen more easily on a common C grain, as there is no necessity for particle collision as with the physical mixture. As is reviewed and compared in *Appendix*, in terms of productivity towards to FDCA, this Au and Pd catalyst with nanoparticles spatially separated, known as ”binary mixture” can achieve 80 $mol_{FDCA}.mol_{metal}.h^{-1}$, where the current best catalyst from literature among all series of Au and Pd catalysts is 99 $mol_{FDCA}.mol_{metal}.h^{-1}$. Compared to the Au-Pd alloy, which has a productivity number of 21.3 $mol_{FDCA}.mol_{metal}.h^{-1}$, as a breakthrough, the “binary mixture” catalyst shows almost 4 times higher of the activity than the alloy. However, this “binary mixture” contains disadvantages too, where the Au and Pd nanoparticles would migrate on its C grain during reaction, some deactivation is seen after recycle for 3 times, and this deactivation becomes more obvious in the third cycle. Microscopic characterization has confirmed this migration where some nanoparticles of AuPd alloy was observed from the sample after use, and from particle tracking, the mean particle size becomes larger when compared to the fresh sample before use as a catalyst (before reaction: 3.8 nm, after reaction: 4.5 nm). To solve this problem, more experiments are needed in future work, for instance, by immobilizing the Au and Pd nanoparticles onto C support with a different sequence, different ligands can be used in the preparation for the catalyst. In order to apply this the newly discovered catalytic system to versatile alcohols, ethanol and glycerol were then selected to test the catalytic activities. It is known that ethanol and glycerol both have alcohol functional groups, its aqueous oxidation pathway in base is close to HMF oxidation. Indeed, the same catalytic trend is observed over the series of catalysts, namely: (Au + Pd)/C > Au/C + Pd/C > Au-Pd/C > Au/C > Pd/C. Furthermore, based on all these HMF, ethanol and glycerol oxidation as foundations, more future works are featured in agenda to test even a bigger range of molecules, *e.g.*, propanol, butanol and octanol. Beside reactants of alcohol, other molecules for example ketone oxidation to lactone

is also within our interest[3], which would largely expand the discovered CORE effect. In hypothesis, the system of physical mixture would be applicable as long as there is CORE effect. More details are discussed in next future work *Section 6.3.* These evidences have clearly supported that by spatially separate the Au and Pd nanoparticles, the enhanced activity could be extended to aerobic oxidation of different alcohols. For future work, more alcohols are worth going to be tested, *i.e*. propanol, butanol, benzyl alcohol, which are all within our interest.

Finally, the catalytic system demonstrated good performance in cyclic voltammetry in *Chapter 5*, where the electro-catalysis aligned very well to the thermo- catalysis. The maximum current density 40 mA/cm^2 appeared at 0.9 V *vs*. RHE for the "binary mixture" catalyst, which is almost 6 times higher compare to the literature where 7 mA/cm^2 net current density was observed over Au-Pd/C alloy. Nevertheless, the illustration of onset potential remained challenging in this work. Especially for the monometallic Au where the lowest onset potential is observed compared to the other catalysts, which indicates the ease of converting HMF over Au, the smallest driving force is provided. In contrast, the Au shows a lower activity in thermal catalytic oxidation of HMF in terms of a lower initial rate, 2.4x10^{-5} M.s^{-1}. The results are consistent to what had been reviewed in *Chapter 1*, Fig. 1.12, however considering the step of HMFCA oxidation to FFCA was reported to be the rate limiting step[4,5], it would be beneficial to conduct another CV starting with HMFCA, implicated from the same work reviewed in *Chapter 1*, in order to find an explanation for the onset potential from each catalysts.

It is strongly suggested that this discovery of rate enhancement by spatially separating Au and Pd nanoparticles will provide an additional, novel approach to research into bimetallic catalysts. It offers a new foundation for the development of multi-component heterogeneous catalysts. Building on this discovery, more application areas, *i.e*. electrochemical cell, where by one cell, it contains biomass conversion into value-added products, by the other cell contains a second reaction, *i.e*.

hydrogen peroxide synthesis will be looked at. More details are listed in this *Chapter 6, Section 6.3*.

6.2 Final conclusions

In conclusion, this study has provided a new explanation for the enhancement effect between nanoparticles of Au and Pd with a support of carbon black in alcohol oxidation reactions, *i.e*. HMF oxidation, glycerol oxidation and ethanol oxidation. Up to date, there has been no definitive demonstration of the origin of such interesting effect. In this thesis, it investigated how to enhance the rate of a given reaction through spatially separating the metal nanoparticles on a common C granule. Demonstrating that this enhancement, in aerobic aqueous oxidative dehydrogenation of alcohols, is attributable to a continuous redox cooperation in the bimetallic catalysts. Alongside, experiments on electrochemistry have been set out to further supports to this new phenomenon and establish the validity of the proposed mechanism.

Though, a new and highly efficient AuPd catalyst series have been heavily investigated in this thesis, additional works are required with regards to the rate limiting step and how to expand this system with other metals, *i.e*. Pt, Ru, Cu. Building on this discovery, we will seek to identify further reactions where such ‘CORE’ might give rise to analogous separation effects, involving its application in the research area of electrochemical cell, see *section 6.3*.

6.3 Future plans

As was discussed in the conclusion section, performing a reaction of D-HMF (α-hydrogens are deuterated) oxidation would be very important as it could be revealing on how kinetic isotope effect (KIE) for ODH change throughout. KIE indicates the change in the reaction rate of a chemical reaction when one of the atoms in the reactants is replaced by one of its isotopes[6]. To establish whether electron transfer is rate determining over catalyst of physical mixture, it should be plausible to demonstrate that this occurs by introducing an electron trap into the reaction solution, thereby uncoupling the ODH and ORR, to stop the overall chemical transformation. The performance of the other catalysts should be relatively unaffected by adding trap. Such a trap might be a viologen or crystal violet, especially in reactions using bicarbonate as base, and this could provide a colorimetric check on the trapping process. Such experiments seem essential to support our general thinking on this mechanism of catalysis enhancement. Building on the 'CORE' effect between Au and Pd, different metals will be interested to test on its activity for ODH and ORR, to prove such 'CORE' effect is well applicable in bimetallic catalyst with different metals, including the size effect from each metal. Insight into coupling of ODH and ORR between different metals would provide more evidences on what the driving force is for the electron transfer.

Additional electrochemical reactions of cyclic voltammetry are in the list of future plans too. Apart from the tested HMF molecule, HMFCA and FFCA are targeted as the reactant molecules over catalysts of Au/C, Pd/C, Au-Pd/C alloy, Au/C + Pd/C physical mixture and (Au+Pd)/C under an identical reaction condition to fully understand the catalytic trend of onset potential and current density. It would be helpful to have a comprehensive comparison between thermal and electrical catalysis as onset potential is a close concept to activation energy and current density is a close meaning to turnover numbers[7]. Lower is the onset potential, higher is the current density, easier is occurence of the reaction. Therefore, it could also distinguish the

rate limiting step during alcohol oxidation reaction, especially for cascade reactions.

6.4 References

1 P. Liu, V. Degirmenci and E. J. M. Hensen, *J. Catal.*, 2014, **313**, 80–91.

2 J. K. Nørskov, J. Rossmeisl, A. Logadottir, L. Lindqvist, J. R. Kitchin, T. Bligaard and H. Jónsson, *J. Phys. Chem. B*, 2004, **108**, 17886–17892.

3 J. H. Maalouf, K. Jin, D. Yang, A. M. Limaye and K. Manthiram, *ACS Catal.*, 2020, **10**, 5750–5756.

4 B. Siyo, M. Schneider, M.-M. Pohl, P. Langer and N. Steinfeldt, *Catal. Letters*, 2014, **144**, 498–506.

5 N. K. Gupta, S. Nishimura, A. Takagaki and K. Ebitani, *Green Chem.*, 2011, **13**, 824–827.

6 S. Trasatti, *Electrochim. Acta*, 2007, **52**, 2729–2730.

7 R. Holze, *Experimental electrochemistry: a laboratory textbook*, John Wiley & Sons, 2019.

Appendix

Table S1. Summary of HMF oxidation over versatile bimetallic AuPd catalysts in literature.

Catalyst	Solvent	T (℃)	P (bar)	HMF/metal (mol/mol)	Time (h)	FDCA productivity ($mol_{FDCA}.mol_{metal}^{-1}.h^{-1}$)	Ref
Au_3Pd_1/ZOC	$NaHCO_3$	80	3	100/1	4	19.8	1
Au_2Pd_1/ZOC	$NaHCO_3$	80	3	100/1	4	22.5	1
Au_1Pd_1/ZOC	$NaHCO_3$	80	3	100/1	4	24.8	1
Au_1Pd_2/ZOC	$NaHCO_3$	80	3	100/1	4	21.8	1
Au_1Pd_3/ZOC	$NaHCO_3$	80	3	100/1	4	17.3	1
Au_1Pd_1/MG20	$NaHCO_3$	80	3	100/1	4	22.5	1
Au_1Pd_1/CeO_2	$NaHCO_3$	80	3	100/1	4	19.3	1
Au_1Pd_1/TiO_2	$NaHCO_3$	80	3	100/1	4	12.5	1
Au_1Pd_1/AC	$NaHCO_3$	80	3	100/1	4	8.8	1
Au-Pd/MgO	Base free	100	5	100/1	12	8.3	2
Au-Pd/HT	Base free	100	5	100/1	12	7.6	2
Au-Pd/CNT	Base free	100	5	100/1	12	7.8	2
Au-Pd/AC	NaOH	60	3	200/1	4	49.5	3
Au-Pd/AC	NaOH	60	3	200/1	2	99.0	3
Pd_1Au_6/TiO_2	NaOH	70	10	100/1	4	20.0	4
Au_1Pd_1/IRA-743	Na_2CO_3	100	10	100/1	4	23.3	5
Au_1Pd_1/IRA-900	Na_2CO_3	100	10	100/1	4	1.3	5
Au_1Pd_1/IRA-400	Na_2CO_3	100	10	100/1	4	6.5	5
AuPd/La-CaMgAl-LDH	Base free	100	5	100/1	6	15.0	6
AuPd/CaMgAl-LDH	Base free	100	5	100/1	6	14.2	6
Au_1Pd_1/PECN	K_2CO_3	90	O_2 flow: 10 mL/min	100/1	12	8.3	7
$Au_1Pd_{1.18}/Fe_3O_4$	K_2CO_3	RT	1	100/1	24	3.8	8
$Au_1Pd_2@Co_3O_4$	NaOH + Na_2CO_3	90	1	50/1	1	47.5	9
Au_4Pd_1/HT	NaOH	60	O_2 flow: 60 mL/min	50/1	6	7.5	10

Table S2. Summary of HMF oxidation over versatile monometallic Au catalysts in literature.

Catalyst	Solvent	T (℃)	PO_2 (bar)	HMF/metal (mol/mol)	Time (h)	FDCA productivity ($mol_{FDCA}.mol_{metal}^{-1}.h^{-1}$)	Ref
Au/ZOC	$NaHCO_3$	80	3	100/1	4	18.3	1
Au/TiO_2	NaOH	60	3	110/1	6	15.6	11
Au/HY	NaOH	60	3	110/1	6	18.2	11
Au/AC	NaOH	60	3	110/1	6	14.7	11
Au/TiO_2	NaOH	70	10	100/1	4	4.8	4
Au/MgO	Base free	110	26 (air)	50/1	2	22.8	12
Au/NiO	Base free	110	26 (air)	50/1	2	8.3	12
Au/ZrO_2	Base free	110	26 (air)	50/1	2	1.5	12
Au/C	NaOH	70	10	100/1	4	23.0	13
Au/Al_2O_3	NaOH	70	10	100/1	4	25.0	14
Au/CeO_2	NaOH	70	10	100/1	4	23.0	15
Au/HT-AC	Base free	100	5	100/1	24	4.1	16

Table S3. Summary of HMF oxidation over versatile monometallic Pd catalysts in literature.

Catalyst	Solvent	T (℃)	PO_2 (bar)	HMF/metal (mol/mol)	Time (h)	FDCA productivity ($mol_{FDCA}.mol_{metal}^{-1}.h^{-1}$)	Ref
Pd/ZOC	$NaHCO_3$	80	3	100/1	4	12.5	1
Pd/TiO_2	NaOH	70	10	100/1	4	2.0	4
Pd/MnO_2	K_2CO_3	100	1	48/1	4	10.6	17
Pd/$MgAlCO_3$	Base free	100	O_2 flow:	40/1	8	5.0	18
Pd/C	NaOH	RT	6.9	150/1	6	17.8	19

Table S4. Summary of HMF oxidation over series of Au and Pd catalysts in this study.

Catalyst	Solvent	T (℃)	PO_2 (bar)	HMF/metal (mol/mol)	Time (h)	FDCA productivity ($mol_{FDCA}.mol_{metal}^{-1}.h^{-1}$)
Au/C	$NaHCO_3$	80	3	200	2	6.3
Pd/C	$NaHCO_3$	80	3	200	2	0.0
Au/C + Pd/C	$NaHCO_3$	80	3	200	2	43.5
Au-Pd/C	$NaHCO_3$	80	3	200	2	17.0
(Au+Pd)/C	$NaHCO_3$	80	3	200	2	64.0
* Au/C + Pd/C	$NaHCO_3$	80	3	200	2	54.4
* Au-Pd/C	$NaHCO_3$	80	3	200	2	21.3
* (Au+Pd)/C	$NaHCO_3$	80	3	200	2	80.0

* Productivity calculated based on moles of Au only

Table S5. Summary of BET surface area from different materials as catalyst supports.

Entry	Supports	Surface area (m^2/g)
1	BN	28
2	TiO_2	51
3	XC72R	324

Table S6. Raw data from HMF oxidation using catalyst of (Au+Pd)/C. *Reaction conditions*: HMF (0.1 M), $NaHCO_3$ (0.4 M), H_2O (16 mL), (Au+Pd)/C: 143.1 mg, 80 °C, pO_2 = 3 bar, 120 min.

Reaction Time (min)	HMF Conversion (%)	Error bar (%)	HMFCA Yield (%)	Error bar (%)	FFCA Yield (%)	Error bar (%)	FDCA Yield (%)	Error bar (%)
0	0.0	±0.0	0.0	±0.0	0.0	±0.0	0.0	±0.0
5	20.3	±4.2	10.0	±2.5	5.1	±1.2	0.0	±0.2
15	53.9	±4.3	29.0	±1.7	17.6	±2.0	1.5	±0.1
30	84.4	±5.0	46.1	±4.1	28.6	±1.1	4.0	±0.6
45	100.0	±0.5	49.1	±1.2	33.9	±2.5	12.0	±2.3
60			41.0	±2.4	31.1	±3.4	24.5	±4.4
90			28.5	±2.5	24.5	±2.0	46.3	±4.9
120			18.6	±2.9	17.3	±2.2	63.9	±3.4

Table S7. Raw data from HMF oxidation using catalyst of Au/C+Pd/C. *Reaction conditions*: HMF (0.1 M), $NaHCO_3$ (0.4 M), H_2O (16 mL), Au/C: 72.1 mg, Pd/C: 71 mg, 80 °C, pO_2 = 3 bar, 120 min.

Reaction Time (min)	HMF Conversion (%)	Error bar (%)	HMFCA Yield (%)	Error bar (%)	FFCA Yield (%)	Error bar (%)	FDCA Yield (%)	Error bar (%)
0	0.0	±0.0	0.0	±0.0	0.0	±0.0	0.0	±0.0
5	14.7	±2.6	7.4	±1.1	2.7	±0.5	0.0	±0.2
15	40.9	±2.7	23.1	±5.0	11.2	±2.7	1.1	±0.6
30	72.3	±5.0	41.4	±3.9	21.3	±3.5	2.9	±0.6
45	90.9	±2.7	52.0	±4.1	27.4	±2.9	5.5	±1.2
60	100.0	±2.2	54.3	±3.2	28.7	±1.5	10.8	±2.6
90			45.2	±4.1	23.5	±1.7	28.4	±4.9
120			36.0	±3.2	18.4	±1.8	43.5	±4.8

Table S8. Raw data from HMF oxidation using catalyst of Au-Pd/C alloy. *Reaction conditions*: HMF (0.1 M), $NaHCO_3$ (0.4 M), H_2O (16 mL), Au-Pd/C: 143.1 mg, 80 °C, pO_2 = 3 bar, 120 min.

Reaction Time (min)	HMF Conversion (%)	Error bar (%)	HMFCA Yield (%)	Error bar (%)	FFCA Yield (%)	Error bar (%)	FDCA Yield (%)	Error bar (%)
0	0.0	±0.0	0.0	±0.0	0.0	±0.0	0.0	±0.0
5	11.3	±2.2	5.5	±1.1	1.9	±0.4	0.0	±0.1
15	30.7	±3.5	18.0	±2.5	7.9	±0.9	0.0	±0.3
30	54.5	±2.7	34.3	±2.5	15.1	±0.4	1.5	±0.1
45	72.3	±1.9	46.1	±1.7	20.1	±0.6	2.4	±0.1
60	86.1	±1.8	55.5	±1.0	23.9	±1.1	3.6	±0.3
90	100.0	±0.5	61.9	±1.8	25.9	±0.1	8.2	±2.7
120			59.0	±4.7	23.2	±1.4	16.9	±6.4

Table S9. Raw data from HMF oxidation using Au/C. *Reaction conditions*: HMF (0.1 M), $NaHCO_3$ (0.4 M), H_2O (16 mL), Au/C: 72.1 mg, 80 °C, pO_2 = 3 bar, 120 min.

Reaction Time (min)	HMF Conversion (%)	Error bar (%)	HMFCA Yield (%)	Error bar (%)	FFCA Yield (%)	Error bar (%)	FDCA Yield (%)	Error bar (%)
0	0.0	±0.0	0.0	±0.0	0.0	±0.0	0.0	±0.0
5	7.5	±0.2	5.1	±0.7	0.0	±0.3	0.0	±0.0
15	20.5	±0.5	16.0	±1.7	1.7	±0.6	0.0	±0.3
30	39.8	±2.3	32.7	±2.9	3.5	±1.0	0.0	±0.4
45	57.8	±1.6	47.9	±0.6	5.1	±1.1	1.1	±0.0
60	73.0	±2.3	60.5	±1.3	6.3	±0.2	1.5	±0.1
90	94.1	±1.0	77.7	±0.5	7.8	±0.9	2.6	±0.2
120	100.0	±0.0	83.1	±0.0	7.6	±1.1	4.6	±0.1

Table S10. Raw data from HMF oxidation using Pd/C. *Reaction conditions*: HMF (0.1 M), $NaHCO_3$ (0.4 M), H_2O (16 mL), Pd/C: 72.1 mg, 80 °C, pO_2 = 3 bar, 120 min.

Reaction Time (min)	HMF Conversion (%)	Error bar (%)	HMFCA Yield (%)	Error bar (%)	FFCA Yield (%)	Error bar (%)	FDCA Yield (%)	Error bar (%)
0	0.0	±0.0	0.0	±0.0	0.0	±0.0	0.0	±0.0
5	0.8	±1.2	0.1	±0.3	0.3	±0.0	0.0	±0.0
15	1.0	±0.4	0.4	±0.4	0.4	±0.1	0.0	±0.0
30	2.3	±0.8	0.6	±0.6	0.6	±0.4	0.0	±0.0
45	3.4	±1.8	0.8	±0.5	0.5	±0.7	0.0	±0.0
60	4.6	±1.6	1.1	±0.7	0.7	±1.1	0.0	±0.0
90	5.0	±2.4	1.5	±0.9	0.9	±1.6	0.0	±0.0
120	5.3	±2.8	1.9	±1.7	1.7	±1.5	0.0	±0.0

Standard deviation from error bars and particle size distribution were calculated based on the mean size of nanoparticles, the equation is listed below:

$$\sqrt{\frac{(X_1 - X_{mean})^2 + (X_2 - X_{mean})^2 + ... + (X_n - X_{mean})^2}{n-1}} \qquad \text{eq. (1)}$$

X_1, X_2...X_n is the particle size from each nanoparticle;

n is the numbers of nanoparticles;

X_{mean} is the mean particle size for all.

Table S11. Geometric model used to estimate the number of Au atoms associated with the exposed particle surface, entire particle volume and interfacial perimeter length as a function of Au particle size. The total number of exposed surface atoms, atoms per particle and interfacial periphery atoms estimated for Au particles of different sizes using the Mackay icosahedral model. The left half of the Table shows selected values of surface and total number of atoms from Mackay icosahedra having different diameters. The particle diameter d was estimated using the equation d = (2n + 1) · 0.288 (nm), where n is the number of shells in the Mackay model; the total atoms per particle (N_{total}) was calculated using the equation $N_{total} = \frac{10}{3}n^3 + 5n^2 + \frac{11}{3}n + 1$; the total number of exposed surface atoms ($N_{surface}$) was calculated using the equation $N_{total} = 10n^2 + 2$. The Mackay icosahedron chosen to best represent each binning interval was that which had the closest value to the median value of the binning interval[21].

N (number of Shells)	Diamater (nm)	N_{total} (Number of total atoms)	$N_{surface}$ (number of surface atoms)
1	-	1	1
2	0.9	13	13
3	2	147	92
…	…	…	…
10	6	3871	1002
…	…	…	…

Given that these estimates are underpinned by numerous assumptions, we consider that the most appropriate method of presenting the data is from metal weight loadings. We therefore have not made any changes to the figures presented in the primary manuscript. We unreservedly agree that accurate TOF measurements would be the most suitable way of presenting this work, but given the difficulties addressed above, we trust what we have provided is a suitable compromise.

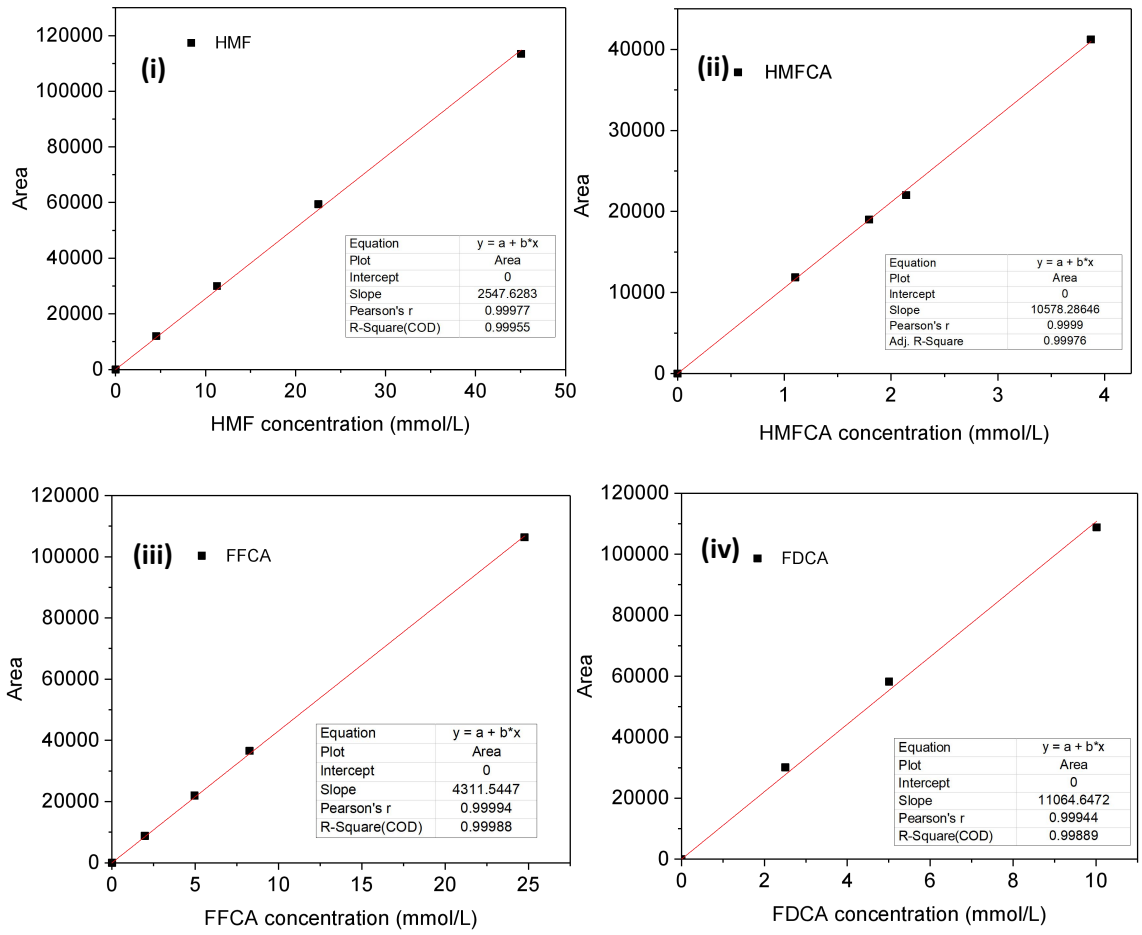

Figure S1. Calibration curves from HPLC for (i) HMF; (ii) HMFCA; (iii) FFCA and (iv) FDCA. *Reaction conditions*: mobile phase 0.7 mL/min 5 mM aqueous H_2SO_4; room temperature; wavelength 254 nm.

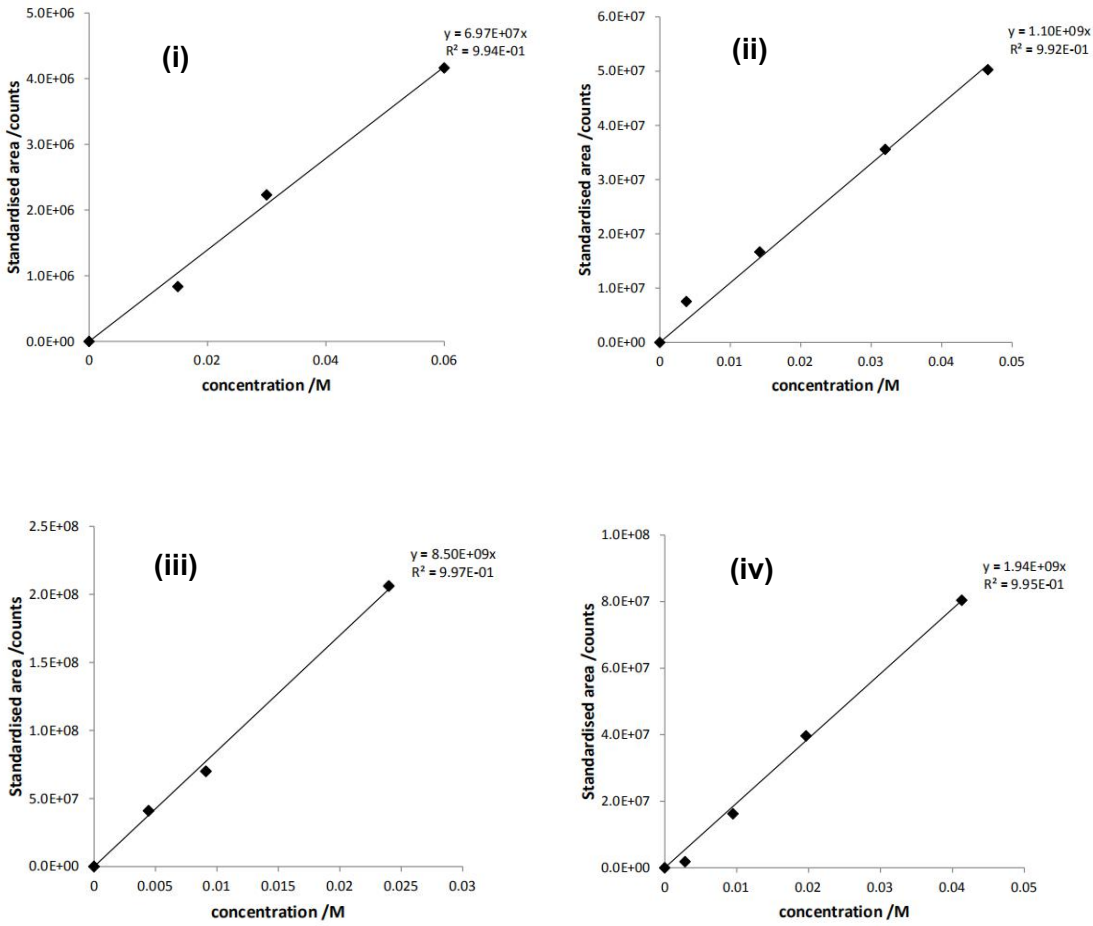

Figure S2. Calibration curves from HPLC for (i) glycerol; (ii) glyceric acid; (iii) oxalic acid and (iv) tartronic acid[20]. *Reaction conditions*: mobile phase 0.5 mL/min 10 mM aqueous H_3PO_4; room temperature; wave length 254 nm.

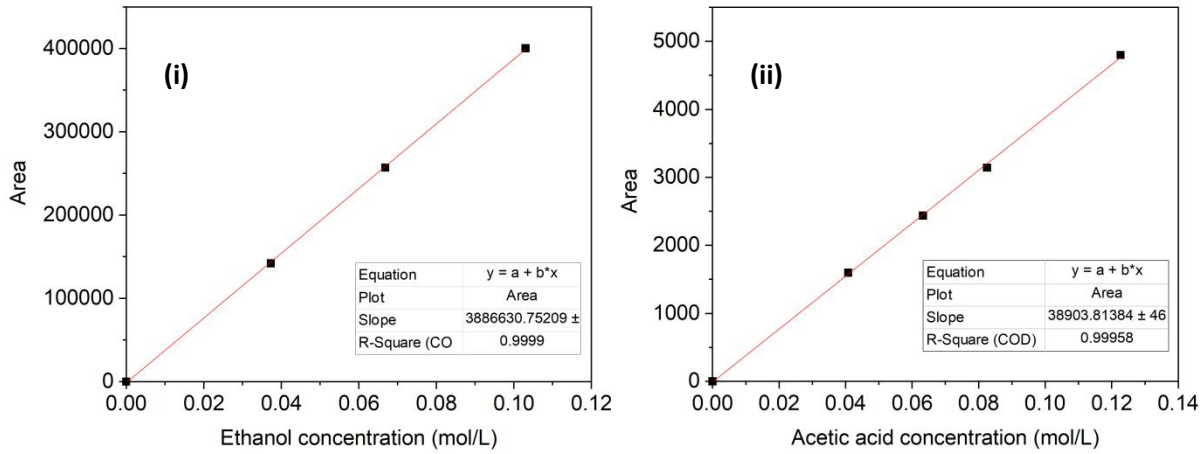

Figure S3. Calibration curves from HPLC for (i) ethanol; (ii) acetic acid. *Reaction conditions*: mobile phase 0.5 mL/min 10 mM aqueous H_3PO_4; room temperature; wave length 254 nm.

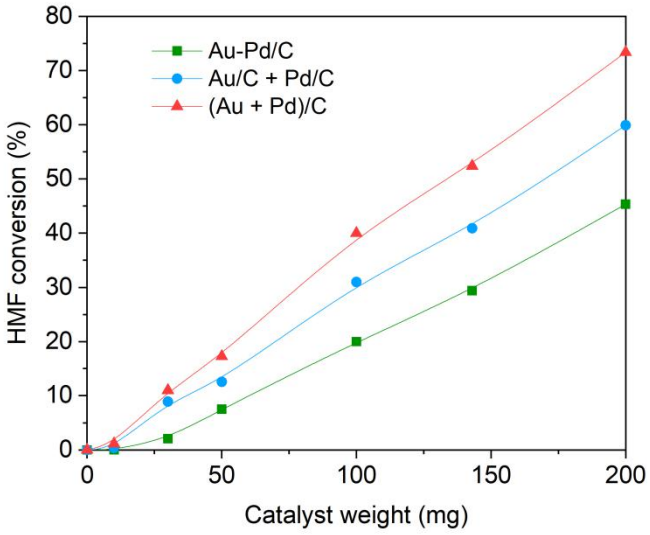

Figure S4. Aqueous HMF oxidation using series of catalysts with different weight. *Reaction conditions*: HMF (0.1 M), $NaHCO_3$ (0.4 M), H_2O (16 mL); 80 °C; pO_2 = 3 bar; 15 min.

References

1 Z. Gui, W. Cao, S. Saravanamurugan, A. Riisager, L. Chen and Z. Qi, *ChemCatChem*, 2016, **8**, 3636–3643.

2 X. Wan, C. Zhou, J. Chen, W. Deng, Q. Zhang, Y. Yang and Y. Wang, *ACS Catal.*, 2014, **4**, 2175–2185.

3 A. Villa, M. Schiavoni, S. Campisi, G. M. Veith and L. Prati, *ChemSusChem*, 2013, **6**, 609–612.

4 A. Lolli, S. Albonetti, L. Utili, R. Amadori, F. Ospitali, C. Lucarelli and F. Cavani, *Appl. Catal. A, Gen.*, 2015, **504**, 408–419.

5 C. A. Antonyraj, N. T. T. Huynh, S.-K. Park, S. Shin, Y. J. Kim, S. Kim, K.-Y. Lee and J. K. Cho, *Appl. Catal. A, Gen.*, 2017, **547**, 230–236.

6 Z. Gao, R. Xie, G. Fan, L. Yang and F. Li, *Acs Sustain. Chem. Eng.*, 2017, **5**, 5852–5861.

7 Q. Wang, W. Hou, S. Li, J. Xie, J. Li, Y. Zhou and J. Wang, *Green Chem.*, 2017, **19**, 3820–3830.

8 A. Cho, S. Byun, J. H. Cho and B. M. Kim, *ChemSusChem*, 2019, **12**, 2310–2317.

9 Y.-T. Liao, V. C. Nguyen, N. Ishiguro, A. P. Young, C.-K. Tsung and K. C.-W. Wu, *Appl. Catal. B Environ.*

10 H. Xia, J. An, M. Hong, S. Xu, L. Zhang and S. Zuo, *Catal. Today*, 2019, **319**, 113–120.

11 J. Cai, H. Ma, J. Zhang, Q. Song, Z. Du, Y. Huang and J. Xu, *Chem. - A Eur. J.*

12 C. P. Ferraz, M. Zieliński, M. Pietrowski, S. Heyte, F. Dumeignil, L. M. Rossi and R. Wojcieszak, *ACS Sustain. Chem. Eng.*, 2018, **6**, 16332–16340.

13 C. Megías‐Sayago, A. Lolli, D. Bonincontro, A. Penkova, S. Albonetti, F. Cavani, J. A. Odriozola and S. Ivanova, *ChemCatChem*, 2020, **12**, 1177–1183.

14 C. Megías-Sayago, A. Lolli, S. Ivanova, S. Albonetti, F. Cavani and J. A. Odriozola, *Catal. Today*, 2019, **333**, 169–175.

15 A. Lolli, R. Amadori, C. Lucarelli, M. G. Cutrufello, E. Rombi, F. Cavani and S. Albonetti, *Microporous Mesoporous Mater.*, 2016, **226**, 466–475.

16 T. Gao, T. Gao, W. Fang and Q. Cao, *Mol. Catal.*, 2017, **439**, 171–179.

17 X. Liao, J. Hou, Y. Wang, H. Zhang, Y. Sun, X. Li, S. Tang, K. Kato, M. Yamauchi and Z. Jiang, *Green Chem.*, 2019, **21**, 4194–4203.

18 Y. Wang, K. Yu, D. Lei, W. Si, Y. Feng, L.-L. Lou and S. Liu, *ACS Sustain. Chem. Eng.*, 2016, **4**, 4752–4761.

19 S. E. Davis, L. R. Houk, E. C. Tamargo, A. K. Datye and R. J. Davis, *Catal. Today*, 2011, **160**, 55–60.

20 G. L. Brett, *PhD Thesis*, 2012.

21 A. L. Mackay, *Acta Crystallogr.*, 1962, **15**, 916–918.